HIGH RESOLUTION STUDIES OF XNR1 SIGNALING AND LEFT-RIGHT ASYMMETRY IN *XENOPUS*

By

Lindsay T. Marjoram

Dissertation

Submitted to the Faculty of the

Graduate School of Vanderbilt University

in partial fulfillment of the requirements

for the degree of

DOCTOR OF PHILOSOPHY

in

Cell and Developmental Biology

December, 2010

Nashville, Tennessee

Approved:

Dr. Christopher V. E. Wright

Dr. Chin Chiang

Dr. David Bader

Dr. Mark de Caestecker

Dr. Joshua Gamse

ACKNOWLEDGEMENTS

Several people were integral to my success during graduate school at Vanderbilt. First and foremost, I would like to thank my mentor, Chris Wright, for his tireless dedication and support. One of the most valuable things Chris has taught me is the art of parallel processing multiple projects, such that there was never an excuse for dull moment in lab. I also want to thank Chris for setting the bar high and encouraging me not to settle for less. Chris is an incredible writer and strives for his students to be good writers too and, for that, I know I am leaving here a much stronger writer than when I started. On a less professional note, I am grateful to Chris for indulging in my love of terrible television shows (American Idol), high-quality music (Leona Lewis), and wine. I would also like to thank my committee members, Dr. David Bader, Dr. Chin Chiang, Dr. Joshua Gamse, and Dr. Mark DeCaestecker for their continued enthusiasm, insight and suggestions. I am indebted to members of the Wright lab past and present, especially Young Cha, JJ Westmoreland and Yuki Ohi for teaching me everything there is to know about *Xenopus* embryology, and to Dan Boyer, Fong Cheng Pan, and Jessica Sweatt for keeping our lab bay a light-hearted and entertaining place to do experiments. I am incredibly grateful for Mike Ray (lab ninja extraordinaire) and Kim Kane (my Jersey girl partner in crime) for their hard work and dedication, which keep the Wright lab running smoothly.

I will never be able to adequately express how appreciative I am for the love and support my family and friends have provided through the years. To my parents, Bob and Patti, and to my sister Michelle, thank you for being with me every step of the way and reminding me of the bigger picture—I can honestly say, I could not have done this without you guys. To my granddad Kolloff, thank you for taking me to Hewlett Packard on ‘take your daughter to work day’, which served as my first introduction to science, and

to my grandparents, Bill & Shirley, thank you for your infinite wisdom and support. I would like to sincerely thank Elizabeth McCain for giving me my first research position at Muhlenberg College and for introducing me to sea urchin embryology and scanning electron microscopy to show me just how beautiful developmental biology can be. To Matt and Leslie and my Sarahs, thank you for being amazing and supportive friends who have been my Nashville family. Last, but definitely not least, I want to thank my husband, Robin, who has been my partner and my best friend throughout graduate school. His unconditional love and devotion have been a constant support and I would not be here without him.

TABLE OF CONTENTS

Page

LIST OF TABLES

LIST OF FIGURES

CHAPTER I

INTRODUCTION

A fundamental understanding of vertebrate embryogenesis requires a definition of how various signaling networks establish tissue patterning programs, in a focal or distributed manner, and with appropriate dynamics. Several models, many with supporting experimental evidence, have been proposed to explain potential mechanisms of tissue patterning by a secreted signaling molecule (for the purposes of this introduction, a receptor ligand). In the ratchet model, proposed by Gurdon and colleagues (Gurdon et al., 1995), the secreted signaling molecule is released from a localized source, such that it travels away from the source to, in canonical terms, form a spatial 'morphogen gradient'. Surrounding cells then interpret the spatial gradient based on their position within it by responding to the absolute number of ligand-occupied receptors (Gurdon et al., 1995). When the morphogen concentration exceeds a particular threshold, cells can 'ratchet-up' their response according to the highest concentration of secreted molecule received. The ratchet model, however, does not account for the dynamic movement of cells within an embryo or the time during which they might be exposed to a particular concentration of the gradient, as the experiments supporting the ratchet model were performed in tissue explants. In an alternate model, Dougan and colleagues proposed that the response to a particular morphogen is a function of both space *and* time. In this spatiotemporal model, a cell makes a fate choice not based on the absolute number of receptors bound to ligand, but rather cumulatively by integration of the total time the cell was exposed to the morphogen, in addition to the distance of the cell from the morphogen source (Hagos and Dougan, 2007).

Many factors regulate the transport, perdurance, and routes of travel of the secreted protein and, for the most part, these parameters are difficult to study and thus still poorly defined. To address these concepts, my thesis studies focused on two members of the Transforming Growth Factor beta (TGFβ) family of secreted ligands: Nodal (specifically Xnr1 or Nodal1 of the six Nodal-related genes *Xenopus*) and Lefty. Nodal and Lefty are highly conserved amongst the vertebrates, and are secreted ligands that work as an activator and inhibitor, respectively. First identified as critical factors in induction of mesoderm and endoderm, Nodal and Lefty were also later shown to be essential for the generation of left-right (L-R) asymmetric patterning, which ensures the proper organ shaping and positioning (the normal embryonic asymmetry is referred to as *situs solitus*). The general picture is that Nodal induces tissue responses and has an autoregulatory loop stimulating its own expression, while Lefty is induced as a feedback inhibitor of Nodal signaling, serving to prevent overactivity of Nodal in space or over time (Wright, 2001). Because Nodal and Lefty are essential for early tissue layer induction and left-right asymmetric morphogenesis, with highly deleterious consequences in their absence, the parameters that govern their secretion, processing and transport have begun to be explored in several accessible model organisms during the period of mesendoderm induction. Loss or gain of function manipulations of this signaling pathway, however, often cause gastrulation failure and therefore preclude accurate analysis of ligand behavior in subsequent stages, such as those relevant to L-R patterning. Thus, it is unclear whether the factors defined as regulating secretion, processing and transport during blastula and gastrula stages are relevant or applicable during L-R patterning. In this introduction, I will briefly explain the identification of Nodal as an important factor in mesendoderm induction and how positive autoregulation and inhibitory signals are essential for spatiotemporal control of asymmetric gene expression and pattern formation. This foundation will be followed by a description of the current

understanding of the roles Nodal and Lefty play during L-R axis patterning and the steps necessary to impose asymmetry within an otherwise bilateral body plan. Finally, I will end with a brief discussion of how asymmetric *Nodal* expression becomes translated into the later morphogenetic movements that govern organ situs.

The TGFβ Superfamily

The TGFβ superfamily is a highly conserved family of proteins integral in cell specification, proliferation and differentiation in the developing embryo and the adult. Misregulation of TGFβ signaling has been implicated in both congenital disorders and cancer. Two main branches exist within the TGFβ family: the Nodal/Activin/TGFβ subfamily and the Bone Morphogenetic Protein (BMP)/Muellerian Inhibiting Substance (MIS)/Growth and Differentiation Family (GDF) subfamily. Both arms play indispensible roles in patterning the dorsal-ventral (D/V), anterior-posterior (A/P) and L-R axes of the early embryo. In this introduction, I focus on the Nodal/Activin/TGFβ ligands.

The function of Nodal in mesendoderm induction and asymmetric patterning is conserved within the deuterostomes. Outside of the deuterostome family, the presence of Nodal was more difficult to uncover, though it should be noted that it was recently identified for the first time in the protostome clade Lophotrochozoa, and connected to a role as a determinant of snail shell chirality (Grande and Patel, 2009). Despite their stereotypical chiral organ formation, a Nodal ortholog has not yet been identified within flies or nematodes, members of the ecdysozoan clade.

Ligand Structure

Most TGFβ ligands share conserved sequence similarities that are associated with structural hallmarks important for ligand activation and receptor-binding. After a

cleavage event releases the mature ligand from a proprotein precursor, the active, mature form of TGFβ homodimerizes. Intra-ligand disulfide bonds that generate a cysteine knot structure stabilize the β-strands within each monomer and, in turn, expose three hydrophobic α-helices, essentially to one face of the monomer. A better understanding of Nodal and Lefty structure comes from analysis of the predicted secondary structure of each ligand modeled against the known secondary structure of TGFβ2 generated by X-ray crystallography (Daopin et al., 1992). The mature domain of human TGFβ2 (112 amino acids) was shown to contain short, two-stranded antiparallel β-sheets and 3 α-helices (Daopin et al., 1992). The authors describe the tertiary structure as resembling a "slightly curled left hand with fingers", where the α3 helix is the heel of the hand, and the ten amino-terminal residues resemble the thumb of the hand (Daopin et al., 1992). Two-fold symmetry and a lack of overtly exposed hydrophobic surfaces in the crystallographic characterization of TGFβ2 indicate that the stable form of TGFβ2 in solution is a homodimer, with the hydrophobic domains of each monomer facing each other.

As inferred from the X-ray crystallography, dimerization occurs after interaction between the hydrophobic helices of two monomers, an interaction that is further stabilized by an inter-subunit disulfide bond (Kingsley, 1994; Shi and Massagué, 2003). Lefty, a divergent member of the Nodal/Activin/TGFβ subfamily and a direct inhibitor of Nodal, has a substantially extended C-terminal tail when compared to other mature ligands of this family and also lacks some of the hallmarks of classical TGFβ ligands. For example, absence of a hydrophobic α-helix containing a cysteine involved in dimerization, in combination with biochemical and structure:function analyses has indicated that Lefty may function as a monomer (Kingsley, 1994; Meno et al., 1996; Thisse and Thisse, 1999). A direct sequence comparison of Nodal to Lefty quickly

highlights how different Lefty is. How do these differences, from the structural level, dictate the diversity in their biological regulation, production, or overall stability?

Extrapolating the crystal structure of TGFβ2 and BMP to Nodal and Lefty, using the available information on the regions that are involved in binding their cognate cell-surface receptors was integral to my thesis studies, as I tried to take into account the way in which Nodal or Lefty tertiary structure might be amenable to the placement of epitope-tags, with respect to the maintenance of receptor binding and signal transduction. Currently, immuno-detection of Nodal or Lefty is not possible, likely because of lack of antibody specificity, low endogenous protein levels, and overall ligand instability. Analyses of Nodal ligands in several species have often reported difficulties in adding an epitope tag without rendering the protein inactive (Williams et al., 2004). The crystal structure of mature dimerized TGFβ ligands showed a close physical interaction between the C-terminus of each monomer, with the final C-terminal residues (Cys-X-Cys-X) essentially buried within this interface. This finding indicates that adding any epitope tag to the C-terminus of Nodal could potentially disrupt dimerization and thus protein function. In agreement with this idea, I showed that C-terminal addition of a 6Myc tag to Xnr1 renders the protein inactive in animal cap mesoderm induction assays. As described above, Lefty contains an extended C-terminal tail and lacks a conserved cysteine residue required for dimerization, and we have shown that Lefty function is not affected by addition of a C-terminal tag, perhaps because of the C-terminal externalization per se, or because the greater flexibility in the C-terminal region allows the epitope tag to more freely 'flop' away from the monomer (Westmoreland et al., 2007).

Proprotein cleavage produces the functional mature ligand

Nodal, Lefty, and most other TGFβ proteins are initially translated as pre-proproteins, with a 15-25 amino acid signal sequence, a pro-domain ranging from 50-375 amino acids and a mature ligand domain, which ranges from 110-140 amino acids. Cleavage of the pro-domain is a significant regulatory step in the production of active Nodal and Lefty proteins: Nodal and Lefty ligands require proteolytic cleavage from their proprotein precursors before becoming active. Precise regulation of protein levels ensures the appropriate activity and Nodal-Lefty balance to establish the proper dynamics of positive and negative feedback loops between them. Members of the subtilisin-like proprotein convertase (SPC) family of calcium-dependent serine endoproteases are key regulators of Nodal/Lefty processing from proprotein to mature ligand by recognition of the dibasic cleavage site, RXXR (Constam and Robertson, 1999; Molloy et al., 1992). A combination of mouse knockouts, *Xenopus* biochemistry, tissue separation experiments and cell culture analyses have specifically identified Spc1 (Furin), Spc4 (Pace4), and potentially Spc6 as being integral for proper Nodal and Lefty function (Beck et al., 2002). While Nodal contains only one cleavage site, Lefty contains two cleavage sites capable of producing a long and short isoform of the mature ligand. JJ Westmoreland, a previous graduate student in our lab, demonstrated that the long isoform of Lefty is the active isoform during mesendoderm induction and is preferentially produced *in vivo* while the short isoform may represent an unstable clearance intermediate (Westmoreland et al., 2007). The cellular location of Nodal/Lefty proprotein cleavage is still somewhat unclear as it has been demonstrated that Nodal and Lefty can be cleaved intracellularly as well as extracellularly, by secreted soluble forms of SPC1 and SPC4 (Beck et al., 2002).

TGFβ Signal Transduction: An overview

Much of our understanding of signal transduction in the Nodal pathway is based on discoveries initially made from other closely related receptor ligands. Generally, Nodal is believed to follow the model established for related ligands such as TGFβ, in that it activates via a 'tetrameric' complex of two serine-threonine Type II receptor kinases (ActRII-B, ActRII-A) that subsequently recruit and phospho-activate two Type I receptor kinases (ALK4, ALK7) in their C-terminal GS-rich region, which then cross-phosphorylate and activate downstream effector components (Smads) (Schier, 2003; Shi and Massagué, 2003). Interestingly, the timing of receptor activation in this model is not applicable to all TGFβ-related proteins: BMPs have a higher affinity for the Type I receptor and initiate the formation of the tetrameric receptor complex by binding the Type I receptors first (Shi and Massagué, 2003). At almost every level of this pathway, there exist important regulatory steps to prevent aberrant Nodal signaling. At the receptor level, Nodal (as well as Vg1 and GDF) cannot activate downstream components of the pathway without the presence of a coreceptor (Gritsman et al., 1999). While the presence of a co-receptor is not required for activin, Nodal is quite distinct in requiring the GPI-linked co-receptor EGF-CFC (FRL1 in frog; Cripto/Cryptic in mouse; One Eyed Pinhead [OEP] in zebrafish) to mediate signal transduction. Genetic removal or morpholino-mediated knockdown of EGF-CFC prevents *Nodal* expression and mesendoderm formation. The phenotype of EGF-CFC knockdown is phenotypically equivalent to an embryo lacking Nodal itself (Gaio et al., 1999; Gritsman et al., 1999). EGF-CFC/Cripto has been shown to interact independently with Nodal and Alk4 (Reissmann et al., 2001), but the mechanism by which this confers pathway activation is still unclear: Nodal conformation may change when in complex with Cripto to more efficiently activate the pathway or, it may be that there are still unknown components that specifically require an intact Nodal/Cripto/Alk4 complex for pathway activation. More

recently, the Constam lab has demonstrated that Cripto is also required for the proper processing and 'presentation' of Nodal to its proprotein convertases (Blanchet et al., 2008).

After Nodal has formed a complex with its receptors at the cell surface, phosphorylated Type I receptors fairly rapidly phospho-activate the receptor-Smads 2 and 3 (Smad2/3), the downstream cytoplasmic transducers of Nodal signaling. Smad proteins, which contain a conserved MH1 and MH2 domain separated by a more divergent linker region, are phosphorylated at an SSXS motif of the MH2 region. This phosphorylation event is required for nuclear pore contact by the Smads (Xu et al., 2000), as signal transduction in the Nodal pathway requires nuclear translocation of the activated Smads to cause changes in transcription. The Smad MH1 domain is subsequently required for DNA-binding following translocation of the Smad complex into the nucleus. Smad-binding to Type I receptors is facilitated by 'Smad anchor for receptor activation' (SARA) proteins, which operate to keep Smad2/3 tethered near the cell membrane for optimal activation by receptors (Shi and Massagué, 2003). Following phosphorylation by the Type I receptor, activated phospho-Smad2/3 (pSmad2/3) bind the common Smad, Smad4, and shuttle into the nucleus where the Smad complex binds transcriptional activators or repressors to alter gene expression. In the case of Nodal signaling, pSmad2/3:Smad4 complexes often form a transcriptional complex with FoxH1, which is known to function as an 'on/off' transcriptional switch. During left-right patterning, activation of Nodal signaling causes the Smads and FoxH1 to activate gene expression of Nodal itself (positive autoregulation), Lefty (its antagonist) and Pitx2 (downstream effector) (Fig. 1.1).

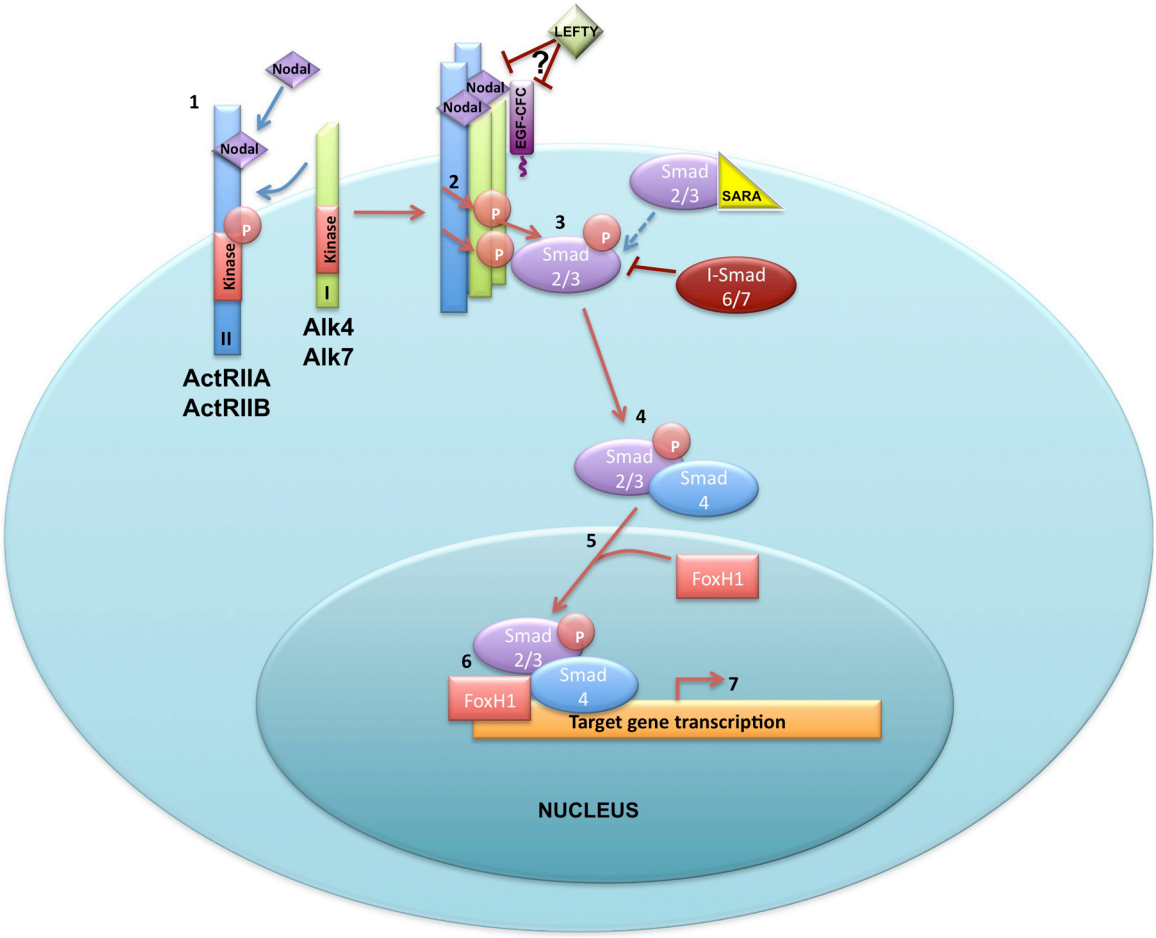

Figure 1.1 Nodal signal transduction pathway. Dimerized Nodal ligand (only one shown for simplicity) binds to the type II receptor (**1**), which subsequently recruits the type I receptor and the EGF-CFC co-receptor to form a tetrameric activated receptor complex (**2**). Phosphorylation of the type I receptor by the type II receptor recruits Smad2/3 to the activated receptor complex, which phosphoactivates Smad2/3 (**3**). SARA proteins keep Smad2/3 tethered at the plasma membrane for faster recruitment to the receptor complex. Phospho-Smad2/3 recruits the common Smad4 (**4**), and the Smad complex translocates into the nucleus (**5**). The Smad complex then binds to the transcription factor, FoxH1 (**6**), which allows the initiation of target gene transcription (**7**).

Nodal as a mesendoderm inducer

Seminal studies in mouse, chicken and frog identified Nodal as a required, potent mesendoderm inducer during gastrulation. A mouse mutant—containing an insertional mutation (413.d) in the Nodal locus, originally dubbed *hyperplastic ectoderm* —was unable to form the primitive streak, and thus failed to undergo gastrulation (Conlon et al., 1994; Zhou et al., 1993). A time-course examination of *Nodal* gene expression revealed that it was expressed prior to and during gastrulation in mouse, chicken and frog, which put Nodal in the right place at the right time to play a role during gastrulation (Agius et al., 2000). This was an exciting discovery because although several potential mesendoderm inducers had been identified (e.g., Vg1, Activin), studies were unable to demonstrate a clear loss-of-function-based requirement in the induction of a range of mesodermal cell types at the proper time during development (Sokol et al., 1991; Sokol et al., 1990; Weeks and Melton, 1987). For example, while activin was able to induce a broad range of mesendodermal cell types, it was not endogenously expressed in the embryo during gastrulation stages. Studies in frog, however, strongly demonstrated that *Xenopus* Nodal-related 1 (Xnr1; provisionally renamed Nodal1) was a potent inducer of mesoderm, as it could both dorsalize ventral marginal tissue and rescue patterning in UV-irradiated embryos (Jones et al., 1995). Similar types of experiments in *Xenopus* were repeated using mouse Nodal to induce mesoderm, which indicated a significant level of conservation in the capacity for Nodal to induce mesendoderm. These experiments were strengthened by improved *in situ* hybridizations showing that *Xnr1* RNA was present in a graded fashion, with higher levels on the dorsal side than the ventral side (Agius et al., 2000). Studies from the Heasman lab and others (Kofron et al., 1999; Lee et al., 2001; Osada and Wright, 1999) also demonstrated a strong link between the maternally deposited factors VegT and Vg1 and mesendoderm induction. Maternal-zygotic depletion experiments of VegT/Vg1, and rescue with exogenous Nodal,

showed that VegT/Vg1 were required to directly induce *Nodal* expression just prior to gastrulation (Agius et al., 2000).

Nodal functions as a morphogen

Following the discovery that Nodal was the primary mesoderm *inducing*-factor, several labs demonstrated that activin, and later Nodal, had the capability of behaving as a mesendoderm patterning factor, i.e. as a 'classical' morphogen (Green et al., 1992; Green and Smith, 1990). Intricate experiments from the Smith and Gurdon labs showed that radiolabeled activin could be secreted and travel long distances away from a localized source, across a field of cells rendered incapable of responding to the activin signal, effectively forming a gradient of protein (Green et al., 1992; Green and Smith, 1990; McDowell et al., 1997). More recent studies that examined Nodal protein mobility were performed on Xnr2 (*Xenopus* Nodal related 2, which has high sequence conservation with Xnr1) in *Xenopus* animal cap assays. Animal caps injected with Xnr2 were sandwiched with uninjected animal caps (Nodal-naïve), cultured for several hours and analyzed for induction of mesendoderm gene expression in the uninjected, 'responder' animal cap (Williams et al., 2004). Prior to the studies from the Smith lab, it was shown that high levels of Nodal signaling were required to induce the gene *goosecoid (gsc)* whereas lower levels of Nodal signaling were sufficient to induce the pan-mesodermal gene *Xbrachyury* (*Xbra*) (Green et al., 1992). In the animal cap sandwich experiments, the Smith lab demonstrated that higher levels of Xnr2 induced *gsc* only in the cells closest to the injected animal cap whereas responding cells that were several cell diameters away from the injected animal cap could express *Xbra* (Williams et al., 2004). In experiments performed thereafter, the morphogen status of Nodal became less clear, as there were several pieces of confounding data from within the Smith lab on whether or not Xnr2 could travel long distances. GFP-tagged Xnr2 was

initially classified as a short-range molecule (Jones et al., 1996) but later as long-range (Williams et al., 2004). Somewhat frustratingly, these conflicting results were not directly addressed by the lab that produced them though we assume they are likely due to differences in experimental manipulation. Our own studies with epitope-tagged Xnr1 (presented in Chapter III) indicate that it is able to signal over long distances.

Nodal ligand mobility

Although the studies mentioned in the previous section depict Nodal as a morphogen, the lack of antibodies against Nodal made it difficult to directly assess Nodal protein traveling long distances and forming a gradient. In addition to Nodal directly traveling long distances, it was also possible that Nodal protein induced a second, 'relay' factor, which traveled long distances and induced mesodermal gene expression. One of the more elegant experiments to address this point was performed in zebrafish. Taking advantage of zebrafish with a maternal-zygotic Oep mutation (MZ-Oep), which are incapable of responding to a Nodal signal because of the loss of the obligate receptor cofactor (described above), the Schier lab first demonstrated that injection of Nodal RNA fails to induce mesodermal gene expression in surrounding cells deficient for the EGF-CFC co-receptor (Chen and Schier, 2001). The authors then set up an experiment where a population of wild-type cells (which contain Oep and are thus Nodal-responsive) were transplanted into the MZ-Oep mutant embryo after it had been injected with Nodal RNA in 1 cell (lacks Oep, nonresponsive to Nodal) at the 128-cell stage. The authors showed a robust induction of mesodermal genes in the transplanted wild-type cells, which indicated that Nodal was secreted from the previously injected producer cells (incapable of responding to the Nodal signal) and directly triggered appropriate downstream target gene expression in a population of cells several cell diameters from the source (Chen and Schier, 2001). The majority of studies examining morphogen

properties of Nodal have been performed in gastrula stage embryos, however, embryonic architecture changes dramatically after gastrulation, which could significantly alter the ligand transport behavior of Nodal. In heterologous electroporation experiments in chicken embryos (when *Nodal* is asymmetrically expressed endogenously), Sakuma et al. (2002) demonstrated that both GFP-tagged mouse Nodal and Lefty2 could move far from a localized source, with Lefty2 moving farther than Nodal. This experiment did not examine which tissue layer Nodal or Lefty2 were found in after electroporation and it was unclear if the mechanisms of long-distance travel utilized in gastrulation stages were similar to those used during these later stages when L-R patterning is established. These experiments raise an important question in the L-R field: do Nodal or Lefty also function as morphogens in embryos with more complicated embryonic architectures?

Cell Memory of the Nodal Signal

After ligand-receptor interaction activates the pathway, how long do cells then 'remember' the signal they received? Studies examining the time window during which cells recognize (via receptor binding) and remember the Nodal signal (via persistent nuclear localization of p-Smad2) have not been performed, but they have been done with activin. Gurdon and colleagues showed that the rate of mesoderm induction by activin binding to its type II receptor is dependent on the concentration of activin in solution: rapid binding occurs at high concentrations whereas slower binding occurs at lower concentrations (Dyson and Gurdon, 1998). Pulse-chase experiments with [^{35}S]-labeled activin also demonstrated that the ligand-receptor interaction was highly stable, with 80% remaining bound at 2 hours, 50% after 5 hours and ~30% still remaining bound after 6 hours (Dyson and Gurdon, 1998; Jullien and Gurdon, 2005). In a follow-up to these experiments, the Gurdon lab quantified the amount of Smad2 protein that entered the nucleus after activin treatment and showed that the amount of nuclear Smad2

linearly correlated with the amount of receptors activated, indicating that no amplification of the original signal took place after receptor activation (Shimizu and Gurdon, 1999). Ligand-bound receptors are not necessarily indicative of active, continuous signaling, however. For example, after receptor binding, the ligand-receptor complex could immediately be internalized and targeted for degradation, which would drastically shorten the time during which the cell was actively responding to activin. The Gurdon lab showed, however, that internalization of the ligand-receptor complex into the endocytic pathway, without moving to the lysosome for degradation, allowed for continuous induction of mesodermal genes by activin. Blocking internalization (Dynamin mutant) or ligand binding (activin immobilized on beads) of the ligand-receptor complex failed to induce mesodermal gene expression, leading the authors to define the time spent by the ligand-receptor complex in the endocytic pathway as a "memory complex", another necessary parameter in shaping the morphogen gradient for proper gene induction (Jullien and Gurdon, 2005).

Alternative approaches have been developed to understand the duration of cellular response to Nodal signaling, since ligand-receptor binding is not easily observable in intact embryos. Translocation of pSmad2 into the nucleus serves as a strong readout for active Nodal signaling, though the current antibodies against pSmad2 do not work well in immunofluorescence assays. To skirt the problem of less-than-ideal antibodies, the Smith lab generated a bimolecular fluorescence complementation (BiFC) system to examine Smad2 residence in the nucleus in real time. The Venus fluorescent protein was split into N- and C-terminal halves and fused to Smad2 and Smad4, respectively. Venus fluorescence was only observed in the nucleus after direct interaction of Smad2/4 following pathway activation (Saka et al., 2007; Saka et al., 2008). This system is highly informative in addressing the time it takes cells to register Nodal signaling by nuclear pSmad2 translocation, but in its current form BiFC is not

adequate to determine the total duration of Nodal signaling. Split fluorescent proteins are known to form a tight association and may artificially stabilize the Smad2/4 protein interaction. Importantly, these studies addressed a long-standing question: Why do early embryos not respond to a Nodal signal until after midblastula transition? With their BiFC system the authors showed that, regardless of the timing of cell exposure to activin, pSmad2 could not enter the nucleus until after midblastula transition (Saka et al., 2007). To address the problem of Smad2 nuclear retention as a means of analyzing the duration of Nodal signaling, our lab has generated new p-Smad2/3 antibodies to detect endogenous nuclear pSmad2/3 localization during mesendoderm induction and L-R patterning stages.

Regulation of the Nodal Signaling Threshold

Nodal signaling must be spatiotemporally controlled as overinduction of Nodal can lead to an excess mesendoderm and failed gastrulation. Aberrant Nodal signaling during L-R patterning, possibly even with only quite small deviations from normal, is associated with severe defects in organ morphogenesis, especially congenital heart defects. There are mechanisms in place at almost every level of the pathway intracellularly to provide negative regulatory feedback of signaling. Downstream of the receptors, the inhibitory Smads (6&7) compete with Smad2/3 for binding to the activated Type I receptor, causing E3 ubiquitin ligases (Smurfs) to mark the receptor for degradation (Shi and Massagué, 2003). Additionally, the mechanism of activated receptor/ligand internalization also determines duration of signaling activity.

Factors in the extracellular environment are also critical in controlling the threshold of Nodal signaling. Secreted inhibitors and extracellular matrix can significantly alter the distance traveled or time during which a ligand can actively signal

(Itoh and Sokol, 1994; Jones et al., 1996). Another predominant negative regulation is afforded by blocking Nodal from activating its receptor. One such inhibitor, Lefty, serves as a Nodal antagonist by binding directly to the type II Activin receptor or, potentially, by interfering physically with the normal function of EGF-CFC as a Type I-Type II complex cofactor (Cheng et al., 2004). Extracellular matrix proteins within basement membranes can either positively or negatively regulate Nodal signaling. These mechanisms of Nodal regulation will be covered in the sections below.

Secreted Inhibitors: Lefty and Cerberus

Secreted inhibitors represent an important class of proteins that regulate the activity/range and perdurance of signaling by secreted ligands. For Nodal, at least two different secreted inhibitors are absolutely required to maintain the proper levels of Nodal signaling for mesoderm induction and L-R asymmetry. Lefty, mentioned previously in the ligand structure and signal transduction sections, is a divergent member of the TGFβ family and likely functions as a monomer. Meno and colleagues (Meno et al., 1996) originally identified mouse Lefty from a subtractive screen in P19 embryonal carcinoma cells. Cell culture analyses demonstrated that Lefty, like Nodal, was processed and secreted into culture medium. In mice, *Lefty* was expressed in the primitive streak during gastrulation and later, during somitogenesis, in the L lateral plate mesoderm (LPM) and L anterior endoderm and symmetrically in the ventral midline (Meno et al., 1996). Mouse mutants with L-R situs defects (e.g. *iv/iv* and *inv/inv*) showed that *Lefty* expression was aberrant, demonstrating that Lefty may play an important role in L-R asymmetry specification, though at the time it was not known in what capacity. Subsequently, Lefty homologs were identified in zebrafish, chicken and frogs (Cheng et al., 2000; Ishimaru et al., 2000; Tanegashima et al., 2004; Thisse and Thisse, 1999). Following Lefty identification, genetic knockouts in mice along with knockdown and

overexpression studies in frog and fish demonstrated that Lefty functions as a potent long-range antagonist of Nodal signaling (Branford and Yost, 2002; Cha et al., 2006; Chen and Schier, 2002; Cheng et al., 2000; Meno et al., 1999; Sakuma et al., 2002; Thisse and Thisse, 1999). A Lefty knockout mouse and antisense morpholino-oligonucleotides targeted against Lefty resulted in a dramatic increase in mesendoderm tissue production (Branford and Yost, 2002; Cha et al., 2006; Chen and Schier, 2002; Cheng et al., 2000; Meno et al., 1999). Through *in situ* hybridization and RT-PCR analysis of target gene expression, our lab and others showed that *Nodal* expression was greatly increased and prolonged in Lefty-morpholino injected embryos as compared to uninjected embryos (Branford and Yost, 2002; Cha et al., 2006). The Hamada lab demonstrated a genetic interaction between Nodal and Lefty by showing that a genetic reduction in Nodal levels ($Nodal^{LacZ/+}$), in a $Lefty^{-/-}$ background, partially suppressed the mesendoderm expansion phenotype (Meno et al., 1999). Furthermore, $Nodal^{LacZ/LacZ}$ embryos lacked Lefty expression, which importantly demonstrated that Nodal induced *Lefty* expression (Meno et al., 1999).

The mechanism by which Nodal is inhibited by Lefty is not fully elucidated. Originally, it was hypothesized that Lefty may interfere with Nodal binding to its type II Activin receptor as co-injection of Lefty with excess type II receptor rescued the phenotype induced by Lefty injection alone (Sakuma et al., 2002; Thisse and Thisse, 1999). It was also suggested that Lefty directly blocked Nodal from binding either the type II receptor or the EGF-CFC co-receptor since a direct Nodal-Lefty interaction can be detected by *in vitro* co-immunoprecipitation experiments (Chen and Shen, 2004). More recently, it was shown that Lefty most likely functions at the level of the co-receptor, EGF-CFC/Cripto/Oep. Studies in fish, frog, and cell culture showed that Lefty and Cripto were able to interact and that Lefty and Nodal might compete for Cripto (Chen and Shen, 2004; Cheng et al., 2004).

Another secreted factor identified to play a role in inhibiting Nodal signaling is Cerberus, identified from a dorsal library in *Xenopus* (Bouwmeester et al., 1996). Studies during gastrulation-staged embryos showed that *cerberus* is expressed within the organizer region, albeit in the deeper yolky cells (Bouwmeester et al., 1996). While *cerberus* is expressed in the organizer like other mesendoderm inducers, overexpression studies demonstrated that *cerberus* RNA injection induced the formation of anterior head and neural structures (i.e. brain tissue and cement glands) rather than mesendoderm (Bouwmeester et al., 1996). In a subsequent paper, the De Robertis lab demonstrated that *cerberus* encodes a multifunctional protein with two isoforms: a long form (Cer-L) and short form (Cer-S) (Piccolo et al., 1999). While Cer-L can inhibit Wnt, Nodal and BMP, the Cer-S isoform specifically inhibits Nodal signaling during mesendoderm induction (Agius et al., 2000). Cerberus-like proteins have also been identified in several vertebrate species are expressed during L-R asymmetric gene expression stages. Discovery of Caronte, a chicken Cerberus-like protein, prompted excitement after experiments from two independent labs demonstrated that it was induced by sonic hedgehog (Shh) at the node and expressed in the L LPM in a pattern that partially overlapped with *Nodal* expression (Rodríguez Esteban et al.; Yokouchi et al., 1999; Zhu et al., 1999). More importantly, however, it appeared that Caronte served as a repressor of BMP signaling, known to be active in the R LPM to repress *Nodal* expression (Rodríguez Esteban et al.; Yokouchi et al., 1999). Our lab and others have searched for *cerberus*-like transcripts in *Xenopus* and other model organisms and while orthologs do exist, they are expressed perinodally rather than in the L LPM and they do not antagonize BMP signaling. *Coco*, a *Xenopus* Cerberus-like protein, mouse *Cerberus-like 2* (*Cerl-2*) and zebrafish *Charon* are expressed in a perinodal pattern, with *Cerl-2* and *Charon* expressed more strongly on the right side (Lopes et al., 2010; Marques et al., 2004; Vonica and Brivanlou, 2007). Morpholinos targeted against c*oco*

and c*erl-2* gene inactivation demonstrated that function of this gene was required on the right side of the node to prevent R-sided activation of *Nodal* expression (Marques et al., 2004; Vonica and Brivanlou, 2007). More recently, it has been demonstrated that upregulation of R-sided expression of the perinodally expressed Cerberus-like genes might be influenced directly by nodal flow (Lopes et al., 2010; Oki et al., 2009; Schweickert et al., 2010).

Extracellular Matrix

Ligand interaction with extracellular matrix (ECM) has been shown to promote or restrict mobility for many secreted ligands, depending on the specific ligand examined as well as the developmental context. Specifically, several different proteoglycans have been shown to affect secreted ligand movement. In the mouse, it has been shown that sulfated glycosaminoglycans (sGAGs) are required for FGF8 signaling and gastrulation. The *lazy mesoderm* mouse mutant, deficient in an enzyme required for sGAG side-chain synthesis, prevented FGF signaling, which indicated that intact sGAGs promote FGF activity (García-García and Anderson, 2003). In *Drosophila,* the BMP-4 homolog decapentaplegic (Dpp) requires the glypicans Dally and Dally-like, both heparan sulfated proteoglycans (HSPGs), for long-range signaling during gradient formation (Belenkaya et al., 2004). In *Xenopus* sGAGs are required for BMP signaling but in a different capacity than in flies: sGAGs inhibit the movement and range of frog BMPs. A series of consecutive N-terminal basic residues present in BMP2/4, but not BMP7, interacted with HSPGs. Removal of these basic residues promoted aberrant long-range signaling by BMP2/4, indicating that interaction with HSPGs serves to limit the distance traveled by the ligands (Ohkawara et al., 2002). In differentiating skeletal muscle cells, TGFβ was shown to be sequestered by the ECM proteoglycans decorin, biglycan, and betaglycan (Droguett et al., 2006). Proteoglycan-mediated sequestration of TGFβ ligands formed a

steeper signaling gradient and limited the range over which TGFβ actively signaled (Droguett et al., 2006). Importantly, though, ligand sequestration is a reversible process: certain activating signals caused matrix metalloproteinases to cleave the proteoglycans tethering the TGFβ ligands and liberated them (Droguett et al., 2006).

For Nodal-related proteins, we understand far less about potential interactions with proteoglycans and the effect it might have on mesoderm induction or L-R asymmetric patterning. In late blastula/early gastrula embryos, HSPGs but not chrondroitin sulfated proteoglycans (CSPGs; likely not expressed then) were required for mesoderm induction by Activin, Wnt or FGF (Itoh and Sokol, 1994). It has also been shown that xyloside-mediated removal of sGAGs in frog embryos prevented asymmetric heart looping (Yost, 1990), indicating asymmetric expression of *Nodal* might also require sGAGs. The effects of sGAGs on asymmetric gene expression are unknown as these frog studies pre-dated the discovery of asymmetric *Nodal*. In more recent experiments, xyloside-treated mouse embryos lacked L LPM *Nodal* expression, though symmetric *Nodal* expression at the node was maintained (Oki et al., 2007). The mechanism by which sGAGs are utilized in a gastrula embryo might be very different from the requirement in tailbud stage embryos, as mature basement membranes have not yet formed in gastrulae.

MicroRNA modulation

Two independent research groups have demonstrated that Nodal and Lefty can be regulated by microRNAs (miRNAs). miRNAs are non-coding RNAs approximately 22 nucleotides in length that block translation of target mRNAs by binding to sites in the 3' UTR, thus enhancing target mRNA turnover. In zebrafish, Choi and colleagues (2007) demonstrated that the miR-430 family is required to both dampen and enhance *squint (sqt*; zebrafish Nodal ortholog) and *lefty2 (lft2)*, respectively. By utilizing target-protector

antisense morpholino oligonucleotides (TP-MOs), which bind 3' UTR miRNA target sites on mRNAs, the authors demonstrated that a TP-MO specific for *sqt* caused an expansion of the *gsc* expression domain and an increased specification of endodermal cells (Choi et al., 2007). Contrary to this, injection of a TP-MO specific for *lft2* caused a decreased number of endodermal cells, though *gsc* expression was unchanged (Choi et al., 2007). From these studies, the authors concluded that the miR-430 family represented a novel form of regulation of Nodal signaling levels: miR-430 dampened Nodal signaling by enhancing the degradation of *sqt* while simultaneously balancing Nodal signaling by repression of *lft2* (Choi et al., 2007). In this study, the authors did not examine whether or not these miRNAs were present or required during L-R asymmetry specification.

Current with the publication of the above paper, another lab demonstrated that the miR-15 family (miR-15 and miR-16) was a key modulator in establishing a dorsal-ventral gradient of *Nodal* expression in *Xenopus*. After establishing that these miRNAs targeted the type II receptor for Nodal (ActRIIA), the authors showed that overexpression of miR-15/16 affected ActRIIA protein, but not mRNA, levels (Martello et al., 2007). Overexpression experiments demonstrated that the miR-15 family antagonized the formation of Spemann's organizer and mature miRNA expression, but not pri-miRNA, as enhanced ventrally within the embryo. More importantly, however, the authors created a direct connection between an early dorsal asymmetry observed in nuclear β-Catenin and the enhancement of *Nodal* dorsally prior to gastrulation. Injection of *Xwnt-8* or *β-Catenin* inhibited the production of mature miR-15/16 in the absence of transcription, prior to mid-blastula transition. This led the authors to hypothesize that localized repression of miR-15/16 dorsally allows for the upregulation of *Nodal* and the subsequent formation of Spemann's organizer (Martello et al., 2007).

Generation of Left-Right Asymmetry

Although the anteroposterior (A/P) and dorsoventral (D/V) axes are patterned quite early, the point at which the L-R axis is formed is not well defined. Prior to L-R axis formation, embryos are bilaterally symmetric with respect to the midline. It is known, however, that establishment of this axis is absolutely necessary for the proper stereotypical asymmetric positioning, coiling and lobation of the internal organs. Asymmetric organ morphogenesis is necessary for efficient packing of the organs into a compact body plan as well as for the formation of a unidirectional circulatory system. Failure to establish proper asymmetric positioning of organs (situs solitus) can result in mirror image reversal of internal organ placement (situs inversus totalis) or randomization of organ placement (heterotaxia). Situs inversus is not associated with an increased risk for developmental defects whereas heterotaxia is correlated with severe congenital defects, especially within the heart and its associated vessels (Ramsdell, 2005). An estimated 1.44/10,000 cardiac defects in live births are associated with disruptions in L-R patterning events (Casey, 1998; Casey and Hackett, 2000). The following sections will describe the four steps required for breaking bilateral symmetry in the embryo.

1. Initial Symmetry Breaking Event

In the L-R patterning field, the point at which bilateral symmetry is first broken and whether this event is conserved across vertebrates, is highly controversial. Research from chicken, fish and frogs demonstrated that asymmetries are apparent early during cleavage stages. The Levin laboratory, which pioneered many of these experiments, has demonstrated that there are several very early asymmetries, which are predictors of later organ asymmetric organ morphogenesis. Global inhibition of gap

junctional communication with pharmacological agents in chicken and frog embryos demonstrated that inherent dorsoventral differences in gap junctional communication were required for proper organ situs in early cleavage stage embryos (Levin and Mercola, 1998; Levin and Mercola, 1999). Following this discovery, differences in H^+/K^+-ATPase and H^+-V-ATPase activity showed differential ion channel behavior across the future L-R axis, almost 24 hours before asymmetric gene expression occurs (Adams and Levin, 2006; Adams et al., 2006; Levin et al., 2002). Many of these early biases in asymmetry have also been found in fish and chicken embryos, but to date, none of these have been identified in mice.

In mouse, the first asymmetry observed occurs after gastrulation at the node, a transient structure formed at the posterior of the embryo during gastrulation. The ventral surface of nodal cells contain posteriorly-tilted monocilia that rotate counterclockwise, generating a net leftward flow of extraembryonic fluid (termed nodal flow) (Nonaka et al., 1998). Subsequently, it was determined that all vertebrates examined thus far contain motile nodal cilia that generate a net leftward flow (Essner et al., 2002; Fischer et al., 2002). Disruptions in nodal cilia formation, positioning or function alter L-R asymmetric gene expression. The mouse mutation *inv/inv*, for example, displays sluggish nodal flow and 100% of the mutants display reversed left-right asymmetry, which is attributed to reversed *Cerl2* expression at the node (Collignon et al., 1996; Lowe et al., 1996; Okada et al., 1999; Oki et al., 2009; Ryan et al., 1998; Yokoyama et al., 1993). In the *iv/iv* mouse, a spontaneous mutation in left-right dynein, nodal cilia are shorter and immotile, which abolishes nodal flow (Okada et al., 1999). These mice display randomized asymmetric gene expression and heterotaxic organ placement, indicating that nodal flow is important for specification of left versus right (Collignon et al., 1996; Hummel and Chapman, 1959; Lowe et al., 1996).

Although nodal flow is necessary for proper patterning of the L-R axis, it is not known how flow generates laterality information. Currently, there are two theories: 1. Transport of a "left-determining" morphogen(s), or 2. Mechanosensation by a second population of cilia. It is an attractive idea that nodal flow could transport some "factor" only to the left side, but there is little evidence to support this. Research from Tanaka et al. (2005) identified nodal vesicular parcels (NVPs) in the node vicinity, which potentially contained retinoic acid and sonic hedgehog. Leftward flow was proposed to deliver these packets of signaling molecules to the L side under the control of FGF signaling (Tanaka et al., 2005). There has been no follow-up on NVPs and it was not convincingly shown that the NVPs observed are genuine rather than artifacts of tissue processing.

A second model, termed the "two-cilia hypothesis", was developed after the discovery of a second, nonmotile cilia population at the node periphery (McGrath et al., 2003; Okada et al., 1999). It was thought that the nonmotile cilia might play a mechanosensory role by sensing nodal flow and transducing signals via intracellular calcium release to cause a L-sided symmetry-breaking response. Mathematical modeling, however, has been unable to demonstrate that the velocity of fluid flow generated across the node is sufficient to cause ciliary bending by mechanosensory cilia (Cartwright et al., 2004). This is further supported by mouse mutants that lack motile nodal cilia but display bilateral expression of asymmetric genes rather than absent expression, which would be predicted in the absence of flow.

Although nodal flow is a necessary step during vertebrate L-R patterning, it has yet to be determined if it represents the first symmetry breaking event in mouse. Mouse knockouts of gap junctional proteins implicated in frog and chicken L-R patterning do not have a phenotype, but this may be due to a functional redundancy among gap junctional proteins. More recently, it was shown that removal of mouse *Vangl1* and *Vangl2* (homologues of the *Drosophila* planar cell polarity gene, *Van Gogh*) prevented the

posterior positioning of cilia, which resulted in turbulent nodal flow (Song et al., 2010). It has long been suspected that planar cell polarity (PCP) may play a role in L-R asymmetry, and this paper is the first to demonstrate that PCP is necessary for proper ciliary positioning at the node. It is currently thought that these early asymmetries in frog, fish and chicken generate L-R biases, which subsequently amplified by nodal flow. It is quite uncertain, though, if an evolutionarily conserved mechanism for symmetry breaking exists across vertebrates.

2. Induction of *Nodal* at the node

Following leftward nodal flow, *Nodal* gene expression is induced at the node or homologous structure. In mouse, fish and frog, *Nodal* is expressed around the node (or node equivalent; Fig. 1.2) and in some species this expression is enriched on the left side (mouse) or restricted to the left (chicken) (Collignon et al., 1996; Fischer et al., 2002; Levin et al., 1995; Long et al., 2003; Lowe et al., 1996; Ohi and Wright, 2007). While the requirement for asymmetric *Nodal* in L-R asymmetry appears to be evolutionarily conserved beyond the vertebrate lineage, the initial steps to establishing L LPM expression of *Nodal* currently lack a universal mechanism for initiation. Recent work from the Tabin lab indicates that asymmetric *Nodal* in chickens may occur because of a leftward asymmetric movement of cells at the node, generating a L-enhanced expression domain, as the result of an increase in cell number rather than a side-specific upregulation of *Nodal* (Gros et al., 2009). Expression of *Nodal* at the node is absolutely required for L-R patterning; genetic removal of *Nodal* at the node prevents L LPM *Nodal* expression (Brennan et al., 2002) and results in heterotaxia.

3. Asymmetric transfer of L-R information from node to LPM

Following expression of *Nodal* at the node, asymmetric information is then transferred from the node to the L LPM (Figure 1.2). Several studies have sought to determine whether or not this signal transfer is direct or indirect: Is Nodal protein moving from node to the L LPM to directly initiate its own expression? Tanaka and colleagues (2007) demonstrated that GDF1, another closely related TGFβ ligand, may heterodimerize with Nodal during the period of signal transfer. While GDF1 alone is not an active ligand, its absence at the node causes L LPM absence of *Nodal* expression. Additionally, Nodal:GDF heterodimers increase Nodal activity and the distance it can travel. In a more recent study, mentioned in the ECM section of this introduction, the Hamada lab demonstrated that sGAGs—presumably around the perinodal region—are required for establishment of L LPM *Nodal*. Mouse embryos treated with xyloside, which prevents sGAG attachment to xylosylated proteins, express *Nodal* perinodally but fail to express *Nodal* in the L LPM (Oki et al., 2007). The authors suggested a model whereby sGAGs at the node were required for transfer of an asymmetric cue to initiate L LPM *Nodal* expression. As mentioned previously, studies predating the discovery of asymmetric *Nodal* showed that xyloside-treated frog embryos displayed situs defects, indicating that sGAGs may play a conserved role in the transfer of asymmetric information from the node to the L LPM (Yost, 1990). While both of these studies implicate sGAGs in Nodal signaling, neither study examines how Nodal ligand movement or its rate of transport is affected by sGAG removal. In my own research, I examined epitope-tagged Nodal during L-R patterning in control and xyloside-treated conditions and determined that sGAGs are required for transfer of the asymmetric cue from the node to the L LPM as well as for Nodal ligand localization and transport rate along the LPM.

After the asymmetric signal is transferred from the node to the L LPM, left-sided *Nodal* expression begins within the L LPM. Our lab and others have shown that there is a transient but dynamic shifting of the *Nodal* expression pattern from the posterior of the L LPM to the anterior LPM, before expression turns off (Lowe et al., 1996; Nakamura et al., 2006; Ohi and Wright, 2007; Wang and Yost, 2008; Yamamoto, 2003). *Lefty*, induced directly by Nodal, is also expressed in the L LPM and its expression pattern mirrors that of *Nodal*. L LPM Nodal also induces *Lefty* expression in the L anterior endoderm as well as symmetrically in the midline (Cheng et al., 2000). *Lefty* expression in the L LPM progressively moves anteriorwards, and via a negative feedback mechanism, extinguishes *Nodal* expression. In *Xenopus, Xnr1* and *Lefty* move along the A/P length of the L LPM in just under a 7-hour period, traveling over 500 μm, which is quite an impressive distance.

Immediately following asymmetric *Nodal*/*Lefty* expression, the downstream effector *Pitx2c*, a paired-type homeobox transcription factor, is induced in the L LPM by Nodal (Ryan et al., 1998; Yoshioka et al., 1998). Unlike the transient expression of *Nodal* or *Lefty*, *Pitx2c* expression is quite stable and is maintained by Nkx2.5 through stages of asymmetric organ morphogenesis (Shiratori et al., 2001) and remains restricted to the left side of the developing heart and gut.

Nodal, *Lefty* and *Pitx2c* represent a conserved L-sided gene expression cassette in vertebrates. Although RNA expression patterns have been examined during these stages, we still know very little about protein localization or parameters such as L LPM tissue architecture, which govern secreted ligand route or range during L-R patterning. Two theories, which are not mutually exclusive, have been proposed to explain the L-sided compartmentalization of Nodal (SELI) and spatiotemporal dynamics of Nodal/Lefty (reaction diffusion model) and they will be discussed in the following sections.

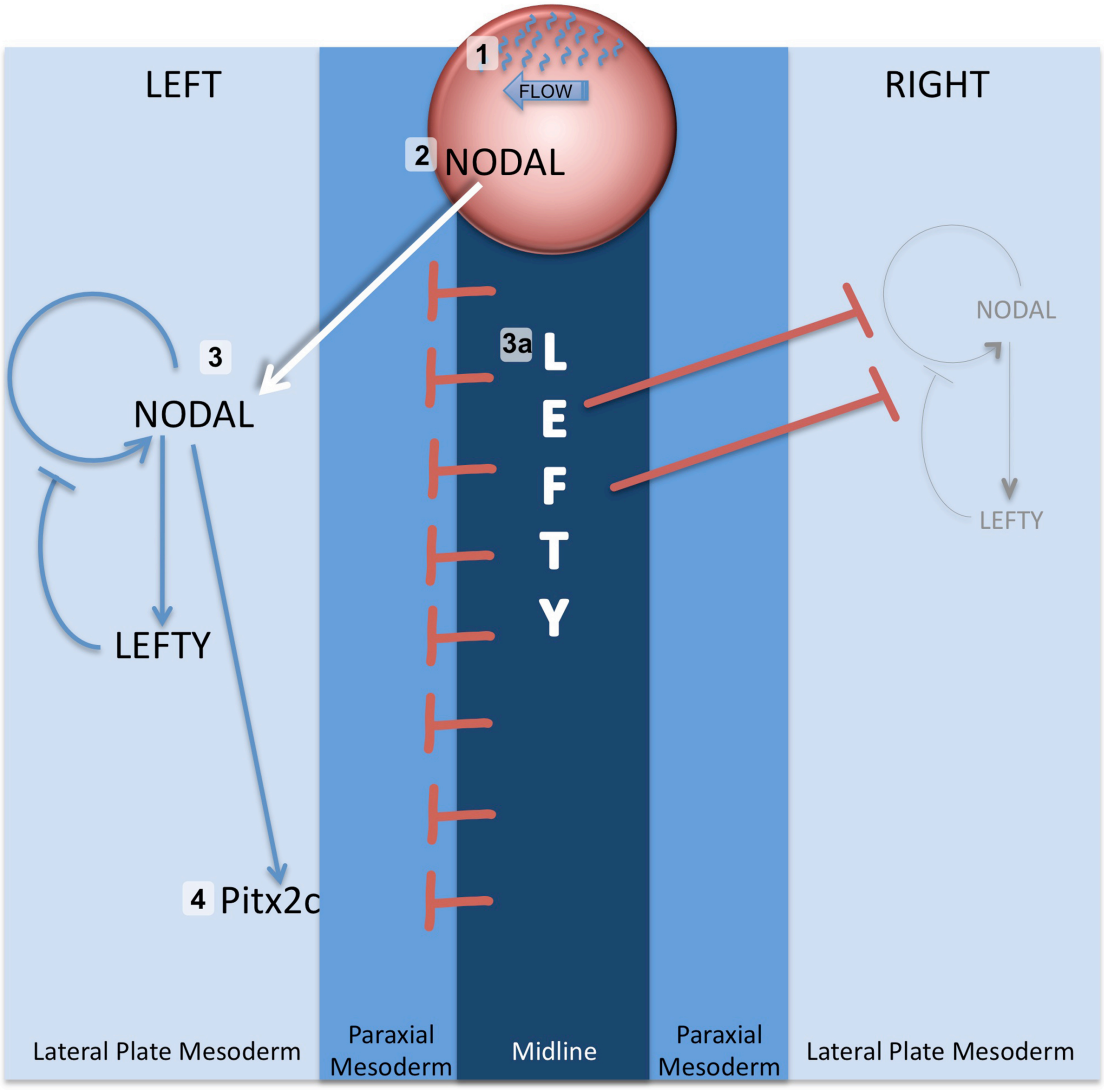

Figure 1.2 Generation of L-R asymmetry in vertebrates. Following gastrulation, cilia on the ventral node surface (**1**) rotate and generate a net leftward flow. *Nodal* expression is initiated within the node (**2**) and subsequently, asymmetric information is transferred to the L LPM (**3**) where *Nodal* expression begins posteriorly and induces the expression of its feedback inhibitor *Lefty*. Nodal also induces *Lefty* expression (**3a**) symmetrically within the midline, which must travel to the R LPM to suppress R-sided Nodal in a self-enhancement and lateral inhibition system (SELI). (**4**) Nodal expression then shifts dynamically from the posterior to the anterior within the L LPM and induces its downstream effector, Pitx2c.

3a. The Self-Enhancement and Lateral Inhibition Model

Though *Nodal* is only asymmetrically amplified on the L side, our lab and others have shown that expression is initially present on the R side, albeit at significantly lower levels. To explain why R-sided Nodal does not also undergo positive autoregulation, Nakamura and colleagues proposed that Nodal and Lefty utilize a Self-Enhancement and Lateral-Inhibition (SELI) system (2006; Tabin, 2006). The SELI model proposes that Nodal-mediated induction of Lefty in the L LPM and midline serves to prevent L-side-produced Nodal signals moving to the R side as well as to squelch any existing R-sided *Nodal*, such that it is unable to undergo positive autoregulation (Fig. 1.2, 3a). Suppression of R-sided Nodal by Lefty is essential for the compartmentalization of the L side from the R. Work from Yuki Ohi, a former graduate student, supports the SELI model: a R-LPM source of Xnr1 initiated R-sided *Xnr1* and suppressed endogenous L-sided *Xnr1* expression (Ohi and Wright, 2007). In this type of grafting experiment, contralateral communication occurs through rapid induction of *Lefty* in the R LPM and at the midline and Lefty protein subsequently suppresses endogenous L-sided *Xnr1* (Ohi and Wright, 2007). This study demonstrated two important features of L-R patterning: 1. The R-side is capable of becoming the L-side and 2. Contralateral communication occurs between the L and R side through induction of *Lefty*. My own experiments have furthered our understanding of this model by examining Lefty protein, provided from an exogenous L-sided source, and showed that Lefty is capable of traveling long-distance from the L LPM directly to the R LPM (see Chapter III).

3b. Nodal and Lefty: a reaction-diffusion relationship

Several different parameters are required to define the transient and dynamic nature of asymmetric *Nodal* expression. As mentioned above, *Xenopus Xnr1* expression shifts from the posterior of the embryo to the anterior in approximately 7 hours. During

this time period, the embryo is actively elongating in the A/P plane from 1.5 to 3 mm, with the LPM itself increasing in length by approx. 500 μm. In order to explain spatiotemporal control required to move Nodal/Lefty great distances in a short time, mathematicians devised an equation, named the reaction-diffusion model (Turing, 1990), to explain pattern formation by an activator/inhibitor pair within an embryo. The model predicts that the activator (Nodal) is induced first and can positively regulate its own expression and subsequently (after a delay) the activator also turns on its own inhibitor (Lefty). To restrict the influence and range of the activator, however, the inhibitor must travel faster than the activator, both to compensate for the lag time in induction as well as to "catch up" to the activator and suppress it. Further extensions of this mathematical model have been developed by Meinhardt and Gierer to include additional variables (2009). For example, protein stability should also play an integral role, with the inhibitor (Lefty) being more stable than the activator (Nodal). There have been a few attempts to study this hypothesis *in vivo*. Focal secretion of GFP-tagged mouse Nodal and Lefty in chickens demonstrated that Lefty2 could travel faster than Nodal in a given time period (Sakuma et al., 2002). As discussed in a previous section, these studies did not examine what tissue layers Nodal and Lefty were electroporated into, given that endogenous RNA expression is limited to the L LPM, nor did they examine what routes of travel Nodal/Lefty utilized. To address Nodal and Lefty transport characteristics, I added smaller epitope tags (Myc in lieu of GFP) and stringently tested the tagged constructs for function equivalent to untagged Nodal/Lefty. Then, utilizing an animal cap grafting system that allowed us to supply a source of Nodal or Lefty directly to the LPM, we measured the rate of movement from the LPM and the routes used by Nodal and Lefty.

3c. LPM as tissue facilitator of Nodal and Lefty signaling

Although asymmetric gene expression is limited to L LPM, very little information about this tissue or its architecture is defined in vertebrates. Scanning electron micrographs of chicken embryos showed that the LPM is bilayered and appears epithelialized, though this conclusion was made without definitive apical and basolateral markers (Meier, 1980). During organ morphogenesis stages in zebrafish, the LPM was shown to be a polarized epithelium (Horne-Badovinac et al., 2003) but the LPM was not characterized in earlier stages. Just as it is important to define the parameters inherent in Nodal and Lefty proteins that affect their transport dynamics, it is also necessary to characterize the tissue within which they are produced. Structural and architectural features (polarity state, ECM, number of cell layers) present in the LPM will directly affect the rates and routes of Nodal and Lefty transfer. Through a broad survey of cell shape, epithelial state, and ECM composition before, during and after *Nodal* expression, we have provided the first high-resolution, anterior-to-posterior cell biological description of the L and R LPM and demonstrated how sGAGs within the ECM flanking the LPM and midline structures are absolutely required for the proper localization and travel rates of Nodal.

4. Asymmetric Organ Morphogenesis

Despite the progress made in understanding the genetic control of laterality and L-R patterning, little is known about how asymmetric expression of *Nodal*, *Lefty* or *Pitx2* is translated into asymmetric morphogenetic movements of the viscera. Only asymmetric *Pitx2c* expression persists through stages of organ morphogenesis, which occurs almost 24 hours after asymmetric *Nodal*/*Lefty* expression. Absence of Pitx2 either by mouse knockout, morpholino-mediated knockdown or misexpression results in discordant situs of the heart and gut (Campione et al., 1999; Logan et al., 1998; Piedra

et al., 1998; Ryan et al., 1998; Yoshioka et al., 1998). Initial studies of the *Xenopus* gut tube from Chalmers and Slack (1998; 2000; 2000) have described in detail the stereotypical bending events that occur over a 3-day period, but these studies do not address the initial asymmetric events that lead to L-R differences in the gut. Studies from the Nascone-Yoder lab have also sought to better characterize asymmetric morphogenesis: late-stage fate mapping by DiI labeling at late tailbud stages showed that the L and R sides contribute equally to the gut tube (Muller et al., 2003). The first mechanistic link between Pitx2 and cell shape change resulted from cell culture experiments in which forced overexpression of Pit2a, a splice isoform of Pitx2c, in HeLa cells resulted in overt changes in the actin cytoskeleton (Wei and Adelstein, 2002). More recent attempts to understand gut looping have focused on effector genes downstream of Pitx2c. In chickens, it was noted that *Islet1* (*Isl1*) expression was enriched within the left dorsal mesentery that surrounded the midgut and this asymmetric expression event was followed by a L-sided asymmetric consdensation of cells, tilting the midgut leftward (Kurpios et al., 2008). Experiments from the Wallingford lab demonstrated that both Pitx1 and Pitx2 were able to directly induce Shroom-3, a known modulator of apical constriction in the neural tube, and that both Pitx1 and Shroom-3 were required for proper gut morphogenesis (Chung et al., 2010). A more detailed analysis of these studies is in the introduction section of Chapter IV.

In the studies presented in Chapter IV, I describe experiments in which we utilized confocal microscopy of cryosectioned embryos before, during and after asymmetric *Nodal* expression to analyze LPM cell shape and cytoarchitectural features to determine where and when the first asymmetries appear within the left versus right LPM. We observe more tightly bundled meshwork of F-actin within the cells of the R LPM versus the L LPM cells, which have a more diffuse actin network.

Aims of the Dissertation

To better understand how L-R asymmetric morphogenesis is established, I sought to define the extracellular (tissue structure/architecture, ECM) and ligand-autonomous features under which Nodal and Lefty are governed. To that end, I created functional epitope-tagged Nodal and Lefty that were properly cleaved and post-translationally modified. I found that the proteins travel very effectively in the dorsal-ward direction, to the extracellular matrix (ECM) surrounding the midline structures (periaxial ECM), as well as anterior-ward within the plane of the LPM. I also found that Lefty could move laterally, through the adjacent endoderm, to the R LPM. My detection of contralateral transfer of Lefty is the first direct evidence that L-side-derived Lefty, which represses the *Nodal* on the R side, is a significant influence in maintaining the unilateral L-side-specific expression of *Nodal* and this data lends further support to the SELI model. In chapter III, I discuss how these movement determinants (transport rates, routes, clearance) are the first set of observations on central parameters that have been proposed in several models as being linked to the dynamic patterns of asymmetric gene expression. I have shown that both Xnr1 and Lefty are capable of traveling remarkable distances (~15 cell diameters/hour, up to 700 microns over 7 hours), and that Lefty can travel faster and farther than Xnr1. The latter finding fits with the proposal that the Nodal-Lefty agonist/antagonist pair act in a reaction-diffusion relationship, which is important in many aspects of embryonic tissue patterning as proposed by Gierer-Meinhardt's models developed from the principles of Turing. Moreover, I have demonstrated that long distance transport of Nodal requires intact sGAGs. Pharmacological inhibition of sGAG assembly significantly diminishes the level of Xnr1 on ECM surfaces, and thus reduces the distance that it can travel. My findings also add a possible mechanism for the directional nature of expansion of the dynamic *Xnr1* expression wave, which shifts

rapidly in a posterior-to-anterior manner. Because there is a progressively higher level of chondroitin-sulfate proteoglycan (CSPG) found towards the more mature, anterior regions of the embryo, the affinity of Xnr1 for CSPG-enriched ECM could provide a forward bias to ligand movement, not only keeping its level above the threshold for maintenance of autoregulatory signaling, but pushing it more effectively in the anterior direction.

To address how the first gut bending events occur in *Xenopus*, I undertook an anterior-to-posterior characterization of cell shape, epithelial state, and cytoarchitectural features of the LPM after *Nodal* expression. From these studies, I have shown that there is an asymmetry in F-actin distribution, whereby the R LPM appears to have more tightly bundled actin filaments than the L LPM.

CHAPTER II

MATERIALS AND METHODS

Embryo Manipulations

Hormonally induced (600 units human chorionic gonadotropin/female) albino and/or wildtype *Xenopus laevis* embryos were collected and *in vitro* fertilized with isolated, homogenized testes preserved in high salt modified Barth's solution (Sive et al., 2000). Embryos were dejellied either 40 minutes after fertilization (for 1-cell stage injections) or after the first cleavage (90 minutes post-fertilization) by gently swirling embryos in 1% thioglycolic acid in 1x Steinberg's Solution, pH 6.0 (1xSS; pH 7.4: 58mM NaCl, 0.67mM KCl, 0.34mM $Ca(NO_3)_2$, 0.83mM $MgSO_4$, 4.6mM Tris) with the addition of 1M NaOH until all embryos were no longer attached (1-2 minutes). Embryos were subsequently cultured in 1xSS (for injections) or 0.1xSS (xyloside experiments) and staged according to Nieuwkoop and Faber (1967). After stage 8-9, all embryos were shifted into 0.1xSS.

Embryo Injections

Embryo microinjections (Narishige IM 200) were performed in 5% Ficoll (Sigma, cat. # F4375) in 1xSS, utilizing a fine mesh screen (0.75-1 mm pore size) to position embryos for injections. Blastomere size defined the injection volume used: 10 nL for one-cell stage, 2.5 nL/cell at 4-cell stage and 1 nL/cell at 32-64 cell stage. Injected embryos were kept in 5% Ficoll until stage 8 and then transferred into 0.1xSS. If embryos were injected with RNA at the one-cell stage for animal cap isolation/grafting, in vitro fertilization and injections were performed in the late afternoon and embryos

cultured in Ficoll at 12.5°C overnight. Embryos injected with plasmid DNA were typically injected in the morning and cultured at 23°C.

One-cell stage injections (RNA)

One-cell stage injections were primarily performed in albino embryos 40 minutes after fertilization and utilized 40-50 pg/nL membrane-bound GFP mRNA (mGFP) as a lineage tracer (gift from John Wallingford). mGFP/pCS2+ encodes eGFP with CAAX Ras membrane localization (Wallingford et al., 2000). Capped mRNAs for microinjection were synthesized using the SP6 mMessage mMachine kit (Ambion) from the following linearized plasmids (several of these plasmids were generated for the purposes of my studies; described further below): pCS2+Xnr1, 25 pg/nL (Jones et al., 1995); pCS2+Xlefty, 50 pg/nL (Cheng et al., 2000); pCS2+Xlefty$^{6MYC-CT}$, 50 pg/nL (Westmoreland et al., 2007); pCS2+Xlefty$^{6MYC-CS}$, 50 pg/nL; pCS2+Xnr1$^{6MYC-CS}$, 25pg/nL; pCS2+Xnr1$^{6MYC-CT}$, 25 pg/nL; pCS2+Xlefty^{GFP-CS}, 50 pg/nL; pCS2+Xnr1^{GFP-CS}, 25 pg/nL; pCS2+Xlefty$^{6MYC-CT/NGM}$, 50 pg/nL (Westmoreland et al., 2007); pCS2+Xnr1$^{6MYC-CS/NGM}$, 25 pg/nL.

8-cell stage injections (DNA)

Injections at the 8-cell stage were performed in wildtype embryos, such that differential dorsal/ventral pigmentation allowed for targeting the right or left four blastomeres with CsCl-purified plasmid and capped LacZ mRNA for lineage tracing. The following plasmids were used for injections (some of which were generated for my thesis work; described below): pCSKA-Xnr1, 80pg/embryo (Sampath et al., 1997); pCSKA-Xlefty, 150pg/embryo (Cheng et al., 2000); pCSKA-Xnr1$^{6MYC-CS}$, 80pg/embryo; pCSKA-Xlefty$^{6MYC-CT}$, 150pg/embryo; pCSKA-Xlefty$^{6MYC-CS}$, 150pg/embryo; pCSKA-Xnr1^{GFP-CS}, 80pg/embryo; pCSKA-Xlefty^{GFP-CS}, 150pg/embryo.

Microdissections and Tissue Transplantations

Microdissections were performed with a Gastromaster® microdissector utilizing 400 or 800 µm platinum square loop tips. All dissections and subsequent culturing were in 0.75x normal amphibian media (NAM; 110 mM NaCl, 2 mM KCl, 1 mM $Ca(NO_3)_2$, 1 mM $MgSO_4$, 0.1 mM EDTA, 1mM $NaHCO_3$, 2 mM sodium phosphate pH 7.4) on 1% agarose-coated Petri dishes (Sive et al., 2000).

Animal Cap Grafts

For animal cap (AC) transplants, albino donor embryos injected with RNA at the one-cell stage were cultured overnight at 12.5^{o}C until they reached stage 9-10. Vitelline membranes were removed with forceps and a 400 µm yellow Gastromaster® tip was used to cut a square animal cap, which was then trimmed of rough edges. Host embryos, isolated from the previous morning and cultured overnight at 18-19^{o}C, were de-membranated at stage 17. The squared corner of a 400 µm yellow Gastromaster® tip was used to remove a shallow pocket (of equal size to donor AC) of epidermis and underlying LPM in the midtrunk region of the embryo. The AC graft was then immediately placed into the newly cut pocket of the host embryo. Blunt forceps were used to put gentle pressure on the cap to help it heal into place. After the graft was secured into its pocket in the host embryo, embryos were turned over, grafted side facing down, to keep pressure on the graft while it healed in (~5 minutes).

For graft removal experiments, AC-engrafted embryos were cultured for 3 hours (Xlefty$^{6MYC-CT}$) or 4.5 hours (Xnr1$^{6MYC-CS}$; Xnr1$^{6MYC-CS/NGM}$), and mGFP-expressing grafts removed with forceps, with the aid of a fluorescent dissecting scope. The host was then immediately fixed in MEMFA (0.1 mM MOPS pH 7.2, 2 mM EGTA, 1 mM $MgSO_4$, 3.7%

formaldehyde) for time 0, or into 0.75x NAM for thirty (T30) or ninety (T90) minutes post-graft removal and then fixed.

LPM Grafts

When donor wildtype embryos were injected with plasmid DNA to target the left or right side at the 8-cell stage, they were cultured until stage 17 and de-membraned; unmanipulated hosts were also de-membraned at stage 17. A yellow 400 µm Gastromaster® tip was used to remove a midtrunk explant containing LPM and overlying epidermis, which was then placed into an equivalent pocket in a host embryo, created by using the corner of the 400 µm Gastromaster® yellow tip to remove host epidermis and LPM. Occasionally endoderm was also present on donor explants and residual endodermal cells were shaved away with the Gastromaster® tip prior to engraftment. Blunt forceps were used to gently push the graft into place. The embryo was then turned onto its grafted side and allowed to heal (~5 minutes).

Animal Cap Assays

Mesoderm Induction assays

One-cell stage embryos were injected with either untagged Xnr1 or Xnr1$^{GFP\text{-}CS}$ RNA. Embryos were de-membraned at 8.5/9 and ACs were cut using the Gastromaster® red 400 µm tip. ACs were cultured in 1x SS in 1% agarose-coated 6 well dishes until sibling-staged embryos reached stage 10.5, at which point ACs were flash frozen in a dry ice/ethanol slurry for radioactive RT-PCR analysis.

Protein secretion from Animal Caps or Animal Halves

One-cell stage embryos were injected in the late afternoon with 250 pg/10 nL Xnr1$^{6MYC-CS}$ or Xnr1$^{6MYC-CS/NGM}$ RNA and cultured overnight at 12.5°C in 5% Ficoll. At stage 9, embryos were demembranated and ACs cut with a Gastromaster ® yellow 400 µm tip. For Xnr1$^{6MYC-CS/NGM}$, animal halves, cut with a surgical knife along the animal-vegetal equator, were used in lieu of ACs. The following procedure was modified from Westmoreland et al. (2007): Ten ACs or animal halves were cultured in 30 µL of Calcium-Magnesium free media (CMFM; 88 mM NaCl, 1 mM KCl, 2.4 mM $NaHCO_3$, 7.5 mM Tris•HCl, pH 7.6, 0.1 mg/ml BSA) with or without 10 mM xyloside, in a 96 well dish. A total of 50 animal caps were used for each condition. After 2 and 4 hours (Xnr1$^{6MYC-CS}$, xyloside experiment) or 4.5 hours (Xnr1$^{6MYC-CS/NGM}$), 25 µL/well of supernatant was collected and analyzed by western blot analysis for Myc.

RT-PCR

RNA was isolated either from 3 whole embryos or 25-30 animal caps first by vortexing in 100 µL volume of TRIzol (Invitrogen, cat. # 15596-018) until smoothly mixed, at which point an additional 900 µL of TRIzol was added. After this, the manufacturer's protocol was followed. cDNA synthesis was performed with 1 µg of RNA, 1 µL Oligo(dT)$_{12-18}$, 1 µL of 10 mM (each) dNTP mix, and DEPC–treated water up to a volume of 12 µL, at which point the mixture was heated to 65^{o}C for five minutes and chilled on ice. The following reagents were then added: 4 µL 5x First Strand Buffer, 2 µL 0.1 M DTT, 1 µL RNAsin and 1 µL SuperScript II RT (Invitrogen, cat. # 18064-022). After a 1.5-hour incubation at 42^{o}C, the reaction volume was adjusted to 50 µL with DEPC-treated water. All reactions were run alongside a control reaction without reverse transcriptase. PCR reactions that analyzed mesoderm gene induction were set up as follows: 4 µL cDNA from above reaction, 0.75 units Taq polymerase (Fisher), 0.25 mM

(each) dNTP mix, 0.2 μM gene-specific primer mix, 2 μCi of [α-^{32}P]-dATP (GE Healthcare). PCR cycle program: 5 minute denaturation step at 95^{o}C, [1 minute at 94^{o}C, 1.5 minutes at 55^{o}C, and 1 minute at 72^{o}C]$^{\textbf{24-28 cycles}}$, final 5 minute extension at 72^{o}C. Cycle number and primer sequences can be found in Table 2.1.

TABLE 2.1 PCR Primer sequences and cycle numbers

Gene Name	Direction	Primer Sequence	Cycle Number
Goosecoid	Forward	ACAACTGGAAGCACTGGA	28*
	Reverse	TCTTATTCCAGAGGAACC	
Chordin	Forward	CCTCCAATCCAAGACTCCAGCAG	26*
	Reverse	GGAGGAGGAGGAGCTTTGGGACAAG	
Noggin	Forward	AGTTGCAGATGTGGCTCT	27*
	Reverse	AGTCCAAGAGTCTCAGCA	
Brachury	Forward	GGATCGTTATCACCTCTG	28*
	Reverse	GTGTAGTCTGTAGCAGCA	
ODC	Forward	GGAGCTGCAAGTTGGAGA	24*
	Reverse	TCAGTTGCCAGTGTGGTC	
Cardiac Muscle Actin	Forward	GCTGACAGAATGCAGAAG	28
	Reverse	TTGCTTGGAGGAGTGTGT	
MyoDa	Forward	AGGTCCAACTGCTCCGACGGCATGAA	31
	Reverse	AGGAGAGAATCCAGTTGATGGAAACA	
xMyf5	Forward	CTATTCAGAATGGAGATGGT	33
	Reverse	GTCTTGGAGACTCTCAATA	

*Denotes radioactive RT-PCR

β-Galactosidase activity staining

To detect LacZ in engrafted embryos analyzed by *in situ*, we used Red-Gal reagent (6-chloro-3-indolyl-β-D-galactoside; Research Organics cat. # 1364C). Embryos were MEMFA-fixed for one hour at room temperature, washed in 0.1% Triton X-100 in PBS (PBT) and stained for up to one hour in a Red-Gal (1X PBS, 5 mM $K_3Fe(CN)_6$, 5 mM $K_4Fe(CN)_6$, 2 mM $MgCl_2$, 1 mg/ml Red-Gal) reaction (Sive et al., 2000). Once a deep red color appeared, embryos were washed in 1x PBS, post-fixed in MEMFA for 1 hour and stored in 100% MeOH at -20^{o}C for *in situ* hybridization.

In situ hybridization analysis

In situ hybridizations were performed as described previously (Sive et al., 2000), with modifications previously published by our lab (Ohi, 2007; Ohi and Wright, 2007).

Frog Embryo Powder

Healthy pigmented or albino embryos (n=100) were collected between stages 25-30 and homogenized by vortexing vigorously in 400 µl 1x PBS in a 2 mL eppendorf tube, after which 1.5 mL cold acetone (stored at -20^{o}C) is added. The mixture is vortexed again and chilled on ice for thirty minutes and spun at 10,000 rpm for 10 minutes. The supernatant is removed, the pellet washed with 1 mL cold acetone and re-spun for 5 minutes. The supernatant is then discarded and the pellet is allowed to dry at room temperature for 30 minutes to one hour. The pellet is crushed to a fine powder with a motorized pestle and stored at -20^{o}C.

Pre-cleaning Antibodies with Embryo Powder

To pre-clean antibodies with higher background levels, a dash of embryo powder was put into a 1.5 mL Eppendorf and heat inactivated for 1 hour at 65^{o}C in either 1x PBS (for immunofluorescence) or maleic acid buffer (MAB; for *in situ* hybridization). After incubation, the tubes were spun for 5 minutes at 10,000 rpm and supernatant removed. Half of the total volume of blocking reagent (AB Block for immunofluorescence [described below]; 2%BMB/20% Lamb Serum in MAB for *in situ* hybridization) required for antibody dilution is then added to the embryo powder pellet, along with the appropriate dilution of primary antibody (for the final concentration). The embryo powder/antibody/block mixture was placed on a nutator at 4^{o} for at least 2 hours and spun at 15,000 rpm for 5 minutes. The supernatant was put into a new tube and the remaining volume of blocking reagent added to make the final dilution for the antibody being used.

Cryosectioning

Embryos were processed for immunofluorescence as described in Kucenas et al. (2008) with modifications. Embryos were embedded in microwave-heated 3% bacto agar/5% sucrose in plastic peel-away molds (Polysciences; cat. # 18985), trimmed to small squares with a notch in one corner, which denotes the proper block orientation for cryosectioning, sunk in glass vials of 30% sucrose overnight at 4^{o} and frozen on super chilled 2-Methylbutane in stainless steel beaker by immersion in liquid nitrogen. To survey embryos from anterior-to-posterior (A-to-P), 14μm transverse or longitudinal sections were collected using a Leica cryostat 1800 microtome (chamber temperature: -24^{o}, arm temperature: -18^{o}, angle of base: 3-4) and every 8th section analyzed, which allowed for a broad A-to-P analysis of the entire LPM from an embryo.

Immunofluorescence on Cryosections

Cryosections were rehydrated in 1x PBS and blocked with AB Block (2% Normal Donkey Serum, 2% BSA in 1x PBS) and sections incubated with primary antibody diluted in AB block overnight at 4^{o}. For primary antibodies used, see Table 2.2.

Sections were washed extensively with PBS after primary antibody incubation, secondary antibody added for 2 hours at room temperature, after which slides were washed continuously for 30 minutes and mounted. Secondary antibodies (1/200; Jackson Immuno) were either donkey-α-mouse or donkey-α-rabbit conjugated to Cy2, Cy3 or Cy5 fluorophores. Where applicable, sections were incubated with Alexa488-conjugated Phalloidin and washed extensively before mounting. Sections were mounted in Prolong Gold Antifade + DAPI (Invitrogen; cat # P36931).

Images were obtained using an Olympus Fluoview FV-1000 laser scanning confocal microscope with Olympus Fluoview Software. To avoid over-processing of images where tagged protein was deliberately supplied in a limited amount, images were not post-processed after confocal acquisition; therefore, immunofluorescence data is best viewed at high-resolution on a computer monitor rather than after printing. Where indicated, signal intensity was analyzed in ImageJ (version 1.43g, National Institutes of Health) line-scan tool. Comparisons of 3-pixel line-scans through LPM or dorsal periaxial regions from each analyzed section, from embryos receiving epitope-tagged grafts, were made against a background average determined from at least ten identically processed embryos with untagged Nodal or Lefty grafts. Genuine Myc signal was thresholded at more than three standard deviations above the background average. In some cases, signal was lower with little background, and signal/background was then defined by averaging ten 3-pixel line-scans taken from the same section's background areas, with 'real signal' again thresholded at 3 standard deviations above this level.

Table 2.2 Primary antibodies used for immunofluorescence and western blotting

Antibody	Source	Dilution Factor	
		Immunofluorescence	Western Blot
ZO1	Zymed, cat. # 33-9100	1/500	--
aPKC	Santa Cruz, cat. # C20 SC-216	1/200 *	--
E-Cadherin	BD Biosciences, cat. # 610182	1/500	--
β1-Integrin	D.S.H.B., cat. # 8C8	1/200	--
β-Catenin (gift, Pierre McCrea, M.D. Anderson Cancer Center)	(McCrea et al., 1993)	1/500	--
Fibronectin (4H2) (gift, Douglas DeSimone, University of Virginia)	(Ramos and DeSimone, 1996)	1/1000	--
Laminin	Abcam, cat. # ab11575	1/500	--
HSPG	Seikagaku, cat. # 370255	1/100	--
CSPG	Sigma, cat. # C8035	1/250	--
Myc (9E10) mouse monoclonal	Vanderbilt Monoclonal Antibody Core, cat. # VU0003	1/400 *	1/1000
Myc tag (A7) mouse monoclonal	Abcam, cat. # ab18185	1/100 *	1/1000
Myc tag rabbit polyclonal	Upstate/Millipore, cat. # 06-549	1/400 *	1/1000
c-Myc (A-14) rabbit polyclonal	Santa Cruz, cat. # sc-789	1/400 *	--
Alexa488-conjugated Phalloidin	Invitrogen, cat. # A12379	1/100	--
GFP	Clontech, cat. # 632460	1/100	1/1000

For immunofluorescence, slides were incubated with primary antibody overnight at 4°C. All Myc antibodies were pre-cleaned with embryo powder to avoid excess nuclear background.
(*) Signifies use of Neutravidin/Biotin amplification step for immunofluorescent detection.

Immunofluorescence Signal Amplification

Weak immunofluorescence signals were amplified using a Neutravidin-Biotin amplification system. Briefly, after slides were incubated with primary antibody (e.g. Myc), they were washed for one hour with PBS. Slides were then blocked with 0.1 mg/ml Neutravidin (Thermo Scientific; cat. # 31000) in wash buffer (TBS [25 mM Tris, 150 mM NaCl, pH7.2], 1% BSA) for 15 minutes, washed once with PBS and blocked with 0.5 mg/ml Biotin (Sigma) in wash buffer, followed by another PBS wash. Biotinylated-α-mouse antibody (1/1000; Vector Labs; cat. # BA-9200) in PBS was added to slides for 1.25 hours at room temperature. Slides were subsequently washed for 45 minutes with PBS, at which point 1/200 Neutravidin-DyLight-549-conjugated secondary antibody (Thermo Scientific; cat. # 22837) was added for two hours, covered at room temperature. Slides were then washed for one hour with PBS and mounted as described above.

Immunoprecipitation & Western Blots

Whole embryos, LPM explants or animal caps injected or engrafted with Xlefty$^{6MYC-CT}$ or Xnr1$^{6MYC-CS}$, Xnr1$^{6MYC-CS/NGM}$ ACs were collected and immediately frozen in minimal media at -80°C. Embryos were then homogenized (30 µL/embryo or cap) in RIPA Buffer (50 mM Tris•HCl pH7.4, 1% NP-40, 0.25% Sodium Deoxycholate, 150 mM NaCl, 1 mM EDTA) + 1% SDS to aid in solublization of ECM-associated proteins (Dzamba et al., 2009; Westmoreland et al., 2007). After a fifteen minute incubation on ice, samples were spun at 14,000 rpm for five minutes at 4°C, after which the soluble protein fraction was transferred to a new tube and spun once more under the previous conditions. Lysate (300 µL) containing tagged protein was added to 10 µL C-Myc-conjugated agarose bead slurry (bead slurry was pre-washed 3x in 500 µL TBS; Pierce, cat. # 23620) and spun end over end at 4°C overnight in a Pierce Handee^{TM} Spin

Column (cat. # 69705). Lysate/bead mixtures were then washed three times with 500 µL 0.05% Tween in TBS (1x; 25 mM Tris•HCl, 0.15 M NaCl; pH 7.2) followed by a ten second pulse centrifuge. Myc-tagged protein was eluted from the columns with 25 µL 2x non-reducing sample buffer (0.3 M Tris•HCl, pH6.8, 5% SDS, 50% glycerol, lane marker tracking dye; cat #23620), heated to 100°C for five minutes and pulse centrifuged for ten seconds. Following elution, 2 µL 2-mercaptoethanol was added to each sample. Samples were run on precast 4-12% Bis-Tris NuPAGE SDS-PAGE gels (Invitrogen; cat # NP0301Box) in NuPAGE MES SDS running buffer (Invitrogen; cat. # NP0002-02) at 180 volts. Proteins were transferred onto Immobilon-P PVDF (Millipore; cat. # IPVH00010) at 36 volts for 2 hours in transfer buffer (Invitrogen; cat. # NP0006) in 20% MeOH. Blots were blocked for 2 hours in 5% nonfat dry milk (Kroger) in 1x TBS•Tw (100 mM Tris•HCl, pH7.6, 150 mM NaCl, 0.1% Tween-20). Primary antibody (Millipore rabbit αMyc) was diluted 1/1000 in blocking solution and blots incubated overnight at 4°C. Membranes were washed 4 times (20 minutes per wash) in TBS•Tw at room temperature. Secondary antibody (goat α rabbit IgG-HRP; Santa Cruz cat# sc-2004) was diluted 1/2000 in block and membranes were incubated in secondary for 1 hour. Membranes were then washed in TBS•Tw 4 times for 20 minutes each. SuperSignal® West Femto Maximum sensitivity substrate (1 mL; Pierce, cat. # 34095) was added to membranes for 2 minutes to detect HRP by chemiluminescence. If a result was needed rapidly, blots were incubated in rabbit-α-Myc primary antibody for 6 hours at room temperature in lieu of an overnight incubation at 4^{o}C and all subsequent steps performed as stated above.

Western blots on conditioned medium

Western blots on conditioned medium did not require Myc immunoprecipitation and were performed as previously published (Westmoreland et al., 2007). 5 µL of 5x

non-reducing sample buffer (Pierce, cat. # 23620) and 2 µL β-mercaptoethanol were combined with lysate (7 AC or 2.5 animal half equivalents), boiled for five minutes and loaded on a precast 4-12% Bis-Tris NuPAGE SDS-PAGE gel as described above.

Enzymatic Removal of N-Linked Glycans with PNGaseF

PNGaseF treatment (New England Biolabs, cat. # P0704S) was performed according to manufacturer protocol on whole embryo lysates following Myc immunoprecipitation or on conditioned medium prior to gel electrophoresis with the following modifications: PNGaseF was diluted 1:4 in buffer (50 mM NaCl, 20 mM Tris, pH 7.5, 5 mM EDTA, 50% Glycerol). A 10 or 20 µL reaction (2 whole embryo equivalents, 3 animal cap equivalents or 7 conditioned medium animal cap equivalents) including 1x glycoprotein denaturation buffer (0.5% SDS and 2% β-mercaptoethanol) was denatured at 100°C for ten minutes. After cooling to room temperature, the reaction volume was doubled by adding 10x G7 reaction buffer (1x final concentration; 0.5 M sodium phosphate, pH 7.5), 10% NP40 (1% final concentration), 1 µL of 1:4 PNGaseF, and water. Reactions were incubated at 37°C for one hour, mixed with sample buffer and analyzed by western blotting.

Colloidal Blue Staining of Gels

Pre-cast 4-12% NuPage® Novex Bis-Tris gels were loaded with protein and run as described above. Colloidal Blue staining (Invitrogen, cat. # LC6025) was performed according to manufacturer specifications. Briefly, gel was removed from plastic casing (wells and foot of gel removed), fixed with gentle shaking for ten minutes in Fixing solution (20 mL deionized water, 25 mL Methanol, 5 mL Glacial Acetic Acid), then transferred into Staining Solution A (27.5 mL deionized water, 10 mL Methanol, 10 mL Stainer A) for ten minutes with gentle agitation. After ten minutes, 2.5 mL Stainer B

solution was added directly to the Stainer A solution; the gel was gently agitated overnight at room temperature. Gels were destained in deionized water for several hours before imaging.

Generation of Injection Constructs

Xlefty$^{6MYC-CT}$

Xlefty$^{6MYC-CT}$ (stock 1387; also called Xlefty^{myc}; 6xMyc at C-terminus) was generated in pCS2+MT (stock 669; gift from David Turner; University of Michigan) as previously published (Westmoreland et al., 2007). The *coding region for Xlefty^{MYC-CT}* was PCR-amplified with the following primers to add a *Hind*III site at each end: 5'_leftymyc_2- GCGGAAGCTTCAGA*ATGGGTGTCACTACCAAATCT*; 3'_leftymyc_2- GCCGAAGCTTCGCG*TCACTATAGTTCTAGAGGCTCGAG*. The resulting PCR product was digested with *Hind*III and sub-cloned into pCSKA (stock 868) that had been digested with *Hind*III.

Xnr1$^{6MYC-CT}$

Xnr1$^{6MYC-CT}$, Xnr1 with a C-terminal 6xMyc epitope tag, was created by PCR amplification of the *Xnr1 coding region* in pCS2+Xnr1 (stock 831) with the following primers, which added *Hind*III and ***Cla*I** sites on either end of the coding region: Xnr1-5'- ClaI_H3- AT<u>AAGCTT</u>**ATCGAT**AAGC*ATGGCATTTCTGACAGCAGTCCTG*; Xnr1-3'- Cla1_H3- C<u>TAAGCTT</u>**ATCGAT**TG*CCACCACTGCACCCACATTCCTCTACAAT*. The PCR product was digested with *Cla*I and subcloned into pCS2+MT digested with *Cla*I. Xnr1$^{6myc-CT}$ from pCS2+MT was digested with *Cla*I and subcloned into pCSKA digested with *Cla*I. Neither of these constructs was functional when tested in grafting assays for induction of R-sided *Xnr1* expression in embryos.

Xnr1$^{6MYC\text{-}CS}$

Xnr1$^{6MYC\text{-}CS}$ was created to insert a 6xMyc epitope tag four amino acids downstream of the cleavage site, after we determined that a C-terminal 6xMyc epitope tag interfered with Xnr1 function. An *Asc*I site along with **3 Glycine** residues was introduced 4 amino acids downstream of the cleavage site in pCSKA-*Xnr1* (stock 873) and pCS2+*Xnr1* (stock 831) by PCR site-directed mutagenesis with the following primers: Xnr1_AscI_5'-
*AGGAACAGGAATGAA***GGA**GGCGCGCCA**GGAGGA***AACCATCACTTATCA*; Xnr1-AscI-3'- *TGATAAGTGATGGTT***TCC**TCCTGGCGCGCC**TCCTTC***ATTCCTGTTCCT*. Following the insertion of an *Asc*I site into Xnr1, the 6xMyc epitope tag was PCR amplified out of pCS2+MT with the addition of an *Asc*I site on each side with the following primers: 5'-Myc-AscI-
*TCCCATCGATTTAAAGCT*GGGCGCGCC*AATGGAGCAAAAG*; 3'-Myc-AscI-
GAT*T*GGCGCGCC*TTCTAGAGGCTCGAGAGGCCTTGA*

Xlefty$^{AscI\text{-}CS}$

In anticipation of inserting epitope tags 4 amino acids downstream of the cleavage site for Xlefty, site-directed mutagenesis was used to insert an *Asc*I site (flanked by **Glycines**) into pCSKA-Xlefty (stock 1035) and pCS2+Xlefty (stock 1031) with the following primers: Lefty-AscI-5'-
CGACCTGTCAACAAT**GGA**GGCGCGCCA**GGAGGA**GCCAGAGTTAGTGTG; Lefty-AscI-3'- CACACTAACTCTGGCT**CCTCCT**GGCGCGCC**TCC**ATTGTTGACAGGTCG.

Xlefty$^{GFP\text{-}CS}$ *and Xnr1*$^{GFP\text{-}CS}$

The *eGFP coding region*, without a stop codon, was PCR amplified from the Clontech pEGFP-1 plasmid (gift from the Joshua Gamse lab) with the following primers, which also add an *Asc*I site on either side of GFP: GFP-5'-AAGTACGGCGCGCC*AGGCATGGTGAGCAAGGGCGAGGAG*; GFP-3'-GATTGGCGCGCC*GCCCTTGTACAGCTCGTCCATGCC*. eGFP was digested with *Asc*I and inserted into pCS2+Xlefty, pCS2+Xnr1, pCSKA+Xlefty (stock 1035), pCSKA+Xnr1 plasmids (all had *Asc*I site inserted 4 amino acids downstream of the cleavage site by site directed mutagenesis), which had been digested with *Asc*I. It was determined that none of these constructs were functional, either by gene expression analysis, mesoderm induction assays, semi-quantitative radioactive RT-PCR and immunohistochemistry.

Xlefty$^{6MYC\text{-}CT/NGM}$

Xlefty$^{6MYC\text{-}CT/NGM}$ (stock 1386; also called Xlefty^{NGMmyc}; at C-terminus) was generated in pCS2+MT (stock 669; gift from David Turner; University of Michigan) as previously published (Westmoreland et al., 2007).

Xnr1$^{6MYC\text{-}CS/NGM}$

Xnr1$^{6MYC\text{-}CS/NGM}$ was generated using site-directed mutagenesis to mutate the "NET"-glycosylation site to "***A***ET" in pCS2+Xnr1$^{6myc\text{-}CS}$ (construct generation described above). Xnr1 NGM 5': GCTTGTCCAATTCCACTA***GCT***GAGACCTTCAAACCAACA; Xnr1 NGM 3': TGTTGGTTTGAAGGTCTC***AGC***TAGTGGAATTGGACAAGC.

Xyloside Treatments

Dejellied two-cell stage embryos were placed into either 0.5% DMSO (control) in 0.1x SS or 5 mM *p*-nitrophenyl-β-D-xylopyranoside (xyloside; Sigma cat. # N2132) in

0.5% DMSO/0.1x SS through stage 15/16, when vitelline envelopes were removed. Embryos were then switched into 10 mM xyloside with 1% DMSO in 0.1x SS or 1% DMSO in 0.1x SS. At stage 17, embryos were engrafted with Xnr1$^{6MYC-CS}$ + mGFP-expressing ACs in 0.75x NAM ± 1mM xyloside and placed back into 10 mM xyloside/1% DMSO in 0.1x SS or 1% DMSO in 0.1xSS after the graft was healed into the host for 5 hours, fixed (MEMFA) and cryosectioned for analysis of Myc (described above).

Microarray Profiling of Left and Right LPM

Stage 23-25 left and right LPMs were isolated from embryos, anesthetized with 25 drops MS222 into 25 mL 0.1xSS, using a Gastromaster® red 400 tips. The left and right LPM pieces were taken closer to the ventral side, to avoid contamination of muscle (paraxial) tissue, which was previously shown to introduce an artificial asymmetric bias (Cha, 2006). 20 LPMs for each side were isolated and frozen on a dry ice and ethanol bath and RNA was extracted (described above). To confirm lack of muscle contamination, cDNA was generated from RNA and RT-PCR performed with primers for cardiac muscle actin, MyoD, and xMyf5 (Table 1.1). Once lack of contamination was confirmed, RNA from isolated LPMs was sent to the Vanderbilt University microarray core for quantification and quality control (QA/QC) analysis. Once the RNA passed quality control inspection, it was submitted for hybridization to a *Xenopus* Affymetrix™ Microarray.

CHAPTER III

RAPID DIFFERENTIAL TRANSPORT OF NODAL AND LEFTY ON SULFATED PROTEOGLYCAN-RICH EXTRACELLULAR MATRIX REGULATES L-R ASYMMETRY IN *XENOPUS*

Introduction

Nodal signaling at post-gastrulation stages is the primary conserved regulator of the asymmetric left-right (L-R) patterning of the body axis. This process provides the foundation for the large-scale and integrated morphogenetic movements that place the organ anlagen asymmetrically, determine their L-R structural differences, and ensure the formation of a stereotypic, unidirectional cardiovascular system (Massagué, 1998; Schier, 2003; Wright, 2001). The pathway defining the L versus R side of the vertebrate embryo involves the expression of *Nodal (Xnr1* in *Xenopus*; provisionally renamed *Nodal1,* (Bowes et al., 2010)) at the node or an equivalent 'L-R coordinator' structure (Ramsdell and Yost, 1998), including a transient asymmetric expression in this structure in some species. Signals passed from the node lead to the conserved unilateral L-sided expression of *Nodal/Xnr1* within the L lateral plate mesoderm (LPM), and its downstream target genes: the feedback antagonist gene *Lefty*, and the effector transcription factor gene *Pitx2*.

Disruptions in the dynamics of asymmetric *Nodal/Xnr1* expression have been proposed causative in congenital defects of organ placement and structure (Casey, 1998; Casey and Hackett, 2000; Ramsdell, 2005). In current models for L-R patterning (Raya and Belmonte, 2006; Tabin, 2006), cross-regulatory positive-negative feedback between Nodal and Lefty causes the asymmetric amplification of initially small L-R differences in Nodal signaling intensity, leading to an essentially binary readout with L-

sided expression and R-sided absence of *Nodal* and its effector *Pitx2*. In these models, preventing R-sided *Nodal* expression includes an active suppression effect described below.

The L LPM expression pattern of *Nodal* is dynamic and transient. In *Xenopus*, it shifts rapidly and over a large distance from posterior-to-anterior (P-to-A) and is then shut down, with tissue morphogenesis (e.g., gut bending, cardiac looping) only occurring substantially later. *Xnr1* autoinduction is a major contributor to the forward shifting of the L LPM expression domain, while induction of its feedback antagonist Lefty may limit the duration and range of influence of *Nodal* expression (Lowe et al., 1996; Nakamura et al., 2006; Ohi and Wright, 2007; Wang and Yost, 2008; Yamamoto et al., 2003). A self-enhancement and lateral inhibition (SELI) model (Nakamura et al., 2006) has been proposed to explain L-R compartmentalization via *Nodal* regulation. SELI invokes a plausible long-range contralateral communication process for establishing and maintaining distinct L (*Nodal*-on) and R (*Nodal*-off) compartments, to enable later embryo-wide integrated morphogenesis. An orthogonal movement of Nodal from the L LPM leads to axial midline expression of *Lefty*. Transfer of Lefty to the R LPM, from both L LPM and axial midline, is proposed as a suppressive, conditioning influence on the contralateral R LPM, blocking the autoregulatory *Nodal* loop (Nakamura et al., 2006; Yamamoto et al., 2003). It has not been determined that Lefty can in fact move to the R side directly from the L LPM, or if the secondary *Lefty* expression zone in the axial midline tissue is more influential. In addition, the degree to which the rapid P-to-A shift of *Xnr1* expression, occurring over about 7 hours, could be explained solely by *Nodal/Xnr1* autoactivation requires investigation of the parameters affecting the ipsilateral range and speed of movement of Nodal and Lefty along the L LPM. The full forward shift of the *Xnr1/Nodal* expression domain is required for anterior structures such as the heart primordium to receive this asymmetric patterning signal.

The cell biological and tissue structural features that facilitate or limit Nodal and Lefty ligand movement at the time of L-R asymmetric gene expression should be central determinants of the level and duration of Nodal signaling over the embryo. A future goal is to deduce how broad or more focal regions of tissue experience and act upon the dynamic Nodal signaling activity map. Ligand movement and longevity considerations mean that the extent of Nodal signaling could be badly misjudged when based solely upon RNA expression patterns. Detecting the mature Nodal ligand and characterizing its biochemical behavior would help fill such gaps, hopefully making connections with the tissue patterns of downstream signal transducers (e.g., the canonical nuclear localization of phospho-Smad2) and target genes, and to the locations where asymmetric morphogenesis is initiated.

Studies examining Nodal movement have been hindered by the lack of suitable antibodies, with signal-to-noise being the central problem for ligands operating at low levels *in vivo*. A general strategy has been to detect overexpressed epitope-tagged variants, or to infer which cells undergo active signaling through phospho-Smad2 or target gene activation patterns (Williams et al., 2004). Experiments in blastula-gastrula stage embryos and tissue explants have suggested that Nodal and Lefty can travel several cell diameters from a production source (Williams et al., 2004), but with sometimes-variable findings. Xnr2 was initially classified as a short-range molecule (Jones et al., 1996) but later as long-range (Williams et al., 2004). The reasons remain obscure, but variations in the tags used or analytical methods possibly lead to different apparent mobilities. With respect to the SELI mechanism, it would be useful to know more about the movement and perdurance of Nodal and Lefty in tailbud stage embryos. The rapidity of tissue maturation during embryogenesis makes it dangerous to assume that such properties are similar in blastula and tailbud stages. In addition, specific aspects of ligand movement in the tailbud/somitogenesis stage embryo, such as through

spaces between tissues or along extracellular surfaces, might allow conduit-like, rapid travel to sites far from their source.

Here, we define the LPM tissue architecture in *Xenopus* embryos before and during asymmetric gene expression, finding that it is an unpolarized pseudo-epithelial tissue over the period of maximal *Xnr1* and *Lefty* expression. We describe results with functional epitope-tagged proteins, supplied in limited quantities from grafts, which support the differential speed of Xnr1 and Lefty movement, and a role for ECM in aiding their extremely long-range transport. We discuss the possible significance of these features in constraining *Xnr1* expression to the L LPM, while concurrently promoting the dynamic, rapid P-to-A shifting of the L-sided *Xnr1* expression domain as a determinant of asymmetric morphogenesis.

Results

Structure of left and right LPM and ECM composition during tailbud stages.

While LPM has been characterized histologically in several organisms at older stages (Deimling and Drysdale, 2009; Horne-Badovinac et al., 2003; Meier, 1979; Pohl et al., 2005), its layering and epithelial state is poorly understood during the stages of L-R gene expression and leading up to asymmetric morphogenesis. To begin to address how tissue architecture or ECM composition affect unilateral *Xnr1* expression, we analyzed LPM before, during and after *Xnr1/Lefty* expression.

We extensively surveyed cell adhesion and ECM proteins within the L and R LPM from early tailbud to early tadpole stages. We utilized β-catenin, a basolateral marker in polarized epithelia that generically detects cell borders in nonpolarized cells. From stage 17, the cell-surface β-catenin signal showed the LPM beginning to organize into two cell layers with future apical surfaces juxtaposed (Fig. 3.1A,B; Fig. 3.2). Similar results were obtained with β1-Integrin, E-cadherin and α5-Integrin (data not shown), markers that become basolateral when epithelia become polarized. The ECM component fibronectin flanked the somatic and splanchnic L and R LPM (Fig. 3.1A,B; Fig. 3.2). Beginning at stage 23, the splanchnic layer in both the L and R LPM began to appear more columnar (Fig. 3.1C). At the stages examined here, all before the physical separation of splanchnic/somatic layers and coelom opening, these differences were more prominent towards anterior regions, likely attributable to the progressive A-to-P maturation of the embryo's mesodermal layer (Slack and Tannahill, 1992). Splanchnic-somatic cell shape differences were maintained through stage 34, the oldest stage examined (Fig. 3.2).

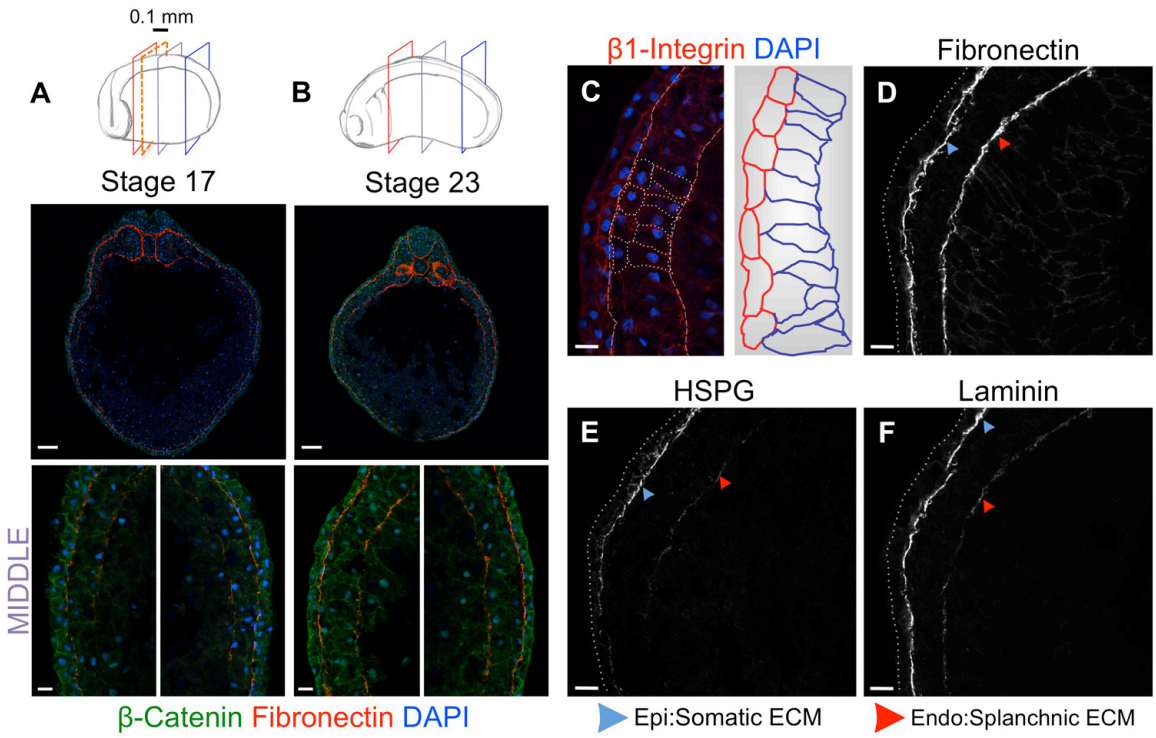

Fig. 3.1 Bilayered LPM is L-R symmetrical from tailbud-tadpole stages. splanchnic-somatic structural differences beginning at stage 23. (**A,B**) Diagrams indicate stage/length and sectional planes. Analysis every 0.1 mm (dashed red frame) was between anterior-posterior LPM extremes indicated by red/blue frames. Representative mid-embryo sections (purple frame): (**A**) Stage 17 (10x, 40x), L and R LPM each comprising two layers. (β-catenin (green); DAPI (blue). Fibronectin (red) flanks epidermal/endodermal faces of L and R LPM. (**B**) Stage 23: maintenance of bilayered L and R LPM. (**C**) L/R LPMs are structurally similar during these stages, but somatic/splanchnic layers become distinct, symmetrically, from stage 23; somatic cells more squamous, splanchnic more columnar. (**D-F**) Somatic and splanchnic LPM show different basal lamina compositions. Somatic: strong fibronectin, HSPG and Laminin signal; splanchnic: much weaker HSPG/Laminin signal, especially laterally. Scale bars: 100 μm, top images A,B; 20 μm, bottom images A,B; C-F.

Fig. 3.2 L and R LPM persist as bilayers following mesoderm formation. (**A-F**) Examination of the L and R LPM before (ST 17), during (ST 20-25) and after (ST 28 & 34) asymmetric *Xnr1* expression, (**C-F**) The LPM is thicker in anterior regions, becoming thinner more posteriorly, beginning at stage 23. The somatic LPM cells are more squamous, splanchnic LPM cells more columnar (see inset in D-F). Scale bars: 100 μm in top 10x images of A-F; 20 μm in all 40x images of A-F.

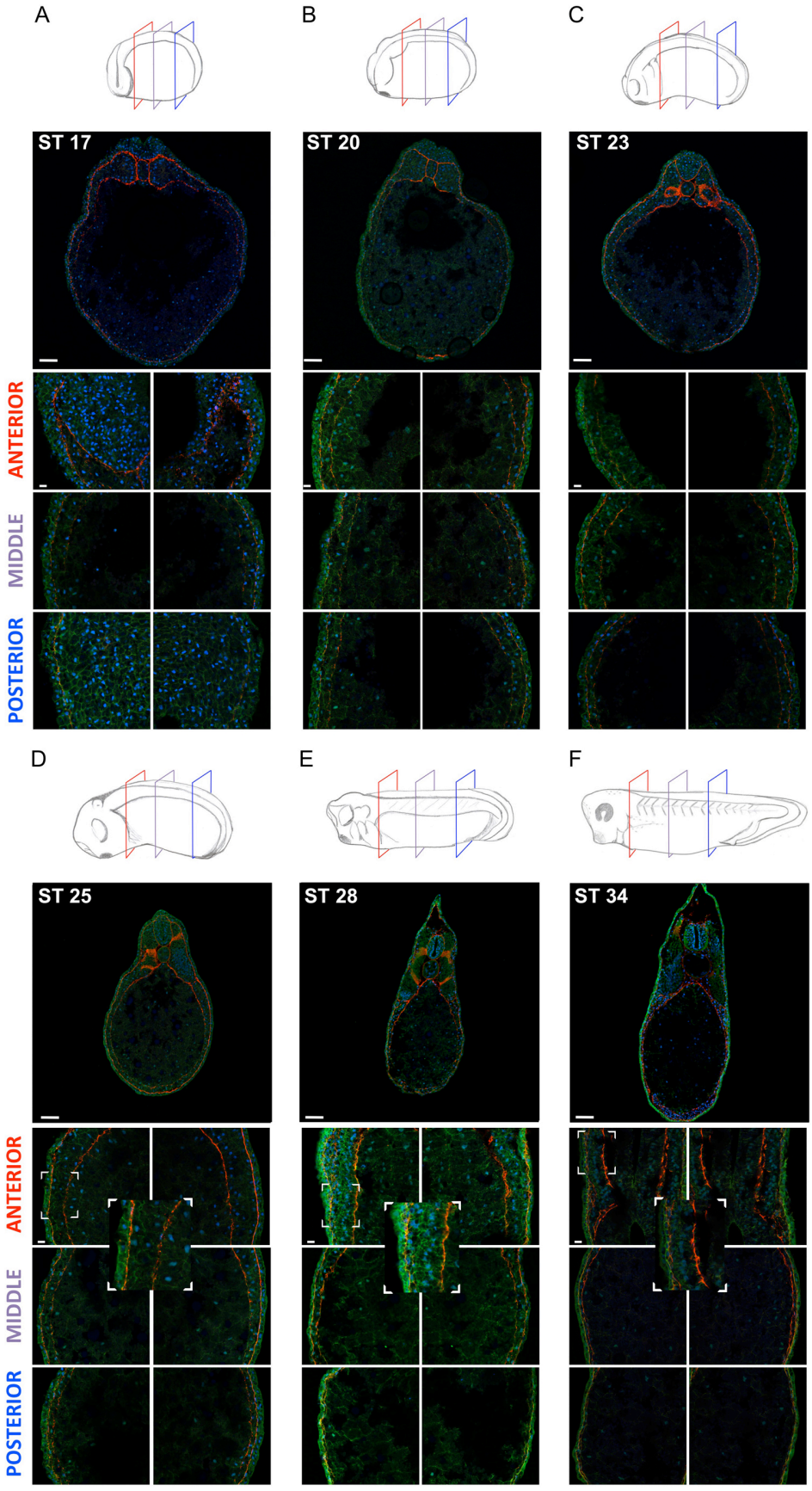
A
B
C
ST 17
ST 20
ST 23
ANTERIOR
MIDDLE
POSTERIOR
D
E
F
ST 25
ST 28
ST 34
ANTERIOR
MIDDLE
POSTERIOR

Because previous studies linked ECM components to the long-range movement of TGFβ ligands (Belenkaya et al., 2004; Guo and Wang, 2009; Oki et al., 2007; Yu et al., 2009), and establishment of asymmetric organ morphogenesis (Kramer et al., 2002; Kramer and Yost, 2002; Yost, 1990), we assessed the expression of other ECM proteins in the basal lamina of the LPM. While fibronectin coated the somatic and splanchnic LPM surfaces at similar levels, other ECM markers were differentially distributed between the epidermal and endodermal interfaces, with apparent L-R equivalence (Fig. 3.1A,B,D-F). Higher levels of laminin and heparan-sulfate proteoglycan (HSPG) were present at the somatic LPM-epidermis interface compared to the splanchnic LPM-endoderm margin (Fig. 3.1D-F). Up to at least stage 25, chondroitin-sulfate proteoglycan (CSPG) surrounded the notochord and ventral neural tube, and was detected in the ECM of the dorsal endoderm and somite boundaries, with anteriorly enhanced levels and posterior absence (Fig. 3.3). If the ECM apposing the LPM contained CSPG, it was below detection with this antibody (Fig. 3.3; not shown). The non-equivalence of the somatic versus splanchnic signal for laminin/HSPG compared to fibronectin was more exaggerated dorsally (Fig. 3.1E,F). These results suggest that ECM proteins could serve a role in movement facilitation or sequestration of Xnr1 and Lefty ligands, both produced from the LPM.

Symmetric apical-basal polarization of LPM following asymmetric gene expression

The epithelial character, ECM border characteristics, or apical/basal direction of secretion could influence the route and range of Xnr1 and Lefty transport from the LPM. We therefore examined various markers strongly accepted as diagnostic of apical or basolateral compartments of a polarized epithelium, for a temporal analysis of the polarization state of the LPM.

Fig. 3.3 CSPG abundance in the dorsal periaxial ECM becomes progressively reduced in an anterior-to-posterior manner. Analysis was focused on the dorsal periaxial regions during asymmetric *Xnr1* expression stages, which are presented schematically with relevant section planes indicated. At stage 20, 23, and 25 HSPG is more uniformly present along the A-P axis whereas CSPG is enriched anteriorly and absent posteriorly. Insets: Laminin represents a control ECM component present at similar levels throughout the embryo and unaffected by any of the manipulations used herein.

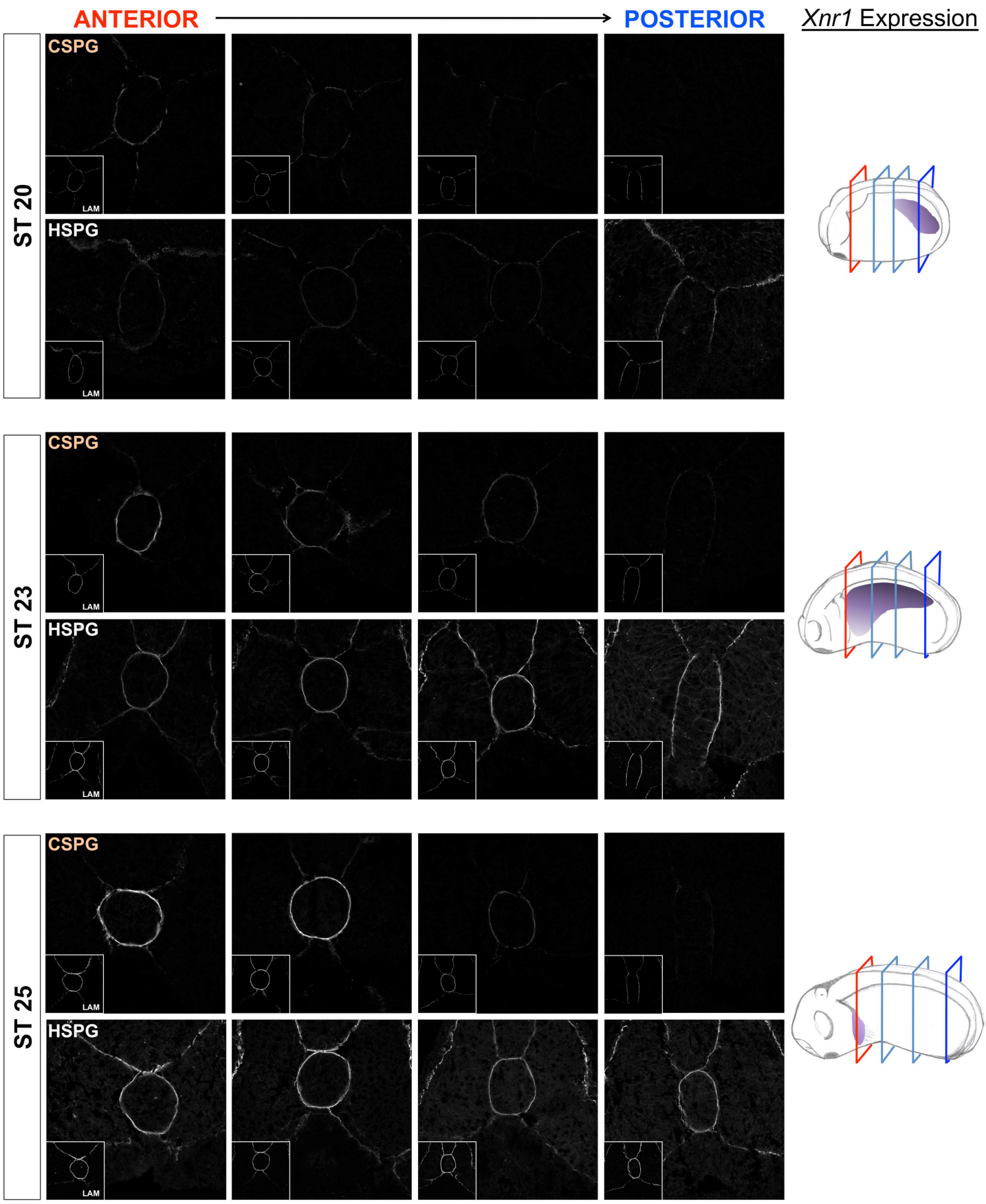
ANTERIOR
POSTERIOR
Xnr1 Expression
ST 20
ST 23
ST 25
CSPG
HSPG
LAM

LPM was characterized with zona occludins 1 (ZO1), a marker of apical tight junctions, between stages 17-34. During the period of asymmetric *Xnr1*/*Lefty* expression (stages 19-23), apical ZO1 localization was not seen in the L or R LPM anywhere along its length. In the same sections, punctate apical ZO1 was detected in polarized epithelia of the neural tube, epidermis, and archenteron (Fig. 3.4A,B; Fig. 3.5). Additional apical-specific marker analysis (aPKC, F-actin, Crumbs3; not shown) confirmed the absence of detectable LPM apicobasal polarity between stages 17-23.

Beginning at stage 24/25, corresponding to the waning of asymmetric *Xnr1*/*Lefty* expression, apical ZO1 was seen in the anterior-most 100 μm of the L and R LPM, the region immediately posterior to the pharyngeal arches (Fig. 3.4C; Fig. 3.5). Later, the apical ZO1 signal spread progressively posterior-ward in both L and R LPM. At stage 34/35, a point just prior to gut looping, punctate apical ZO1 extended along the entire length of the LPM (Fig. 3.5). These results suggest that the Xnr1 and Lefty ligands are normally produced predominantly within an apicobasal non-polarized environment, with LPM only becoming polarized after the cessation of asymmetric gene expression.

Epitope-tagged Xnr1 or Lefty are functional and move rapidly from a graft source

Against this LPM architecture and ECM composition foundation, we sought to determine the parameters of Xnr1 and Lefty transport. Although examination of the endogenous proteins would be most relevant, current antibodies have unfavorable signal-to-noise ratios. We therefore generated several tagged variants of Xnr1 and Lefty (Fig. 3.6A,B; Fig. 3.8A,B) and tested them for normal function (Williams et al., 2004) (Fig. 3.6A-C; Fig 3.9A,B). We placed two different tags (6xMyc or eGFP) just C-terminal to the cleavage site (CS) or at a carboxyl-terminal (CT) location in Xnr1 and Lefty, and tested them by a grafting method.

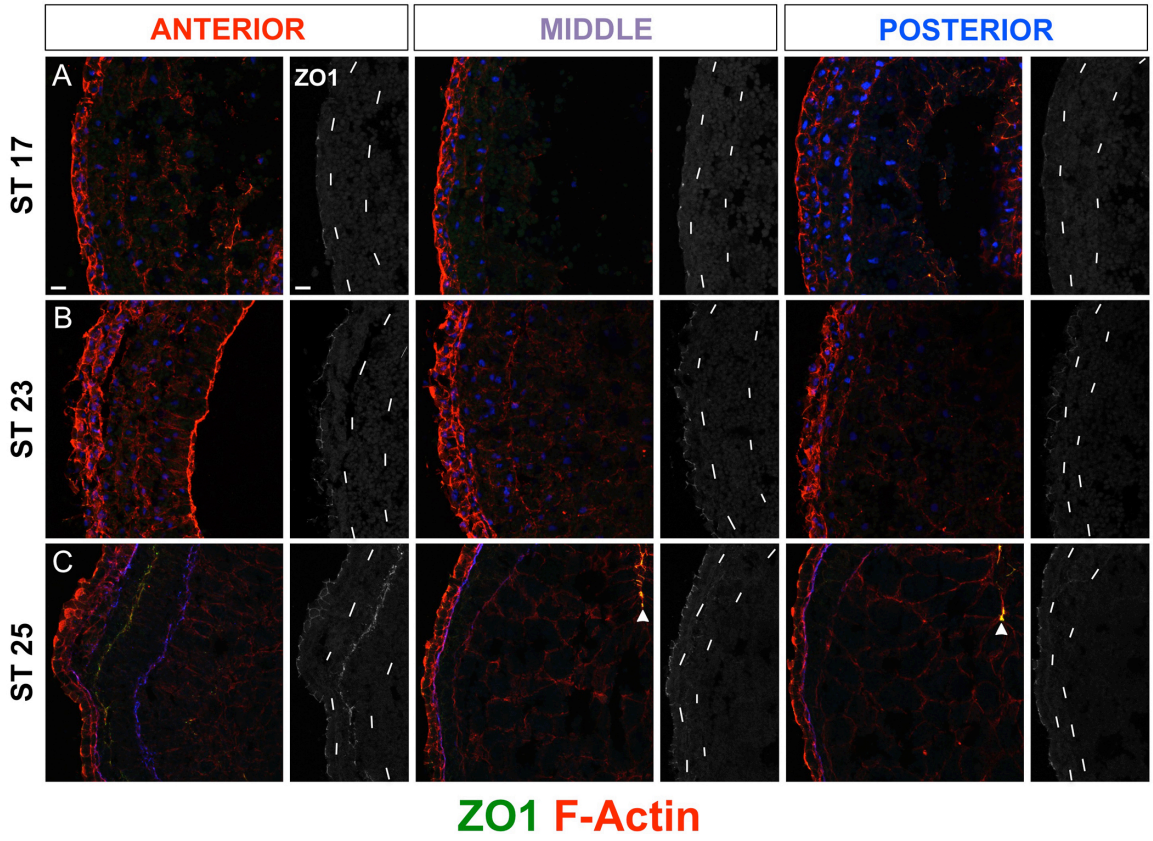

Fig. 3.4 LPM undergoes symmetric epithelial polarization after *Xnr1/Lefty* expression. Anterior, middle, posterior transverse cryosections showing F-actin (Phalloidin, red), ZO1 (green), and nuclei or ECM (blue: DAPI (A,B), Laminin (C)); 40x images. ZO1 alone (L side shown) is in grayscale, chained lines indicating LPM epidermal/endodermal boundaries. (**A**) Stage 17, LPM not yet polarized. ZO1 puncta indicate tight junctions in polarized epidermal layer; no puncta apparent within LPM at stages before asymmetric *Xnr1*/*Lefty* expression. (**B**) Stage 23, unpolarized LPM during peak *Xnr1*/*Lefty* expression. (**C**) Stage 25, punctate ZO1 signal appearing at somatic/splanchnic interface in anterior L and R LPM; at this stage, asymmetric *Xnr1*/*Lefty* expression is waning. Arrows in C: ZO1 in epithelial archenteron. Scale bars: 20 μm.

Fig. 3.5 Progressive anterior-to-posterior spreading of epithelial apicobasal polarization. (**A-C**) No apicobasal polarization (ZO1, marking tight junctions) is observed in L or R LPM from stage 17-23; LPM highlighted by dotted lines in ZO1-only channels. (**D**) Apical ZO1 localization is first seen during stage 25 in the first 100 μm of the L and R LPM, beginning posterior of the pharyngeal arches. Arrows highlight apical surface of archenteron opening. (**E**) ZO1 localization is evident more posteriorly in stage 28 embryos, extending back ~500 μm from the pharyngeal arches. (**F**) By stage 34, the L and R LPM are apicobasal polarized for the entire length of the L and R LPM. Scale bars: 20 μm in A-F.

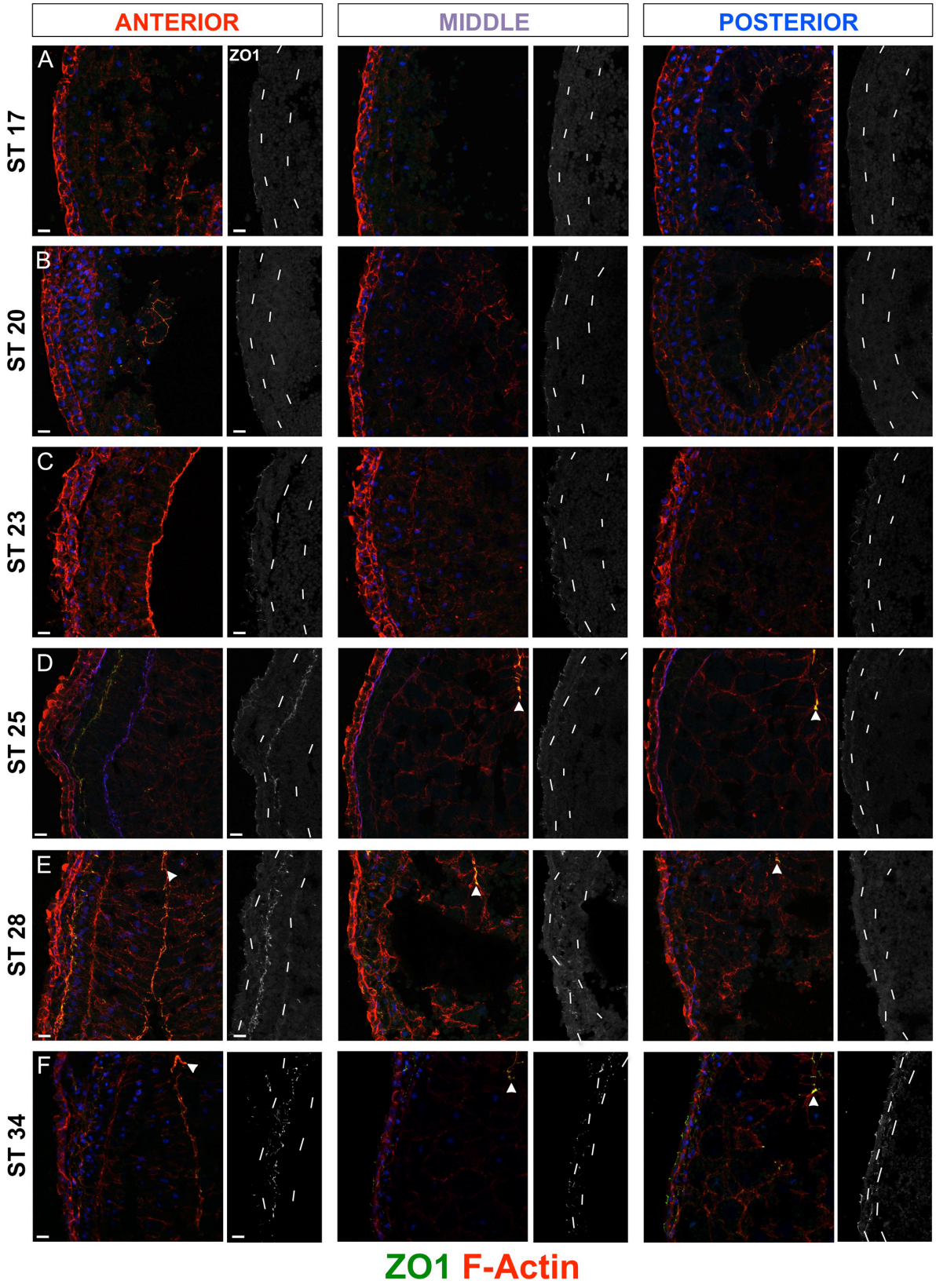
ANTERIOR
MIDDLE
POSTERIOR
ST 17
ST 20
ST 23
ST 25
ST 28
ST 34
A
B
C
D
E
F
ZO1
ZO1 F-Actin

We showed previously that R-sided placement of Xnr1-expressing LPM grafts initiated a R-sided P-to-A wave of *Xnr1* expression, and that L-sided Lefty grafts blocked the endogenous L-sided *Xnr1* expression wave (Ohi and Wright, 2007). Those previous studies (Ohi and Wright, 2007) used plasmid-loaded LPM grafts in which cells inherit the non-integrated plasmid mosaically, therefore expressing the desired protein unevenly and at low levels (data not shown). With that method, we did not reproducibly immunodetect the tagged protein above the ubiquitous yolk autofluorescence. To overcome this problem, we used RNA-loaded animal cap (AC) grafts as the source: trimmed AC explants were engrafted into recipient stage 17 embryos in either the L or R LPM, and cultured for several hours (Fig. 3.8B). The effects on *Xnr1* gene expression were then analyzed. AC grafts healed into hosts somewhat less seamlessly than LPM grafts, but did not hinder embryonic development. While control grafts carrying membrane-bound GFP (mGFP, Methods), did not affect endogenous L-sided *Xnr1* expression (Fig. 3.6C) or gross morphology in stage 45 tadpoles (data not shown), Xnr1 and Lefty from RNA-injected AC grafts had similar effects to the plasmid-based assays described above. This analysis (Fig. 3.6A-C) led to the selection of tagged variants most similar in function to the untagged versions: Xnr1$^{6MYC-CS}$ and Lefty$^{6MYC-CT}$ (Fig. 3.8A). R-sided grafts with Xnr1^{UNTAGGED} or Xnr1$^{6MYC-CS}$ initiated a P-to-A wave of *Xnr1* expression, and L-sided AC grafts producing either Lefty^{UNTAGGED} or Lefty$^{6MYC-CT}$ inhibited equivalently the anterior-ward shift of *Xnr1* expression (Fig. 3.6C).

Western blot analysis of host tissue after graft removal showed that the principal form of Xnr1$^{6MYC-CS}$ and Lefty$^{6MYC-CT}$ secreted from the graft and transported around the embryo was the mature ligand (important because proprotein cleavage is a determinant of signaling range; (Cui et al., 2001)), and that both were N-glycosylated (Fig. 3.7). For Lefty, we detected specifically the 'long isoform', similar to results from blastula/gastrula embryos, and not a putative short isoform that we proposed (Westmoreland et al., 2007)

Fig. 3.6 Assessment of epitope-tagged Xnr1 and Lefty function in LPM induction assays. (A) Xnr1 constructs tested and effects on initiating R-sided *Xnr1* expression. **(B)** Lefty constructs tested and effects on inhibiting L LPM *Xnr1* expression. As in Ohi and Wright (2007), partial *Xnr1* expression suppression is defined as *Xnr1* expression reaching the posterior graft margin whereas complete suppression is defined by an absence of *Xnr1* expression in the L LPM. **(C)** Control and mGFP-grafted embryos display anterior *Xnr1* expression (purple) within the L LPM. Embryos engrafted on the R with $Xnr1^{UNTAGGED}$ or $Xnr1^{6MYC\text{-}CS}$ show R-sided forward-shifting induction of *Xnr1* in the LPM. Embryos engrafted on the L with $Lefty^{UNTAGGED}$ or $Lefty^{6MYC\text{-}CT}$ grafts showed inhibition of L LPM *Xnr1* expression. Dotted lines outline the graft.

A.

Construct	Right *Xnr1* Expression (%)	Left *Xnr1* Expression (%)	Bilateral *Xnr1* Expression (%)
Xnr1^{UNTAGGED} (n=16)	0 (0)	3 (19)	13 (81)
Xnr1$^{6MYC-CS}$ (n=14)	1 (7)	4 (29)	9 (64)
Xnr1$^{6MYC-CT}$ (n=6)	0 (0)	6 (100)	0 (0)
Xnr1^{GFP-CS} (n=16)	0 (0)	16 (100)	0 (0)

B.

Construct	Complete *Xnr1* Suppression (%)	Partial *Xnr1* Suppression (%)	No Suppression (%)
Lefty^{UNTAGGED} (n=12)	4 (11)	7 (78)	1 (11)
Lefty$^{6MYC-CT}$ (n=17)	4 (29)	9 (64)	3 (21)
Lefty$^{6MYC-CS}$ (n=13)	0 (0)	4 (31)	9 (69)
Lefty^{GFP-CS} (n=14)	0 (0)	7 (50)	7 (50)

C.

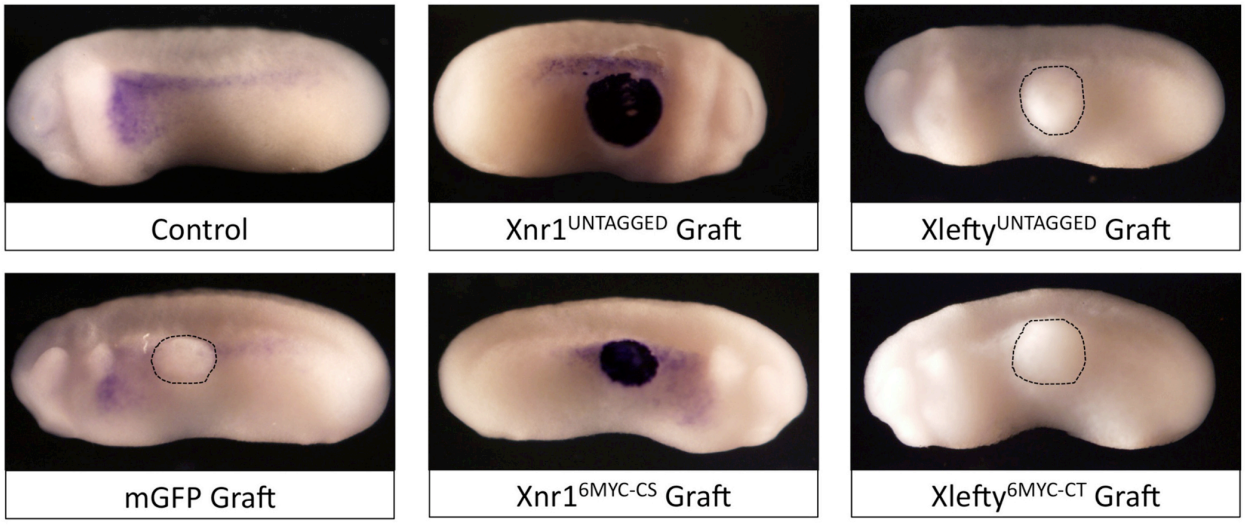

is an unstable clearance intermediate. Our combined biochemical, immunofluorescence and gene expression data demonstrated that these tagged proteins had an appropriate effect on the host embryo tissue signaling systems in terms of the effect on the expression of *Xnr1* (Fig. 3.6; Fig. 3.7).

We then examined ligand movement from AC grafts producing these functional Xnr1$^{6MYC-CS}$ and Lefty$^{6MYC-CT}$ proteins. AC-grafted stage 17 embryos were cultured for several hours until stage 24/25, then systematically sectioned and analyzed for Myc signal outside of the graft, the latter identified by membrane-bound mGFP. Both Xnr1$^{6MYC-CS}$ and Lefty$^{6MYC-CT}$ were readily detected both within and outside the graft source. Outside, there was colocalization with the ECM proteins laminin, HSPG, and fibronectin (Figure 3.8; data not shown). Xnr1$^{6MYC-CS}$ and Lefty$^{6MYC-CT}$ were detected at ECM interfaces flanking the L LPM, and around the dorsal periaxial, paraxial, and neural structures (notochord, somites and ventral neural tube, respectively; Fig. 3.8C-J′). We also detected interstitial signal within the LPM, albeit lower than at the ECM interfaces. Identical processing for Xnr1^{UNTAGGED} and Lefty^{UNTAGGED} AC-grafted embryos (details in Methods) established the background against which to evaluate real Myc signal (Fig. 3.8K-L′; Fig. 3.9A-D). The only substantive background problem was a non-specific epidermal haze (Fig. 3.8K-L′), becoming more apparent if images were post-processed to enhance Myc signal intensity (Fig. 3.9C,D), which precluded us deciding that ligand moved into the epidermal layer rather than remaining excluded. In sections that contained the graft, or nearby, Lefty$^{6MYC-CT}$ was detected interstitially in the adjacent endodermal mass, with an apparently intracellular signal in some cells (Fig. 3.8J′). Moreover, a Lefty$^{6MYC-CT}$ signal was definitely detected at the ECM interface flanking the R LPM, suggesting the long-range, direct contralateral transfer of Lefty from the L-sided graft. This R-sided transfer was confirmed biochemically (Fig. 3.10C).

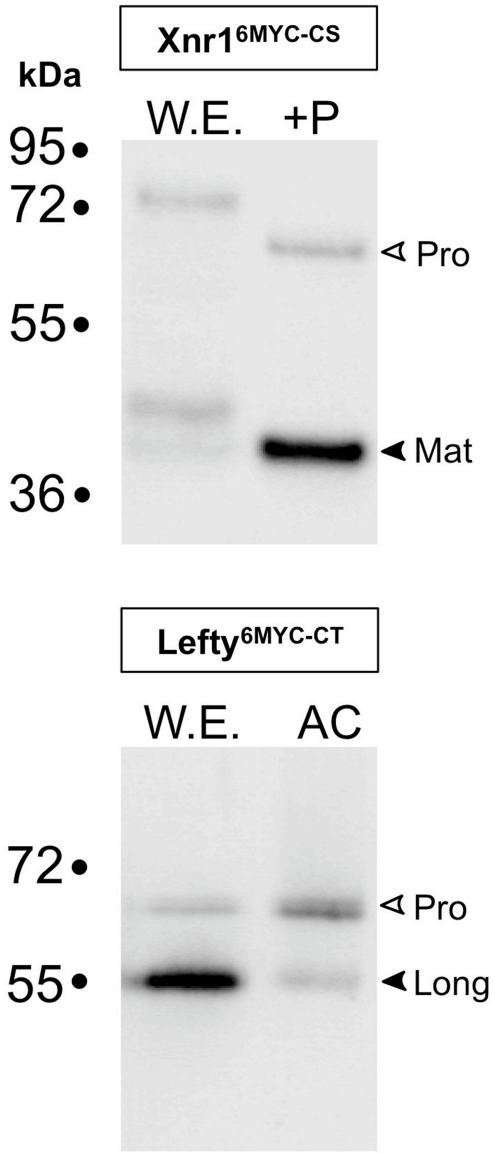

Fig. 3.7 Mature ligands of Xnr1$^{6MYC-CS}$ and Lefty$^{6MYC-CT}$ are the major forms traveling from AC grafts. AC-grafted embryos were cultured for 5 hours, grafts removed using mGFP visualization, and whole embryos (W.E.) and excised grafts processed separately by immunoprecipitation and anti-Myc western blot (2 embryo-equivalents or 4 AC-equivalents per lane). **Top panel**: Xnr1$^{6MYC-CS}$ within previously grafted whole embryos detected predominantly glycosylated mature ligand (+P, extract was PNGaseF-deglycosylated pre-electrophoresis; both proprotein and ligand are glycosylated); a low amount of non-glycosylated Xnr1 was detected. Deglycosylation allows better immunodetection of the nearby epitope tag, therefore giving the best estimate of mature ligand to proprotein ratio. **Bottom panel**: The mature, long Lefty isoform (Westmoreland et al., 2007) is the predominant form outside the graft, whereas the proprotein is the major form remaining within the graft.

Fig. 3.8 Xnr1$^{6MYC-CS}$ and Lefty$^{6MYC-CT}$ move substantially from AC grafts. (**A**) Xnr1 and Lefty constructs: blue box, pro-domain; CS1/CS2, cleavage sites liberating mature ligands; 6MYC tag was inserted just downstream of CS1 (Xnr1) or C-terminally (Lefty). (**B**) AC-grafting schematic. (C-L′) Transverse cryosections were used to detect Myc (red; grayscale in ′ panels), laminin (blue), and nuclei (DAPI, white); dorsal panels focus axially/paraxially, lateral panels on LPM. Membrane-bound GFP (mGFP, green) marks engrafted cells; 2.5 µm optical sections. Open arrowheads, Myc; closed arrowheads, nonspecific epidermal haze. (**C-F**′) Xnr1$^{6MYC-CS}$, (**G-J**′) Lefty$^{6MYC-CT}$, (**K,K**′) Xnr1^{UNTAGGED}, (**L,L**′) Lefty^{UNTAGGED}. (**C,C′; D,D**′) Representative section ~110 µm anterior of graft margin; Xnr1$^{6MYC-CS}$ signal in basal lamina surrounding notochord/neural tube. Dorsal and L LPM Xnr1$^{6MYC-CS}$ signal colocalized with laminin. (**E,E′; F,F**′) Representative images, dorsal and lateral Xnr1$^{6MYC-CS}$ signal within/near graft. Note absence of endoderm signal. (**G,G′; H,H**′) Lefty$^{6MYC-CT}$ signal colocalized with laminin in dorsal and lateral views, ~340 µm anterior of graft. (**I,I′; J,J**′) Dorsal and lateral images of Lefty$^{6MYC-CT}$ signal. Note Lefty$^{6MYC-CT}$ signal within endoderm, not colocalized with laminin. (**K-L**′) AC grafts with Xnr1^{UNTAGGED} or Lefty^{UNTAGGED} reveal artefactual hazy epidermal signal (closed arrowhead). Scale bars: 25 µm.

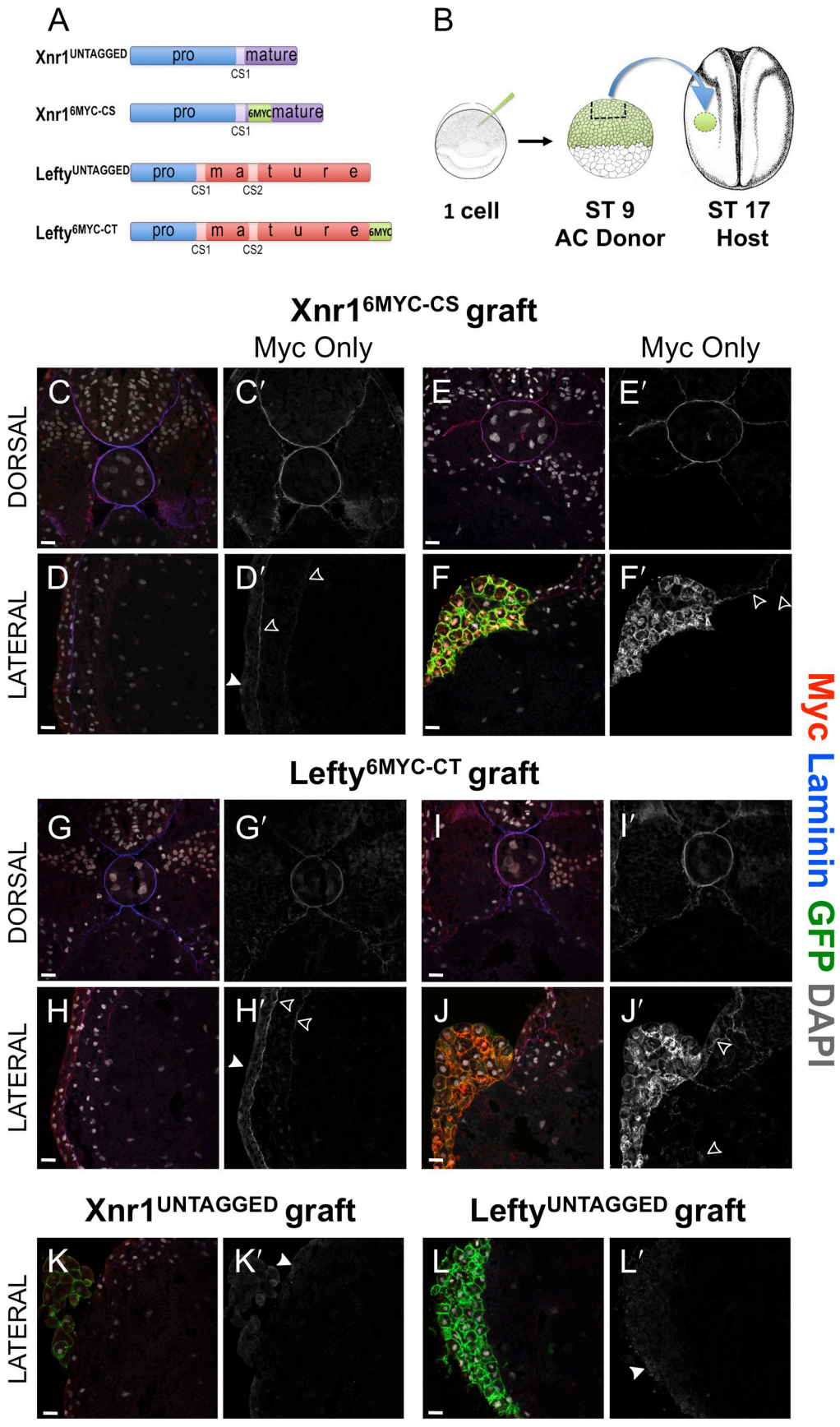
A
Xnr1UNTAGGED
pro
mature
CS1
Xnr16MYC-CS
pro
6MYC
mature
CS1
LeftyUNTAGGED
pro
m a t u r e
CS1
CS2
Lefty6MYC-CT
pro
m a t u r e
6MYC
CS1
CS2
B
1 cell
ST 9
AC Donor
ST 17
Host
Xnr16MYC-CS graft
Myc Only
Myc Only
DORSAL
LATERAL
C
C′
D
D′
E
E′
F
F′
Lefty6MYC-CT graft
DORSAL
LATERAL
G
G′
H
H′
I
I′
J
J′
Xnr1UNTAGGED graft
LeftyUNTAGGED graft
LATERAL
K
K′
L
L′
Myc Laminin GFP DAPI

Although AC engraftment inevitably leads to a reduction (possibly transient) in ECM quality at the LPM-endoderm interface, notably, unlike Lefty$^{6MYC-CT}$, Xnr1$^{6MYC-CS}$ was undetectable by immunofluorescence or biochemical analysis in the endoderm or R LPM (Fig. 3.10B). The timing and fractional contralateral transfer of Lefty$^{6MYC-CT}$ to the R LPM was addressed. Mature Lefty ligand was present predominantly in the L LPM at 3 hours with a high transfer to the R LPM by 6 hours (Fig. 3.10D). Thus, Lefty has a much greater capacity than Xnr1 to move from LPM AC grafts into the endoderm and towards the R LPM. As discussed more below, the affinity of Nodal and Lefty for the ECM adjacent to the LPM cells secreting these ligands may facilitate their rapid, far-ranging, planar movement. At the same time, the retention of Xnr1 in proximity to the LPM, the responsive tissue, would enable appropriate threshold-dependent regulation of gene expression.

Epitope-tagged Xnr1 and Lefty clearance

One caveat in studying misexpressed tagged ligands is what the signal represents: 'active protein', or accumulated overly stabilized, inactive protein undergoing clearance or terminal sequestration. To buttress the significance of the Xnr1 and Lefty signals as related to active transport and signaling, we devised an approach to show that the signal does not represent accumulated protein, and that both Xnr1 and Lefty are being cleared relatively dynamically. The visualization of mGFP-expressing AC grafts aided their removal from host embryos after 'ligand-conditioning' the LPM. Embryos received AC Xnr1$^{6MYC-CS}$ or Lefty$^{6MYC-CT}$ grafts plus mGFP, and were cultured (4.5 hrs for Xnr1$^{6MYC-CS}$, 3 hrs for Lefty$^{6MYC-CT}$) before the graft was removed. Embryos were fixed immediately (reference peak signal), or 30 or 90 minutes after graft removal and analyzed for periaxial Myc signal (Fig. 3.11).

Fig. 3.9 Validation of signal arising from epitope-tagged Xnr1 and Lefty constructs. (**A,B**) A poorly secreted variant, Lefty$^{6MYC-CS}$, bearing an epitope tag near the prodomain/ligand cleavage site (poor secretion established by focal delivery and ligand movement assays at blastula/gastrula stages) was (**A**) not detected in dorsal periaxial ECM or the ipsilateral LPM ECM, but (**B**) was detected strongly within the AC graft. Laminin inset in **A**: tissue landmark reference for periaxial tissues. This analysis provides another robust estimate of the background signal in embryonic tissue not receiving Myc-tagged proteins from AC grafts. A background epidermal haze (closed arrowheads) is again noticeable (Fig. 3 D′, H′, K′ and L′). (**C,D**) Images were post-capture processed (identically increased contrast) to compare Xnr1$^{6MYC-CS}$ signal to the background (closed arrowheads) seen with Xnr1^{UNTAGGED}-engrafted embryos showed Xnr1$^{6MYC-CS}$ localized between LPM cells, and to splanchnic and somatic LPM ECM surfaces (open arrowheads), but absence from endodermal interstitial spaces. [100 μm anterior of graft, same as Fig. 3D′]

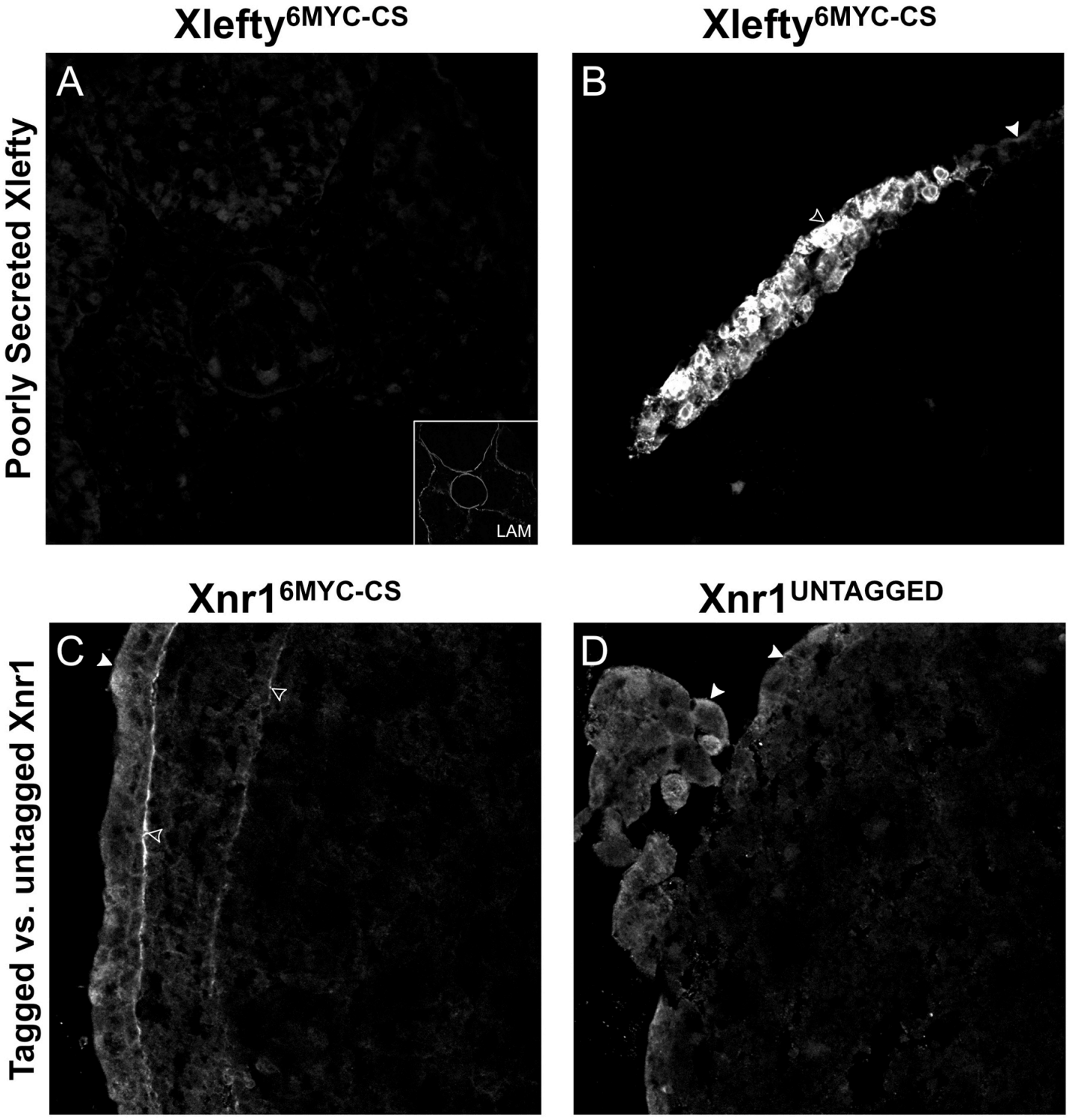
Xlefty6MYC-CS
Xlefty6MYC-CS
Poorly Secreted Xlefty
A
B
LAM
Xnr16MYC-CS
Xnr1UNTAGGED
Tagged vs. untagged Xnr1
C
D

Both Xnr1$^{6MYC-CS}$ and Lefty$^{6MYC-CT}$ signals were principally at periaxial and L LPM ECM. At T30, the Xnr1$^{6MYC-CS}$ signal was decreased 60%, and Lefty$^{6MYC-CT}$ by 40% suggesting that, in the absence of continued replenishment from the AC graft, both ligands were effectively cleared. By T90, approx. 90% of Xnr1$^{6MYC-CS}$ and 80% of Lefty$^{6MYC-CT}$ signal had disappeared. From this analysis, relative half-lives were inferred as approx. 25 minutes for Xnr1$^{6MYC-CS}$ and 45 minutes for Lefty$^{6MYC-CT}$.

Lefty travels more rapidly than Xnr1

A key postulate in the reaction-diffusion model for interactions between an inducer (Nodal/Xnr1) and its feedback antagonist (Lefty) in limiting the range/longevity of the inducer's influence is that the antagonist travels faster than its inducer (Turing, 1990). We therefore addressed the rate and distance of movement in intact embryos during the stages of asymmetric gene expression, especially with reference to the types of tissue transport routes that are used. We performed a time-course comparison of the ability of tagged Xnr1 and Lefty to exit grafts and take a dorsal (producing a periaxial signal around notochord and ventral neural tube) or lateral route (planar movement along L LPM surfaces), both anteriorly and posteriorly.

At 3 hours post-engraftment (hr-PE), dramatic differences were observed between Xnr1 and Lefty. For both ligands, Myc signal was detected in a graded fashion away from the graft, potentially displaying first-order diffusion characteristics, although a careful quantitative biochemical analysis would be required to address this issue (immunofluorescence assays on localized signals are at best semi-quantitative). For the lateral LPM ECM route, anteriorward Lefty$^{6MYC-CT}$ movement was twice that of Xnr1$^{6MYC-CS}$, and posterior Lefty$^{6MYC-CT}$ signal was detected five times farther than for Xnr1$^{6MYC-CS}$ (Fig. 3.12). This difference was observed for the anteriorward dorsal-periaxial route at 3 hr-PE, Lefty$^{6MYC-CT}$ having traveled about 3 times farther than Xnr1.

Fig. 3.10 Contralateral R-sided detection of Lefty$^{6MYC-CT}$ but not Xnr1$^{6MYC-CS}$. (A) Experimental design for biochemical detection of contralateral Myc signal. **(B)** Xnr1$^{6MYC-CS}$ was not detected at contralateral ECM flanking the R LPM in immunofluorescence or biochemical analyses whereas **(C)** Lefty$^{6MYC-CT}$ was robustly detected (open arrowheads) in interstitial endodermal spaces and contralateral splanchnic and somatic ECM surfaces. Note predominance of the mature, glycosylated Lefty$^{6MYC-CT}$ within the R LPM. Closed white arrowheads, background epidermal haze; open white arrowheads, R LPM-ECM signal; Closed yellow arrowheads, endodermal signal. **(D)** To assess the timing and fractional transfer of Lefty$^{6MYC-CT}$ to the contralateral side, mGFP-expressing AC grafts were implanted for 3 or 6 hours, then grafts (expressing mGFP) were removed and L and R LPMs isolated and pooled separately. Complete graft removal was confirmed by absence of mGFP signal on western blot. The proprotein (pro) and mature, long isoform (mat) of Lefty$^{6MYC-CT}$ are predominantly present within L LPM at 3 hrs. but more protein has transferred to R LPM by 6 hrs. Colloidal blue staining comparison of lysates showed that equivalent amounts of protein were subjected to IP (not shown). These data suggest that concentrated Nodal signaling within the L LPM may correlate with a locally enhanced clearance mechanism.

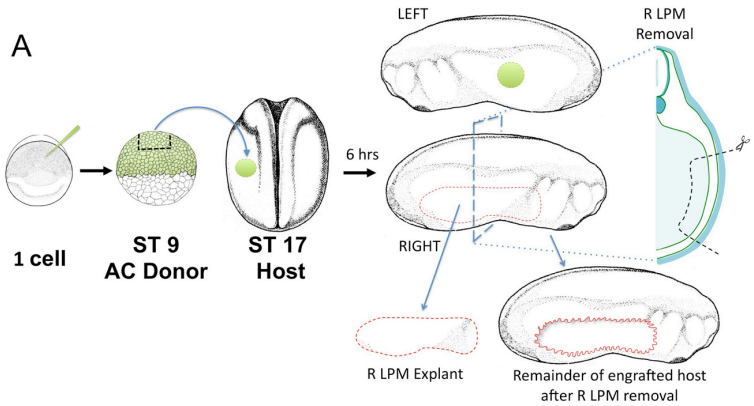

Xnr1$^{6MYC-CS}$

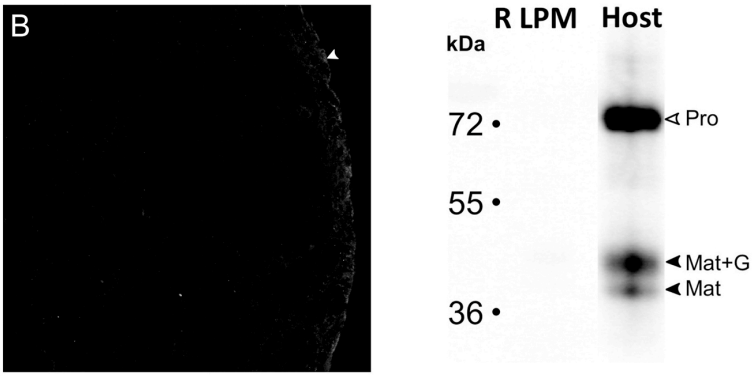

Lefty$^{6MYC-CT}$

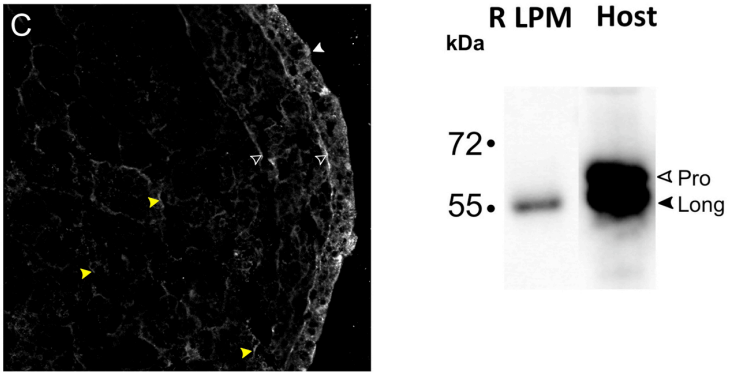

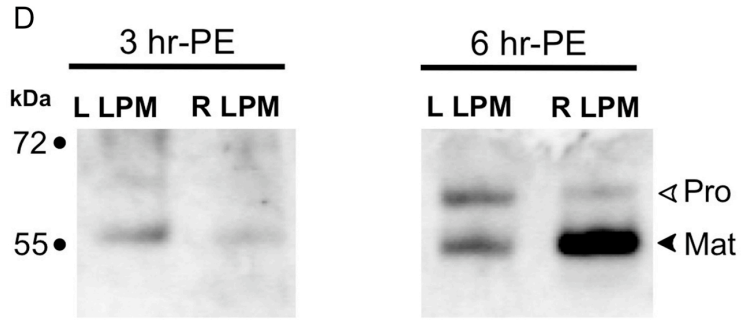

A similar trend was observed for the posterior periaxial route. From these results, we infer an inherent difference in these functional tagged ligands: Lefty travels significantly greater distances in a shorter time period compared to Xnr1. By 5 hr-PE, the distances reached anteriorly and posteriorly in the LPM and periaxial regions by Xnr1$^{6MYC-CS}$ and Lefty$^{6MYC-CT}$ were relatively similar (Fig. 3.12), implying movement up to 700 μm from the source (Fig. 3.12). The long-range transport and 'catch-up' by Xnr1 compared to Lefty were under conditions of prolonged ligand production from the graft and did not result from ligand accumulation, as shown by the clearance findings above. The later 'catch up' of Xnr1 to Lefty may be related to the ligands reaching some type of anterior and posterior tissue limit; we did not detect signal extending posteriorly into the region of nascent mesoderm formation or anterior of the LPM in the pharyngeal arches or presumptive cardiac field.

Xnr1 requires sulfated proteoglycans for fast planar LPM transport and dorsal-ward movement to the midline

Previously, sulfated glycosaminoglycans (sGAGs) were implicated in transporting Nodal from the node to the L LPM in mouse, and sGAG-depleted mouse embryos fail to express L LPM *Nodal* despite the normal perinodal *Nodal* expression (Oki et al., 2007). Here, we examined how sGAG removal might affect Xnr1 movement within and from the LPM. Xyloside (*p*-nitrophenyl-β-D-xylopyranoside) blocks sGAG attachment by competing with xylosylated core proteins as substrate for galactosyltransferase I, with differential effects on heparan- and chondroitin-sulfate pathways. Preferential binding to CS groups blocks CSPG synthesis, and a lower affinity for HS reduces HSPG synthesis more moderately (Lugemwa and Esko, 1991; Oki et al., 2007). For our analysis here, it is relevant that heparan-sulfate-xyloside conjugates are still secreted and may be detected by immunofluorescence (Stevens and Austen, 1982).

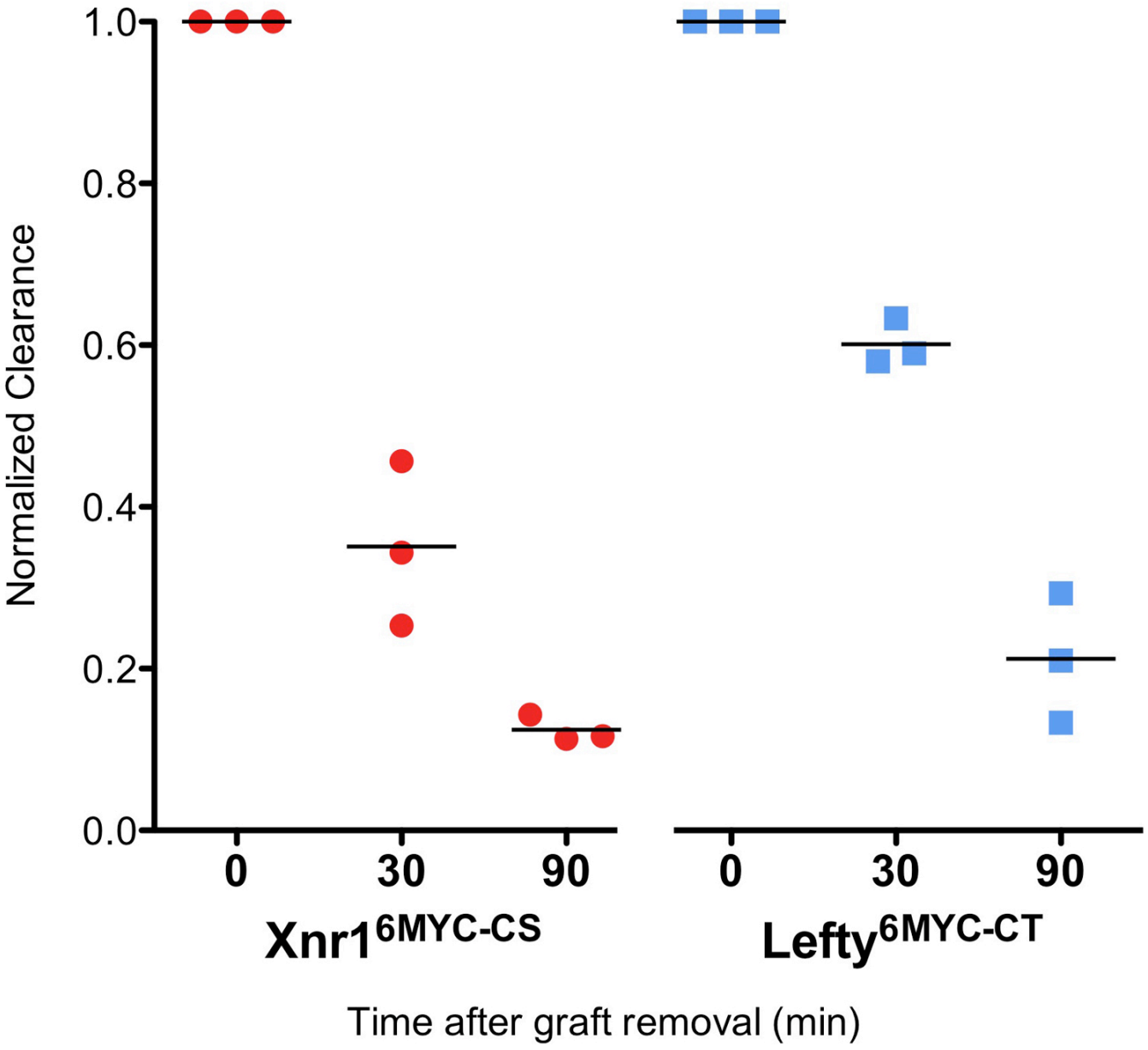

Fig. 3.11 Xnr1 and Lefty clearance. Xnr1$^{6MYC-CS}$ (red) and Lefty$^{6MYC-CT}$ (blue) clearance was measured by conditioning embryos by engrafting for 3 hours, graft removal and analysis (ImageJ line-scan) 0, 30, or 90 minutes post-removal, values normalized to T0.

While xyloside prevents proper cardiac looping in frog embryos (Yost, 1990), it has not been determined how sGAG removal alters ligand movement or, specifically in frogs, its effect on the spatiotemporally dynamic expression of *Xnr1*.

We first tested if xyloside prevented the left-sided LPM initiation of *Xnr1* expression, presumably by blocking transfer of signals from the posterior L-R coordinator (gastrocoel roof plate, the equivalent of the late node in the mouse; (Schweickert et al., 2007), a block expected if asymmetric signal transfer to L LPM requires sGAG as in the mouse (Oki et al., 2007). This effect was indeed detected (Fig. 3.13A,B). The efficiency of sGAG removal was confirmed by analyzing CSPG and HSPG in tissue sections. Embryos treated with xyloside continuously from the two-cell stage completely lacked the CSPG signal in ECM (Fig. 3.13C,D), and therefore completely removed the 'anterior enhancement' of CSPG seen around dorsal periaxial structures (Fig. 3.13C,D; Fig. 3.3). HSPG was still detected, but we note with respect to the caveat above that the current antibody and immunodetection methods might not detect fractional reductions in HSPG.

The absence of endogenous asymmetric gene expression in the presence of xyloside provided an opportunity to test how sGAG deficits affected ligand movement from an AC graft in the absence of endogenous ligands produced within the LPM. Because Xnr1 is the inducer, and *Lefty* the responsive gene, we focused analysis on the movement of Xnr1$^{6MYC\text{-}CS}$. Control and xyloside-treated recipients received, at stage 17, AC grafts producing Xnr1$^{6MYC\text{-}CS}$ and mGFP, and were cultured for 5 hours in the presence/absence of xyloside, a period appropriate to detect an altered speed and range of movement, based upon results described above. Grafted xyloside-treated embryos showed a mislocalization of Xnr1$^{6MYC\text{-}CS}$. In many cases, Xnr1$^{6MYC\text{-}CS}$ was detected interstitially within the endodermal mass, unlike controls (compare Fig. 3.7D′,F′ to Fig. 3.13E-H).

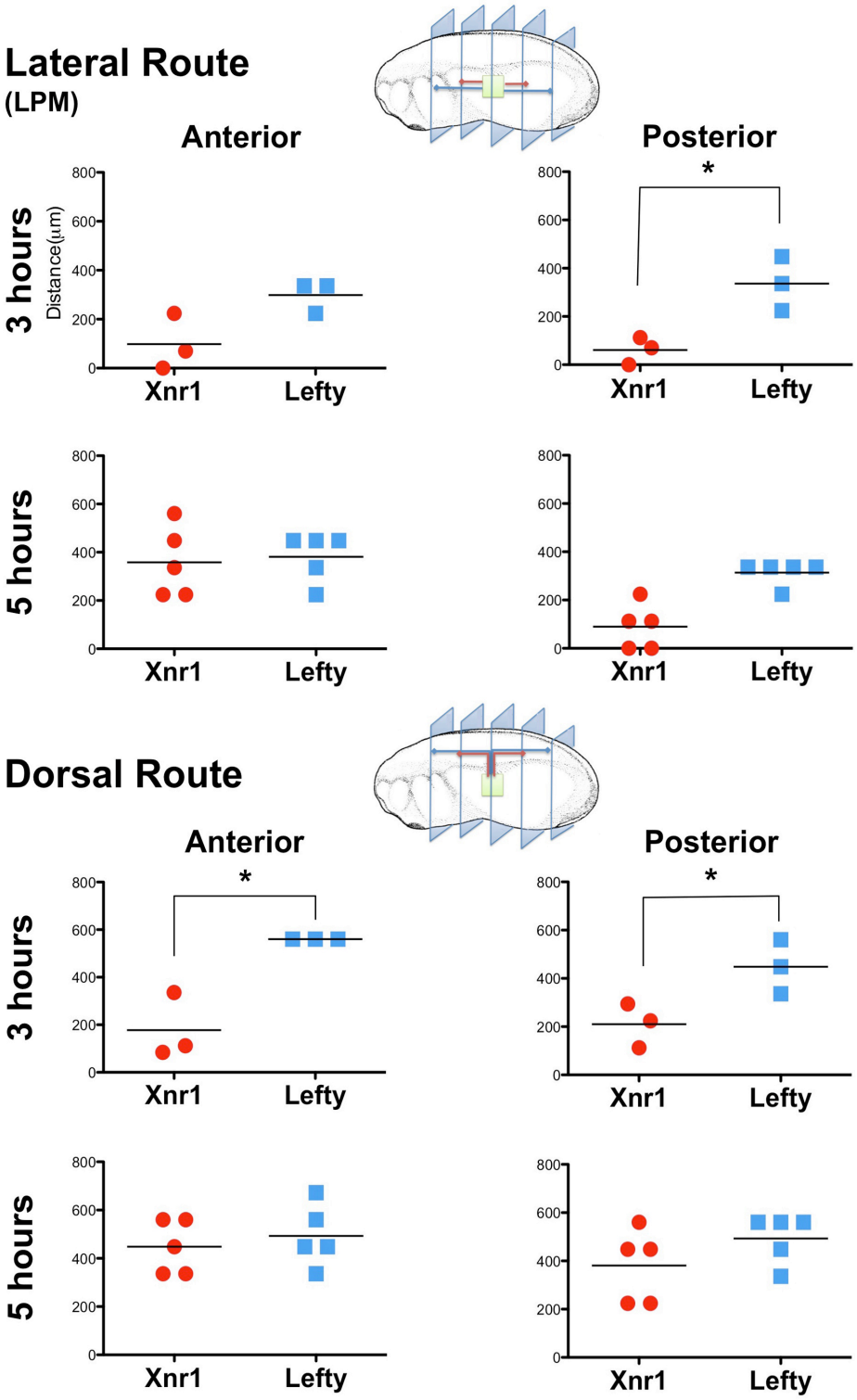

Fig. 3.12 Lefty$^{6MYC-CT}$ travels farther than Xnr1$^{6MYC-CS}$, in less time. Distance of signal detection from graft (ImageJ line-scan) of consecutive dorsal, lateral views, 40x magnification. Note different distances traveled periaxially and laterally between Xnr1 and Lefty at 3 hrs. *Non-parametric Mann-Whitney test; p≤0.05.

While controls displayed long-distance Xnr1$^{6MYC-CS}$ movement along ECM in L LPM and to periaxial tissues after 5 hours (Fig. 3.13I), signal within sGAG-deficient embryos was reduced at the somatic-epidermal ECM interface, relatively increased along the splanchnic-endodermal ECM, and showed significantly decreased transfer along both dorsal-periaxial and lateral routes (Fig. 3.13F,H,I). We note that colocalization of tagged Xnr1 with ECM was not abolished, as many other ECM proteins are still present after sGAG depletion, suggesting that low-affinity interactions between Xnr1$^{6MYC-CS}$ and yet-undetermined ECM proteins persisted. Because AC grafts experienced xyloside only after engraftment, secretion of tagged Xnr1 was have been affected (Fig. 3.14). Moreover, despite the mislocalized signal with xyloside treatments, the signal remaining ECM-associated plus that in endoderm (under identical imaging conditions) also suggests that secretion per se was not grossly affected. As well as suggesting that ligand moves faster and farther on sGAG-rich ECM, we hypothesize an additional role in preventing too much Xnr1 from leaving the vicinity of the L LPM, with the premise that threshold signaling is central to enabling an efficient autoregulation-based spatial propagation of *Xnr1* expression.

Fig. 3.13 Xyloside decreases L LPM-restraint of Xnr1 signal and alters distance traveled. (**A,B**) Endogenous *Xnr1* expression in L LPM of controls but complete absence from 80% of xyloside-treated embryos. (**C,D**) CSPG periaxially (around notochord) and at the somite/dorsal endoderm interface in DMSO-treated (n=9) but absence from all xyloside-treated embryos (n=11). (**E,F**) Xnr1$^{6MYC-CS}$ grafts display dorsal periaxial signal, which is markedly reduced with xyloside treatment. (**G,H**) Dorsolateral L LPM signal on ECM in controls and lack of endodermal signal (inset; graft, green outline). Xyloside-treated Xnr1$^{6MYC-CS}$ engrafted embryos showed increased endoderm signal (inset), interstitial and intracellular. Note increased relative signal at splanchnic:endodermal ECM. Open arrowheads, epidermal:somatic ECM; yellow arrowheads, splanchnic:endodermal ECM. (**I**) Xyloside treatment reduces distance traveled by Xnr1$^{6MYC-CS}$, lateral and periaxial route (Fig. 4). *Non-parametric Mann-Whitney test: p≤0.05. Scale bars: 25 μm.

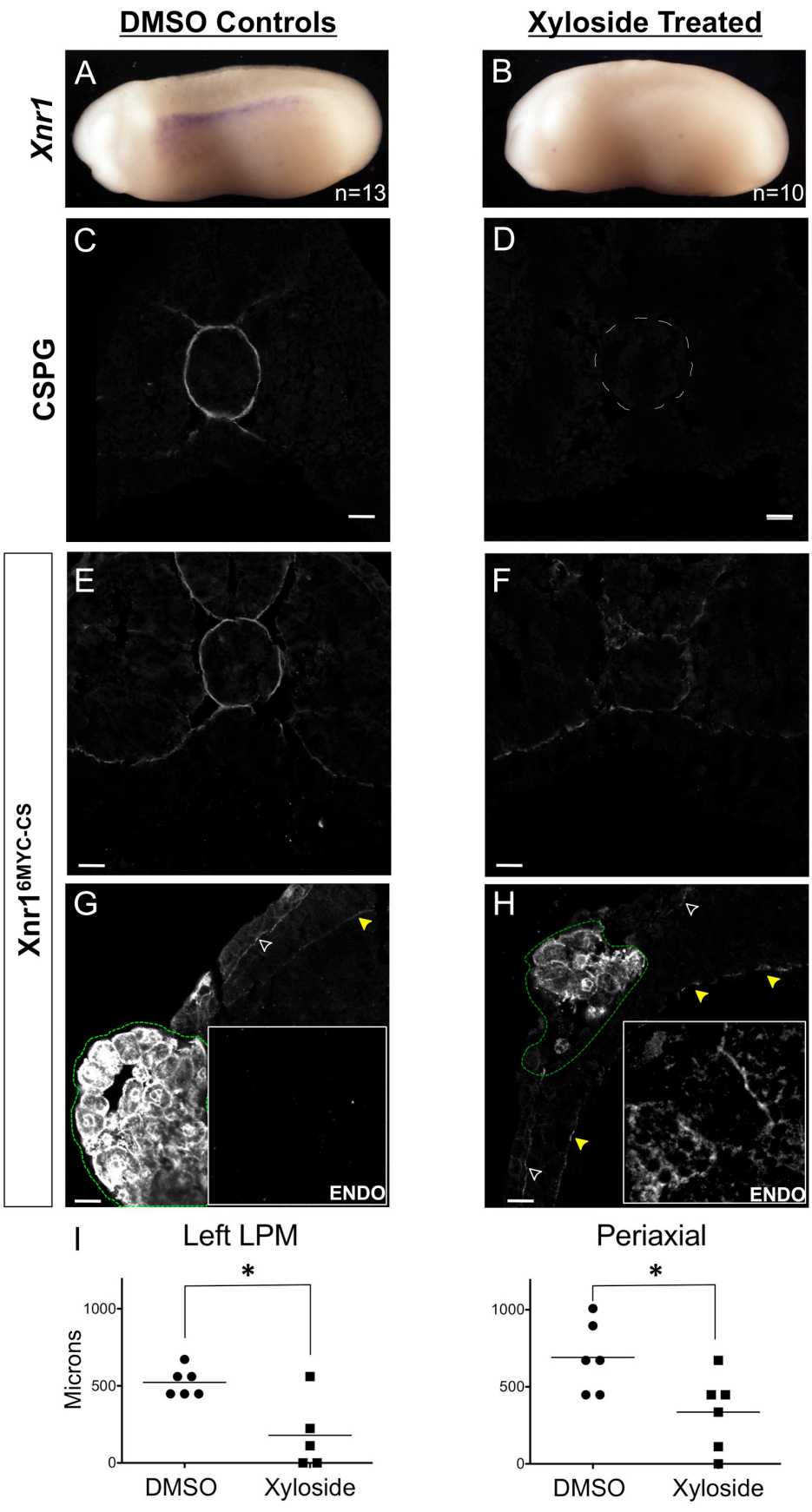
DMSO Controls
Xyloside Treated
Xnr1
CSPG
Xnr1^6MYC-cs
A
B
C
D
E
F
G
H
n=13
n=10
ENDO
ENDO
I
Left LPM
Periaxial
Microns
1000
500
0
DMSO
Xyloside
*

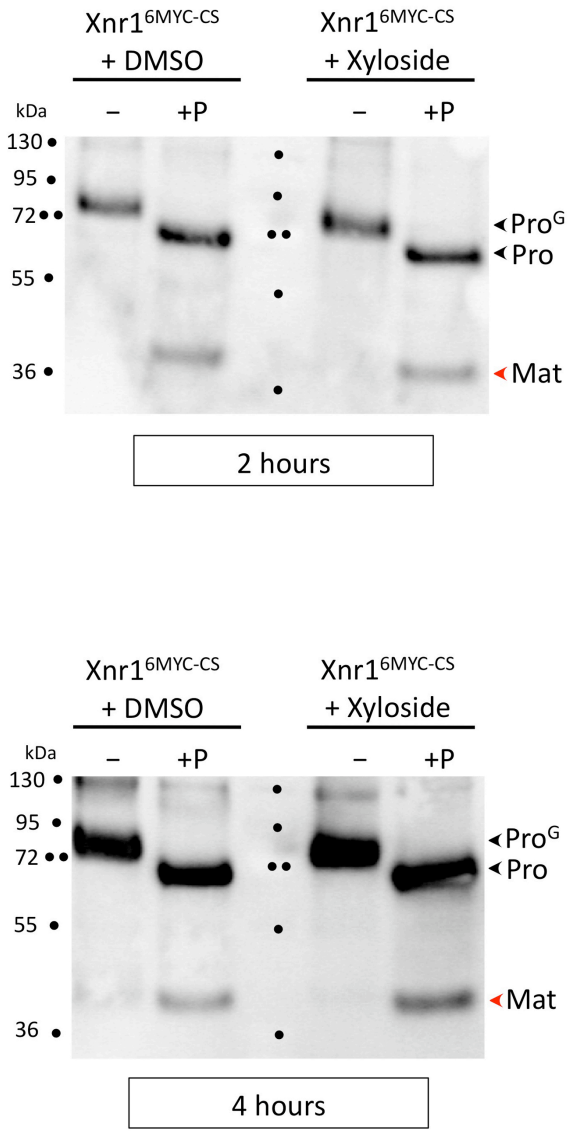

Fig. 3.14 Xyloside does not affect secretion of Xnr1$^{6MYC-CS}$ from AC graft.
At both time points examined, Xnr1$^{6MYC-CS}$ secretion from ACs is not affected by the addition of xyloside. **Top Panel:** Conditioned media collected after 2 hours shows no difference in Xnr1$^{6MYC-CS}$ secretion in the presence of xyloside versus the DMSO control. +P, addition of PNGaseF, reveals fraction of mature ligand that was N-linked glycosylated. **Bottom Panel**: Conditioned media collected after 4 hours shows equivalent amounts of Xnr1$^{6MYC-CS}$ was secreted in xyloside as it was in DMSO controls. Pro^{G}: Glycoslyated proprotein, Pro: non-glycosylated proprotein after PNGase F, Mat: non-glycosylated mature ligand, after PNGase F addition.

Discussion

Few studies exist of Nodal and Lefty movement during the stages of embryogenesis relevant to their asymmetric expression period (Hamada, 2008). It is likely, especially given our results, that ligand movement in blastula-gastrula stages is different from that in tailbud-somitogenesis embryos. Studies on focally secreted GFP-tagged mouse Nodal and Lefty2 in chicken embryos implied that both move far, with Lefty2 traveling farther and faster, supporting a reaction-diffusion relationship (Sakuma et al., 2002; Turing, 1990). More recently, however, movement of tagged Nodal from the node was difficult to detect (Oki et al., 2007). Our findings extend our knowledge of L-R signaling processes driven by Nodal/Lefty, by increasing our understanding of the features affecting tissue penetration and activity of this critical ligand pair. We generated biochemical evidence for the proper cleavage and glycosylation of tagged ligands secreted from AC grafts, measured faster relative movement of Lefty compared to Xnr1, and detected a transfer along CSPG/HSPG-rich ECM that we propose is central to the fast directional expansion and shut-down of *Xnr1* expression within L LPM (Fig. 3.15). Our findings provide a foundation for a future biochemical dissection of ECM-ligand interactions, including determining the relevant structural features, and if there are, for example, differential on-off rates and affinities for CSPG compared to other proteoglycans.

ECM and Nodal signaling

ECM interactions of several TGFβ-family ligands affect tissue transport or cell accessibility either positively (facilitation) or negatively (sequestration) (Bernfield et al., 1999). A permissive role for heparan sulfate in mesoderm induction mediated by activin was reported (Itoh and Sokol, 1994).

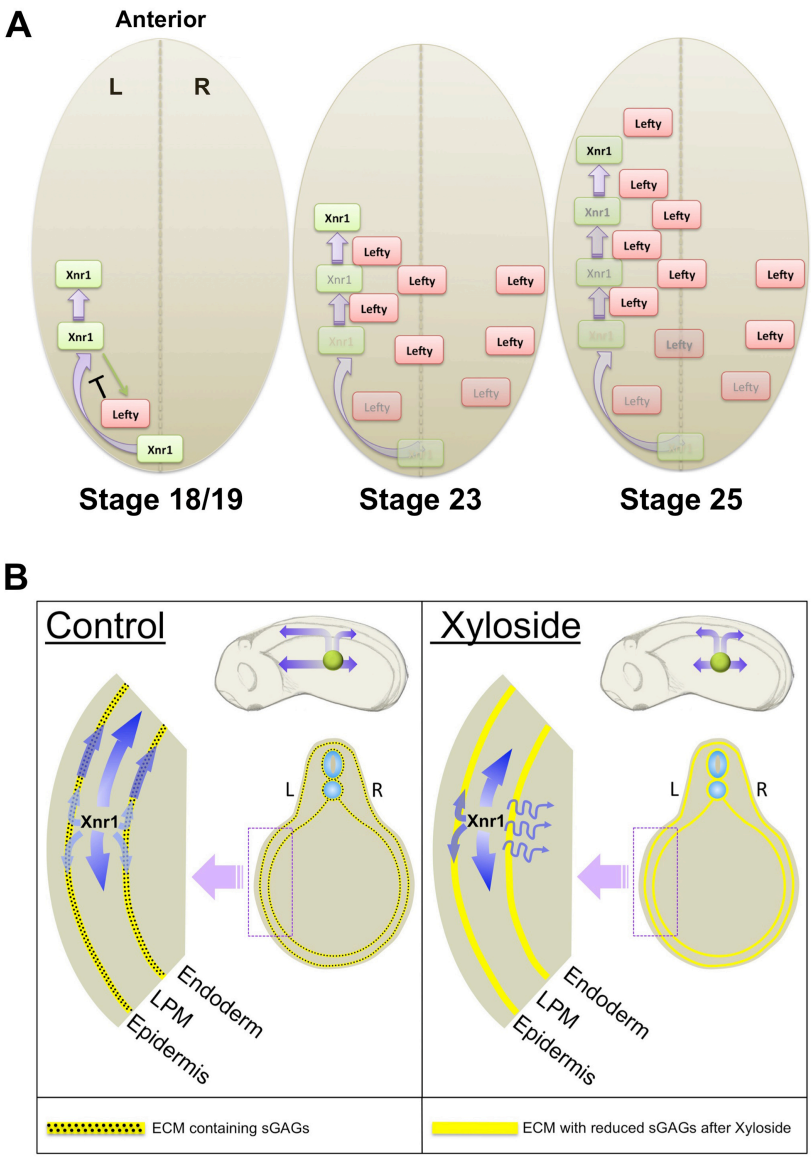

Figure 3.15 Model for effect of sGAGs during asymmetric gene expression. (**A**) Asymmetrically-produced Xnr1 in the L LPM beginning at stage 18/19 begins to move anteriorwards, concentrated over ECM of L LPM/periaxial tissue surfaces, and begins to induce Lefty. Lefty travels anteriorly along L LPM/periaxial ECM more rapidly than Xnr1, and into endoderm. Lefty catches up to Xnr1, shutting down Xnr1 autoregulation. Lefty stability may prevent a second Xnr1 wave from initiating. (**B**) sGAGs (stippling) within LPM and periaxial ECM (yellow line) help retain a significant fraction of Xnr1 in proximity to L LPM, while Lefty (not shown) moves more freely to R LPM either directly through endoderm or 'up-and-over' the dorsal axial midline. sGAG removal allows lateral travel of Xnr1 into endoderm, reducing LPM signal and planar movement. This orthogonal transfer reduces the strength of Xnr1 autoregulation within LPM.

In *Drosophila* and mouse, sulfated proteoglycans aid in transporting BMPs, FGFs, and Nodal (Belenkaya et al., 2004; Bernfield et al., 1999; García-García and Anderson, 2003; Ohkawara et al., 2002; Oki et al., 2007; Scholpp and Brand, 2004; Yu et al., 2009). A conserved HSPG-binding motif identified as an N-terminal basic residue region in some BMPs (Ohkawara et al., 2002) is absent from Xnr ligands, and it is possible that multiple, distributed low-affinity interactions mediate ECM-binding in other TGF-b ligands. Ligand range was explored in the zebrafish Nodal ligands, Cyclops and Squint. Acidic residues in the N-terminal region of Squint but absent from Cyclops, proposed to confer long-range capacity (Jing et al., 2006), are not conserved in Xnrs. We speculate that mature-region Nodal glycosylation, present only in some vertebrates (Le Good et al., 2005), could significantly affect ECM binding (on-off rate, affinity), which as discussed below may be particularly relevant in *Xenopus*. The evidence from pharmacological inhibition of sGAG modification that CSPG and potentially HSPG aid the rapid movement of Xnr1 over extensive distances, possibly with a superimposed directional bias, highlights the importance of extracellular spatial regulation of ligand function.

Apicobasal polarization of LPM and separation into distinct somatic and splanchnic layers occurs only after *Xnr1*/*Lefty* asymmetric expression, meaning that we currently rule out a role for polarized secretion of ligands through specific cell surfaces. Indeed, while ECM showed the highest epitope-tagged Xnr1 signal, it was also distributed around most, possibly all, LPM cells. We currently speculate on a dual role for LPM-flanking ECM: first, to help Xnr1/Nodal move rapidly in the plane of the LPM, both anteriorly and orthogonally towards the dorsal midline (discussed more below), and second, to keep the level of Nodal in the vicinity of the responsive LPM high enough to maintain its feedforward loop, which underlies the expansion of *Xnr1* expression (Ohi and Wright, 2007). These features are important for the relatively unstable Nodal, and

less so for the more stable Lefty, which has the ability to depart the ECM and move contralaterally to prevent spurious activation of *Nodal* expression in the R LPM. The high fractional transfer (Fig. 3.9D) suggests that Lefty produced in spatially restricted fashion could have the remarkable ability to bathe large areas of the embryo, for a significant period, in an anti-Nodal suppressive influence.

We hypothesize that dorsal-ward movement of Xnr1 from the LPM to the midline, necessary for inducing axial tissue expression of *Lefty*, is aided by the relative progressive dorsal enrichment of CSPG/HSPG-containing ECM in LPM, and around axial/periaxial tissues. Although not detected with the current antibody, the dorsal CSPG (Fig. 3.3) could extend lateroventrally, in a graded fashion, towards the splanchnic LPM/endoderm interface, therefore representing a significant directional attractive influence on Xnr1 and Lefty. Ligand flux up this 'ECM gradient' may bring Nodal rapidly to the axial midline where it induces a secondary source of Lefty that can also move towards R LPM.

We also suggest that transport facilitation by dorsally biased CSPG/HSPG within the LPM is overlain by an anteriorward CSPG enrichment, especially noticeable periaxially and correlated to the greater maturity of more rostral regions. Biased ligand movement along both ECM gradients, working together with the relatively high ventral levels of BMP (Hemmati-Brivanlou and Thomsen, 1995), which suppresses Nodal autoregulation, could be major influences defining the dynamic *Xnr1* expression domain. Future real-time tracking of molecular movement, or pulse-chase-labeling, might allow more direct determination of routes and range of movement. We might also assess the relative amount of Xnr1 that moves anteriorly only along LPM, compared to moving orthogonally towards axial regions then forward along the CSPG/HSPG tissue-maturity gradient, to return to the dorsal LPM slightly more anteriorly. The latter route could intensify *Xnr1* expression in dorsal LPM, a feature of endogenous *Xnr1* expression (Ohi

and Wright, 2007; Sampath et al., 1997), as well as help generate an anterior-ward sweep to Xnr1 autoactivation loop.

Lefty travels farther than Xnr1, with different tissue penetration

Our data further support a reaction-diffusion relationship between Xnr1/Nodal and Lefty during L-R patterning, because the feedback antagonist Lefty moves faster and is more stable, than the Xnr1 inducer (Nakamura et al., 2006; Sakuma et al., 2002; Turing, 1990). These properties in Lefty are likely important in limiting the time and range of influence of Nodal by suppressing its autoregulation and finally terminating its expression. In the SELI model (Nakamura et al., 2006; Tabin, 2006), L-sided *Nodal* self-amplification drives expansion of unilateral expression, and R-sided contralateral *Lefty*-mediated suppression is critical for its 'L-on, R-off' pattern. In *Xenopus* embryos, after an asymmetric signal is received from the posterior L-R coordinator region, *Xnr1* expression initiates in posterior L LPM, and begins expanding anteriorly ahead of the expression of *Lefty*. Too brief a delay between *Nodal* and *Lefty* expression, or inappropriate relative movement of inducer and antagonist, would be deleterious. The lack of a timing advantage to *Xnr1* expression would allow Lefty to set off too fast, rapidly squelch Xnr1 feedforward autoactivation, and prevent asymmetric signaling from reaching far enough forward to pattern the cardiac anlage, or even less anterior tissues. Or, Lefty might move to the axial midline too quickly, prevent the orthogonal Nodal-induced *Lefty* expression, and reducing or removing its contribution to the contralateral suppression of *Xnr1* expression, confuse L-R patterning almost immediately. Within this framework, the significant transfer of Lefty to the R LPM after production from L-sided grafts provides direct evidence for an embryo-wide transfer of Lefty. We note, however, that the relative amount of Lefty moving directly through the endoderm or 'up-and-over'

the dorsal axial midline were not determined, and both paths could contribute meaningfully.

We detected a 'loosening effect' on Xnr1 ligand accumulation on ECM when sGAG modification was xyloside-blocked. Ligand signal was reduced on the ECM facing the epidermis and in dorsal periaxial regions, concomitantly increased on splanchnic-endodermal ECM, and detected permeating the interstitial space within endoderm. This loosening effect greatly reduced the overall range and speed of Xnr1 movement. We suggest that such ECM interactions are a substantial directional transport influence, and plausibly explain how a rapid anterior shift of *Xnr1* expression along LPM could be driven solely by autoactivation. We note that in the different context of blastula/gastrula-stage AC tissue, a loosening effect of ECM disruption was proposed to explain the increased range of Xnr2 (inferred by target gene response) in dissociated-then-reaggregated explants compared to non-dissociated ones (Jones et al., 1996).

Ultimately, a complete understanding of L-R patterning will include linking the threshold-dependent shaping of a spatiotemporally dynamic 'Nodal activity contour map' to the cell biological initiation of asymmetric morphogenesis. In different species, the activity map could be related to specific tissue structure and ECM distribution/composition, which may have become adapted to each other in accordance with the embryo's morphology, size, and developmental strategy. Similar influences to those detected here might exist in non-vertebrates that use Nodal signaling to regulate asymmetric embryogenesis.

One should not underestimate the relevance of an ECM-facilitated transfer of ligands within embryos the size of *Xenopus*, which increase in length from 1.5 to 2.8 mm during the ~7 hour period of *Xnr1* expression (Stages 19-25), with LPM lengthening from approx. 0.8 to 1.3 mm. We previously suggested that Nodal autoregulation, working only by cell-to-cell-to-cell relay, might be incapable of working fast enough to expand the

Xnr1 expression domain along the entire LPM within this short time. Despite the significant embryo extension, our clearance estimates (Fig. 3.10) imply that passive ligand conveyance on cells moving away from the AC source cannot account for the long-range movement of Xnr1 and Lefty. Therefore, a prospective Xnr1 movement of, conservatively, 500 microns in 5 hours (Fig. 3.12) results in no need to invoke additional mechanisms to speed up Nodal autoregulatory spreading. This is particularly important considering that a single Xnr1 gene is active in tailbud stages, versus the transcriptional relay between multiple Xnrs existing during blastula-gastrula stages (in which we speculate a reduced effect of ECM interaction).

Ligand processing and clearance

Our assays relied upon expressing epitope-tagged proteins from AC grafts, an approach chosen because of the lack of high signal-to-noise antibodies, and the likely low levels of endogenous Xnr1 and Lefty. Our biochemical analysis strongly supports the idea that the predominant Xnr1 and Lefty molecules moving around the embryo represent properly processed ligands. Such analysis, to our knowledge, was not performed previously and is important in several respects. First, our method did not overwhelm the secretion or proprotein-processing capacities of source/host tissues and, second, the signal detected and perdurance/clearance estimates reflect, for Xnr1 and Lefty, properties of the mature, glycosylated ligands. We cannot rule out that, ultimately, the dynamics of movement of the natural ligands differ from those determined here, but we did compare functional proteins carrying identical Myc tags. It is possible that a larger tag (e.g., GFP) would more dramatically alter ligand movement and ECM-association and, moreover, our experiments showed inactivity for Xnr1^{GFP} and Lefty^{GFP} (Fig. 3.6). A complete understanding of mechanisms regulating ligand movement and tissue responses could require developing new tools and methods for precisely detecting

ligand that is ECM-bound or 'freely moving', versus engaged at its receptor, for quantitative correlation with downstream events such as nuclear translocation of phospho-Smad2.

Structural predisposition of splanchnic and somatic LPM to Nodal signaling

The differential distribution of ECM components at somatic-epidermal compared to splanchnic-endodermal interfaces (laminin, HSPG, and fibronectin are higher in somatic LPM ECM) may be associated with initiating or maintaining the squamous or columnar cell shapes inherent to each LPM layer. A future goal is to determine how Nodal signaling causes unilateral alterations in LPM cell shape (likely those in the splanchnic layer after formation of the coelom), the degree to which they are broad-ranging or focal, and how they cue and drive asymmetric morphogenesis. Differential cell shape alterations between L and R splanchnic LPM have been linked to chick midgut chirality (Davis et al., 2008). Indeed, the formation of a columnar splanchnic layer may be a structural prerequisite for enacting the cell shape rearrangements preceding asymmetric morphogenesis: *Nkx3.2*-null mice do not form columnar splanchnic cells, with subsequently disrupted asymmetric anatomy (Hecksher-Sørensen et al., 2004).

CHAPTER IV

CYTOARCHITECTURAL ALTERATIONS DRIVING TISSUE MORPHOGENESIS IN RESPONSE TO ASYMMETRIC *NODAL* EXPRESSION IN *XENOPUS*

Introduction

This chapter will focus on the current understanding of the mechanisms driving asymmetric displacement of the gut tube from the midline, which presumably serves as the foundation for its overall, more complicated and chiral looping process, identifying several chasms in our understanding and ways that these gaps might be filled. The processes controlling asymmetric placement of internal organs may be quite disparate between model organisms as a result of drastically different embryo size and body plans (such as the amount of yolk present). For example, some of the initial asymmetric morphogenetic movements in the zebrafish gut have been described, and attributed to asymmetric LPM migration behaviors: the left LPM migrates dorsal to the endodermal mass, while the right LPM migrates more ventrolaterally, the latter pushing and exerting a leftward displacement of the endodermal rod (Horne-Badovinac et al., 2003). While this is an important finding, it is likely applicable to other vertebrate model systems: zebrafish LPM does not encircle the entire endodermal rod (perhaps because the entire embryo develops as a 'cap' over the very large yolk mass) unlike gut morphogenesis in frogs or the generation of midgut chirality in chickens. With this diversity in mind, it may be unrealistic to assume that there is one unifying process of gut morphogenesis that occurs across all vertebrates. Conserved patterns of *Pitx2c* expression as well as the ultimate asymmetric positioning of organs, however, indicates that there may be mechanistic elements of asymmetry generation common to many vertebrates. Moreover, while it is unlikely that Pitx2 is solely responsible for driving asymmetric organ

morphogenesis, Pitx2 is currently the only link between asymmetric L-sided *Nodal* expression and subsequent proper organ placement, and thus I feel it is warranted to present a detailed analysis of what is currently known about Pitx2 in addition to the descriptive analyses of gut morphogenesis.

Descriptive analyses of asymmetric organ morphogenesis

Understanding the instructive contributions from each tissue layer (somatic LPM, splanchnic LPM, endoderm) to generate gut chirality is essential. In contrast to the process described in zebrafish above, endoderm in frogs, chickens and mice is fully encased in LPM during the relevant stages where gut bending first occurs. Although only endoderm gives rise to the gastrointestinal tract epithelium, morpholino knockdown of some genes such as FoxF1, which shows LPM-restricted expression (Tseng et al., 2004), severely disrupted gut development. Thus, it is unclear if LPM-driven displacement of endoderm from the midline, endoderm-autonomous cell shape alterations, or a synergistic interaction between the two tissue layers ultimately triggers the process of asymmetric morphogenesis. Potentially, endoderm or LPM explant experiments could address this question but, by disrupting adjacent tissue layer communication and the instructive factors they might secrete, this type of experiment may not generate information relevant to an intact embryo. While *Nodal* is asymmetric within the L LPM, *Lefty* is expressed asymmetrically in the L anterior endoderm in addition to within the L LPM, indicating a registration of Nodal signals within endodermal tissue, which begs the question: Do Nodal signals within the endodermal tissue enact a change in tissue architecture?

If the LPM is, at least in part, directing asymmetric morphogenesis, it is important to note that the somatic and splanchnic LPM (derived as two separate laminae from an initial common LPM layer; see Chapter III) will separate. This separation generates the

embryonic coelom, a buffering fluid-filled space present in all vertebrates to help to protect the organs from external insults. The timing and mechanism of coelom formation is generally poorly understood but could serve as an important structural feature for facilitation of gut chirality, either passively by allowing space for the gut to jog, deform or kink into or, perhaps, since the coelomic cavity is fluid-filled, it could play a more active role by exerting some force of its own, perhaps in response to physical forces from adjacent tissues. It is easier, however, to imagine the coelom playing a passive role. Coelom formation separates the somatic and splanchnic LPM layers, making it uncertain if both LPM layers could play a role in gut tube shaping or if its asymmetric morphogenesis is accounted for by influences generated solely from within the splanchnic LPM, the layer that is in direct contact with the gut epithelial tube. It is also possible that the relative physical contributions from the different tissue layers (LPM versus endoderm) fluctuate along the A/P axis of the embryo. It is easy to see that the extensive process of gut morphogenesis could involve multiple inputs from different tissues, and that the process could include interactions with accompanying basement membranes and tissue spaces. More research is needed to move closer to a comprehensive understanding of the different influences that generate the first asymmetries within the gut tube.

The Slack laboratory has published substantial systematic yet descriptive analyses of the *Xenopus* gut structure to illustrate how the endodermal mass coils over time (Chalmers and Slack, 1998; Chalmers and Slack, 2000; Chalmers et al., 2000). Examination of the frog gut anatomy from 3 to 5 days post-fertilization, in combination with *in situ* analysis of regionally-expressed RNAs and basic histology resulted in a description of the timing and direction of stereotypically reproducible looping events. These studies did not address the initial stages during which the midline-located

endoderm becomes displaced, as they focused only on stages after asymmetric positioning of anteriorly-located organs (e.g. liver) had already begun.

Transcriptional effectors of morphogenesis: *Pitx2*

Pitx2c was introduced in Chapter I as the sole currently identified transcriptional target of asymmetric Nodal signaling and the idea that, as such, it likely represents a key entrance point into understanding any instructive roles that the LPM might contribute to organ chirality. Now it is important to understand how Pitx2c drives cellular asymmetry generation, for example, through processes such as apicobasal constrictions or cytoskeletal contractions. Forced overexpression of Pitx2a (a splice isoform of Pitx2c) in HeLa cells triggered cell shape changes 48-72 hours after Doxycycline-induced expression: Pitx2-overexpressing cells became more relaxed (i.e. spread) and increased their cell-cell contacts by upregulating N-cadherin and β-catenin at the cell periphery (Wei and Adelstein, 2002). Application of soluble inhibitors against different GTPases indicated that Pitx2a was working through Rac1 to cause changes in the actomyosin cytoskeleton (Wei and Adelstein, 2002). Although there has not been any follow up to this study to see if the same pathway is active *in vivo*, these experiments were the first to show that the presence of Pitx2 is sufficient to dictate cell relaxation and spreading. This leads to models where Pitx2c might induce a relative relaxation of L LPM cells whereas R LPM cells, without Pitx2c, might stay relatively constricted.

The Nascone-Yoder laboratory has reported studies that attempted to associate the location of *Pitx2c*-expressing cells with specific tissue architectures that might be responsible for asymmetric gut looping *in vivo*. Late stage fate-mapping experiments showed that L and R cells contributed equally to organs that were asymmetrically placed. Interestingly, the authors discovered a predisposition of cells from the L LPM (those expressing *Pitx2c*) to lie in concave curvatures of the gut tube whereas R LPM

cells (Pitx2c-non-expressors) were more likely found contributing to convex surfaces (Muller et al., 2003), and R-sided overexpression of *Pitx2c* RNA generated local ectopic concave surfaces. Measurement of whole-mount gut tube length from stage 41 to 43 showed that the R side was longer than the L. Observations of L and R LPM mitotic events (unclear if both somatic and splanchnic LPM were examined) within the midgut showed no differences in proliferation rates, indicating that a unilateral increase in cell number could not explain the observed asymmetries at this stage. In this report, the authors proposed that the cells corresponding to the midgut region on the R were more elongated than those on the L, though cell shape was never examined at higher resolution to confirm this idea. This proposal is somewhat contrary to the work from the Adelstein lab, in that it might be expected that L-sided *Pitx2c* would cause cell spreading, allowing the L LPM cells to be more elongated than the R. It is also important to note that the authors never looked at absolute cell number on the R versus L (for example, by DAPI staining) to show that there were not initial biases in L versus R cell number, which would be maintained if the proliferation rates were equal on the L and R sides. Nonetheless, this report raised an interesting point that intrinsic differential cell shapes on the L versus the R might initiate bending events in the gut, but the authors did not follow up these studies. Ideally, one could imagine moving onward to a higher resolution imaging of L- and R-sided cells in thick vibratome sections, or with whole-mount imaging, to allow a 3-dimensional analysis of L- and R-sided cell shape, as well as a spatiotemporal characterization of cell shape changes over time to address this theory.

The studies of chicken midgut chirality reported from Cliff Tabin's lab have potentially elucidated an LPM-instructive role in generating a regional gut asymmetry. The midgut dorsal mesentery, a splanchnic LPM derivative, displays structural L-R differences downstream of asymmetric *Nodal* and *Pitx2c* expression. Dorsal mesentery

(DM) tissue on the L, which asymmetrically expresses the *Pitx2c*-induced transcription factor gene *Islet1*, has a columnar-shaped epithelial layer that faces the coelom and a more condensed mesenchymal layer underneath (Davis et al., 2008). The DM tissue on the R is dramatically different in that it asymmetrically expresses *Tbx18* and has a cuboidal outer epithelial layer with a loosely packed, more spread-out character in the underlying mesenchyme. The authors proposed that it was the differential packing of cells on the right versus the left side that generated a leftward midgut tilt. This mechanism may be regionally conserved in a small part of the mouse midgut as transient left-sided *Islet1* and right-sided *Tbx18* expression were observed in the DM along with left columnar-shaped epithelium versus right cuboidal-shaped epithelium (Davis et al., 2008). To address causality, the authors performed a set of experimental manipulations to alter expression of *Pitx2c.* Pitx2-null mice, which develop discordant organ situs, have bilateral *Tbx18* expression, absent *Islet1* expression, and a midline-located (unbent), non-tilted midgut. Chicken embryos with forced bilateral *Nodal* expression displayed bilateral *Pitx2c* and *Islet1* expression, which also resulted in a midline, non-tilted gut (Davis et al., 2008).

While it may indeed be useful to generate a list of the arsenal of transcription factors expressed differentially in the R or L LPM, it will be more insightful to begin uncovering what effector genes these transcription factors regulate or induce to directly drive cell shape changes that will generate organ chirality. In a follow-up to the previous paper, the Tabin lab utilized *in silico* modeling to propose that differential adhesion properties in the L versus R mesenchymal cells (which underlie the outer DM epithelial cells) could communicate with the overlying epidermal layer and generate a synergistic contraction on one side relative to the other (Kurpios et al., 2008). Immunodetection analyses of N-cadherin, a cell adhesion protein, were interpreted as showing that it was strongly produced in the L mesenchymal cells but absent from the R mesenchymal cells

(Kurpios et al., 2008). The authors suggested a model in which L-sided *Pitx2* expression regulates *Islet1*, which in turn upregulates N-cadherin in L-sided mesenchymal cells only. The study did not show what cellular effectors downstream of *Pitx2* and *Islet1* specify the L-sided outer columnar cell layer shape nor did it determine if N-cadherin is a transcriptional target of *Islet1*. It is, however, important to note that these studies are at least in partial agreement with the original cell culture work from the Adelstein lab demonstrating that N-cadherin is upregulated after Pitx2 expression. It is difficult to assess how the columnar versus cuboidal outer epithelial layer of the DM might relate to Pitx2-induced cell spreading described in the Adelstein paper. Moreover, it might be dangerous to make direct extrapolations from the *in vitro* work performed in HeLa cells to what occurs *in vivo*.

More recently, an effector protein with an endodermal expression pattern restricted to the foregut region of the gastrointestinal tract during gut coiling was characterized by the Wallingford lab. Shroom3 was previously implicated in apicobasal constriction during *Xenopus* neural tube closure, and has now been shown essential in asymmetric gut tube morphogenesis. Chung and colleagues demonstrated that Shroom3 and Pitx1 were coexpressed in the developing foregut endoderm, although it was unclear from the *in situ* images if Shroom3 was also expressed in the overlying splanchnic LPM. In animal cap assays, Pitx1, Pitx2 and Pitx3 directly induced transcription of *Shroom3*, indicating a conserved ability for Pitx family members to activate cell-shape-change effectors (Chung et al., 2010). Morpholino-oligonucleotide-based loss-of-function for Pitx1 or Shroom3 targeted to the ventral endoderm resulted in knockdown of *Pitx1/Shroom3* expression within the archenteron floor at stage 32 and prevented the apicobasal constriction of lumen-facing cells required for the formation of the V-shaped morphology of the archenteron opening (Chung et al., 2010). At later stages, these embryos displayed severely disrupted gut coiling, though this is likely

secondary to improper narrowing of the archenteron. The authors did not examine the interaction of asymmetrically L LPM-expressed *Pitx2c* and Shroom3, which might be more relevant to address the type of LPM:endodermal interactions we suggested in the opening paragraphs of this chapter.

The current understanding of gut morphogenesis is hazy with several major questions unanswered, including how factors such as tissue:tissue interactions, cell shape, tissue thickness, cytoskeletal composition and differential cell adhesion affect the process of asymmetric morphogenesis. Given that previous research mentioned above has demonstrated that *Pitx2c* expression is required for the establishment of *situs solitus* and associated with driving changes in cell shape, the high-resolution examination of the L and R LPM intracellular architecture prior to asymmetric morphogenesis might reveal Pitx2-dependent alterations that represent the initiation of more global cell shape changes on the L versus the R. Specifically, we were looking for LPM-specific changes as a consequence of Nodal signaling that show L-R differences based upon a registration of the Nodal signal within the L but not the R cells during stages when *Pitx2c* is actively and robustly expressed. In this chapter, I present my data on actin cytoskeletal asymmetries, refer to a situs-switching experiment in which Xnr1 might affect focal actin asymmetries and, in the discussion, I will speculate on how broad, continuous L LPM *Pitx2c* expression might serve to prevent an inherent program of cell contractions.

Results

Maturation of the LPM-adjacent basement membrane is concomitant with apicobasal polarization of the L and R LPM

As we previously described (see Chapter III, Figs. 3.4, 3.5), there is an anterior-to-posterior wave of apicobasal polarization that occurs symmetrically within the LPM after *Xnr1* is asymmetrically expressed. In an effort to better characterize the L and R LPM, we also examined the basement membrane on the somatic and splanchnic LPM faces, which we showed to be relatively immature during L-R patterning (see Chapter III, figure 3.1). At stage 17 (prior to asymmetric *Nodal* expression), laminin immunostaining was only detectable at low levels periaxially (i.e. around the notochord, ventral neural tube) (Fig. 4.1, left column). At stage 23, just a few hours later, laminin was detected laterally at the interface between the somatic LPM and epidermis, but was still absent from the splanchnic:endodermal interface (Fig. 4.1). At stage 25, in the first ~100 μm of the L and R LPM just posterior to the pharyngeal arches, laminin was detected flanking both faces of the LPM. Deposition of laminin appeared to follow an anterior-to-posterior maturation process like the apicobasal polarization of the LPM, which could be attributed to the generation of nascent mesoderm posteriorly (Slack and Tannahill, 1992). By stage 28, laminin was detected symmetrically flanking the entire length of LPM (Fig. 4.1).

Asymmetric displacement of the endoderm is first evident at stage 38

To better understand how the LPM might contribute to rearrangements of the gut tube, it was first necessary to better define when asymmetric positioning of the internal organs was evident. According to Muller et al. (2003), the first gut bending events initiate “subtly” between stages 38-40, a period of approx. 10 hours.

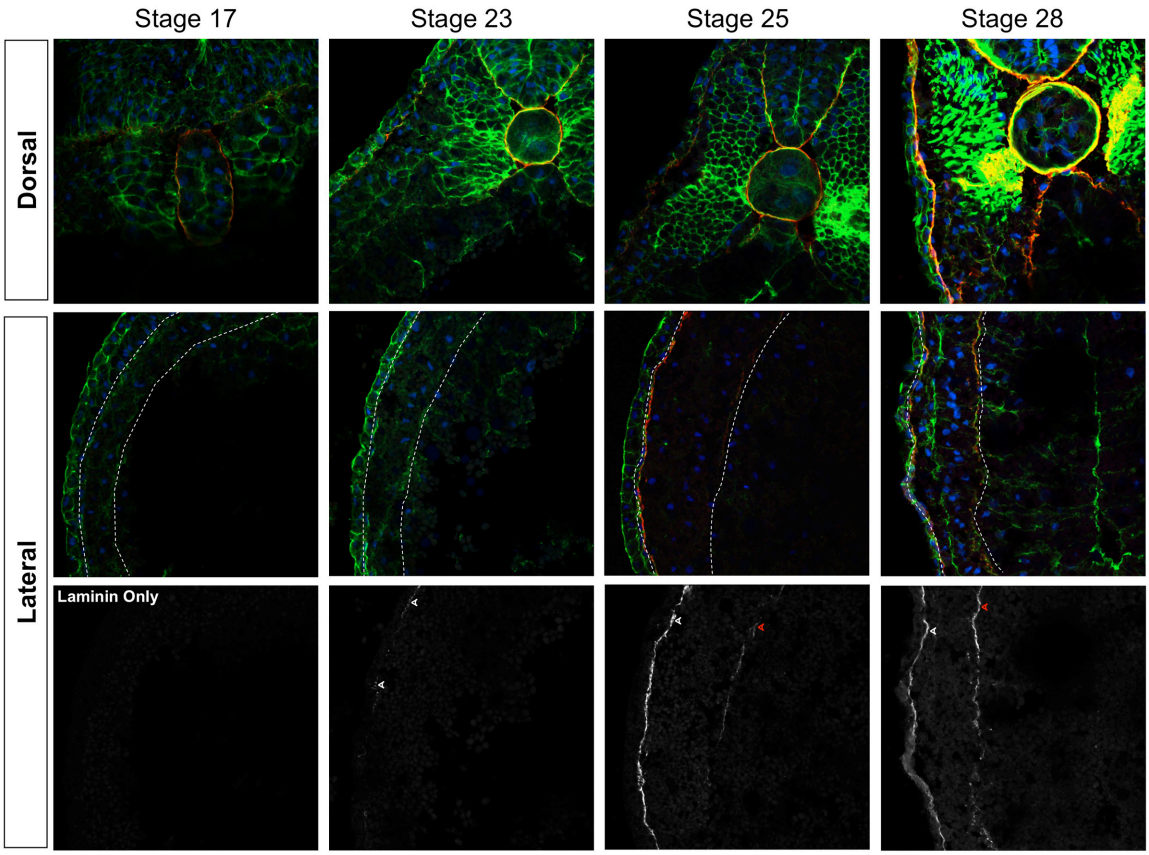

Figure 4.1 Progressive Anterior-to-Posterior maturation of the somatic and splanchnic LPM basement membranes. Transverse cryosections were used to detect laminin (red; grayscale in bottom panel), F-actin (by fluorescent phalloidin; green) and nuclei (DAPI; blue); dorsal panels focus axially/periaxially, lateral panels focus on LPM. White arrowheads, epidermal:somatic LPM ECM; red arrowheads, splanchnic LPM:endodermal ECM. **Top panels**: Laminin is present in the ECM, periaxially around the notochord at all stages shown. Laminin subsequently appears in basement membrane around the somites, ventral neural tube and endoderm border by stage 25. **Middle and bottom panels**: Laminin is not detected at the somatic:epidermal or splanchnic:endodermal interface at stage 17. At stage 23, laminin was detected adjacent to the somatic LPM:epidermal interface (white arrowhead). At stage 25, laminin was also detected within the first 100 µm of basement membrane adjacent to the splanchnic LPM (red arrowhead). By stage 28, laminin was detected along the full A/P length of the somatic and splanchnic LPM.

These conclusions were generated from examination of whole-mount gut tubes, thus we sought to refine this ten-hour window by examining embryos in transverse cryosections. Prior to stage 35-36, the endoderm was a linear tube, consisting of 1-2 cell layers in the anterior and several cell layers (>4) in more posterior regions of the embryo. In transverse sections along the A/P axis, the luminal opening was narrow and displayed apicobasal polarity (Fig. 4.2, top row). It is important to note that, at this point in development, we are already able to differentiate between some of the arising foregut structures such as the liver, based on morphology. At stage 37, the gut tube still appears linear with respect to the midline in transverse sections (Fig. 4.2), and the liver anlage is directly underneath the foregut. At stage 38, the liver anlage was no longer in alignment with the overlying foregut, but had rather become displaced to the R (Fig. 4.2). Just posterior to the liver, however, the gut was still midline-oriented. Thus, we defined stage 38 as the first stage during which morphological asymmetries appear, and they began as expected in the more anterior, mature regions of the developing gastrointestinal tract. Significant displacement of the gut tube (coiling, bending) continues over the next several stages, with progressively posterior localization of these events (Fig. 4.2).

L-R LPM cytoarchitectural differences appear after asymmetric *Xnr1* expression but prior to the first gut bending events

After defining stage 38 as the developmental time point when gross morphological asymmetries first appeared in the endoderm, we extended our characterization of L and R LPM cytoarchitecture during the stages leading up to this point, as a continuation of the LPM characterization reported in chapter III.

Figure 4.2 Transverse sectional analysis of embryos reveals first morphological asymmetries at stage 38. 10x images of transverse cryosections were used to detect laminin (blue), F-actin (via phalloidin; green), E-Cadherin (red) and nuclei (gray). At stage 35-36 and 37 the endodermal mass is midline-oriented from the anterior to posterior. At stage 38, the liver anlage (white arrow) is tilted to the right and the overlying foregut endoderm is tilted slightly to the left (red arrow) and a kink in the endodermal mass, posterior to the liver, is also apparent (white arrow). By stage 40, the liver has shifted further right while foregut endoderm is displaced to the L. Posterior to the liver, the gut tube has begun to coil and the posterior-most part of the gut tube has begun to retract (data not shown). At stage 41, more than half of the endodermal mass has begun to coil.

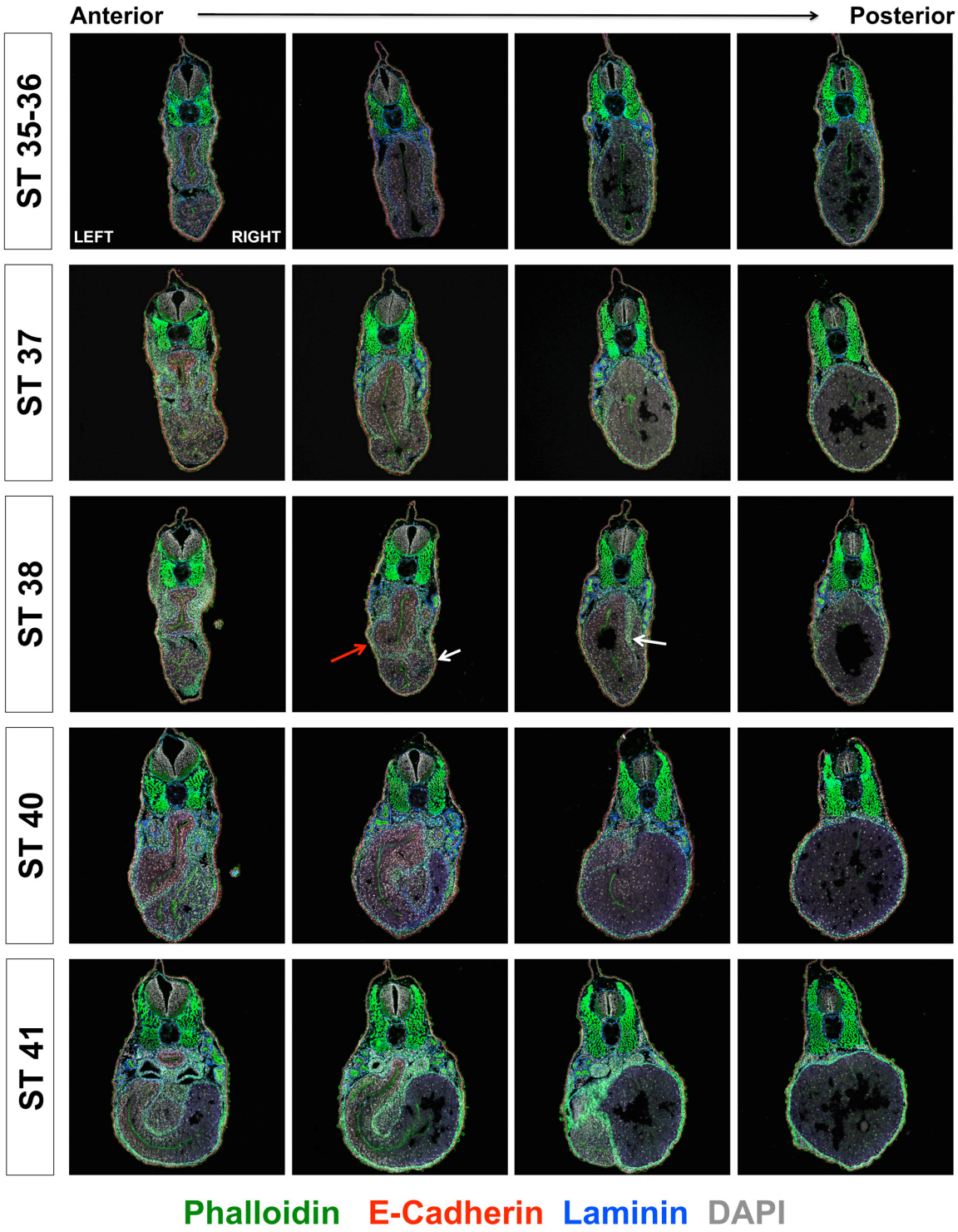
Anterior
Posterior
ST 35-36
ST 37
ST 38
ST 40
ST 41
LEFT
RIGHT
Phalloidin
E-Cadherin
Laminin
DAPI

As reviewed in the introduction above, my focus in this chapter will be to try to associate the architectural alterations I see with the presence of continuous L-sided *Pitx2c* expression to make potential functional correlations.

The same polarity markers mentioned in chapter III (e.g. β-catenin, β1-Integrin, ZO-1, aPKC, phalloidin) were utilized. Similar to stages 17-25, no overt differences were observed between the L and R LPM when we examined E-Cadherin, β1-Integrin, β-catenin, ZO-1, phalloidin or aPKC at stages 28-34 (data not shown). Beginning at stage 35-36 (50 hpf), subtle differences in the intensity of fluorescently-labeled phalloidin, which detects F-actin, were apparent in the R versus the L LPM (Fig. 4.3). Whereas phalloidin fluorescence detected F-actin diffusely, at low levels, and essentially uniformly throughout all cells of the L LPM, cells in the R LPM had more F-actin in a more compact configuration (Figure 4.3, top panel). It was not possible to see more than relatively gross differences in F-actin intensity or organization at this magnification, but it was rapidly obvious that the L-R difference became increasingly amplified at each subsequent stage examined, still remaining focal in the R LPM (Fig. 4.3). At stage 40, after gut bending had initiated anteriorly (Fig. 4.2, stage 40), the R LPM, both in anterior areas surrounding the actively coiling endoderm and posterior locations surrounding midline-oriented endoderm, displayed significantly more intense F-actin.

R LPM actin cables are more thickly bundled

While F-actin intensity differences were apparent at 40x magnification, it was unclear what this information meant. To begin to uncover whether or not the actin bundling in R versus L cells could connect to an active redistribution of the actin cytoskeleton that controls the overall cell shape as part of the asymmetric morphogenesis program, R and L LPMs were examined at higher resolution (100x magnification, 3x optical zoom).

Figure 4.3 R LPM cells show more intense, contracted F-actin whereas L LPM cells have more dispersed F-actin. 40x images of transverse cryosections of L and R LPMs analyzed for F-actin (via phalloidin; green), E-cadherin (red), laminin (blue) and nuclei (gray). Beginning at stage 35-36, F-actin intensity was greater in the R LPM than in the L. This R-L intensity difference became amplified with each progressive stage. Intensity differences are more easily seen in the R-sided panel where a spectral analysis has been applied to only the F-actin channel (blue and green, low signal intensity; red and white, high signal intensity).

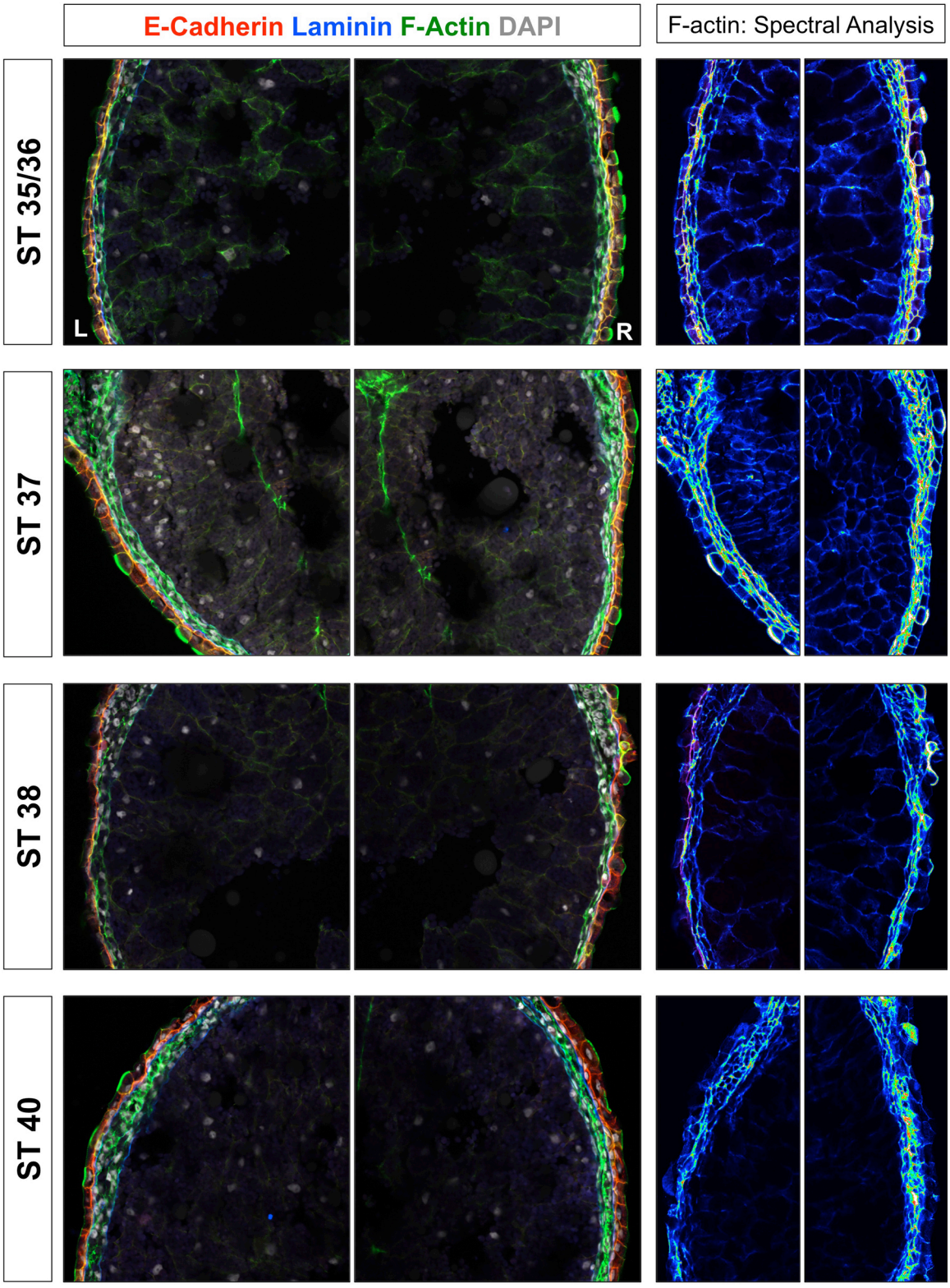
E-Cadherin Laminin F-Actin DAPI
F-actin: Spectral Analysis
ST 35/36
ST 37
ST 38
ST 40
L
R

Transverse cryosections were stained with fluorescent phalloidin (to detect F-actin), laminin (to highlight LPM boundaries with epidermis and endoderm) and DAPI (nuclei) and z-stacks were compiled for each section at 100x. Preliminarily, at this higher magnification, it appeared that the actin bundles in R-sided cells were both thicker and more intensely localized to the cell periphery than in cells within the L LPM, especially in areas of cell-cell contact, in comparison to those surfaces at cell-matrix contacts (Fig. 4.4). These intracellular alterations in F-actin could be indicative of ongoing changes in R LPM cell shape. One interesting observation is that the R LPM fibers seem to be circumferential rather than perpendicular, following the R LPM plane, expanding the dorsal-ventral length of any particular cell. Actin fibers in the L LPM do not have the same alignment seen on the R side in this sectional plane and appear more truncated (Fig. 4.4). Longitudinal sections might address if L LPM fibers are oriented along the A/P axis instead. It is intriguing to think that Nodal signaling might switch the polarity of the actin network from a D/V to an A/P orientation in the L LPM.

R LPM actin redistribution present focally along A/P length of embryo

While this difference in F-actin organization is apparent at several stages, we wanted to address whether these changes were present broadly along the A/P length of the LPM or in a more focal manner, which could serve to prime areas of future asymmetric morphogenetic movements.

F-actin intensity was measured for embryos at stage 35-36 (prior to endodermal chirality) and stage 40 (after anterior coiling has begun) with MetaMorph® morphometric analysis software. After outlining the L and R LPM on 40x images, I measured the F-actin intensity as related to total LPM area and then divided the R LPM by the L to produce a quotient of R/L intensity as a quantitative evaluation of asymmetry in F-actin.

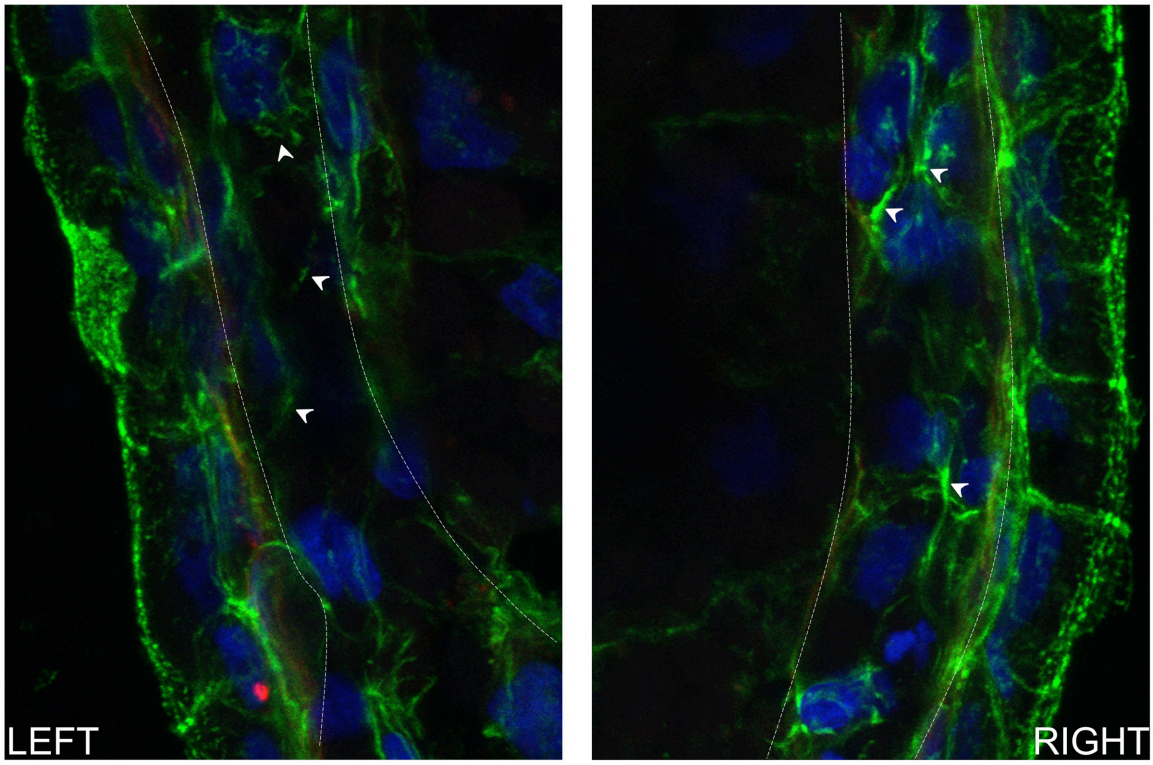

Figure 4.4 F-actin is bundled more thickly in R LPM than L LPM. Transverse cryosections imaged confocally at 100x magnifcation with 3x optical zoom and z-stacked detect F-actin (via phalloidin; green), laminin (red) and nuclei (blue). R LPM F-actin still appears more intense and shows areas of thicker bundles whereas staining within the L LPM is more diffuse. R LPM actin bundles look elongated in this plane (arrow heads) where as L LPM F-actin fibers appear more truncated. Also note the increased intensity at cell:cell contacts in the R LPM.

That is, a result of 1 indicates that R/L intensity equivalence, a number greater than 1 indicates R intensity is greater than the L and a number less than 1 indicates that L F-actin intensity is greater than the R. In keeping with the idea that intracellular alterations could preconfigure architectural events, I was interested in areas where focal F-actin was more organized on the R LPM versus the L. At stage 35, we detected peaks of intensity where phalloidin is significantly more intense on the R than on the L (Fig. 4.5). And with less frequency, we detected some areas where the L intensity was greater than the R. By stage 40 when gut bending has initiated anteriorly but not posteriorly, these peaks of observed intensity difference are far more dramatic than those observed at stage 35-36, and they spread over the full length of the gut tube suggesting that the F-actin alterations observed might be participating in pan-LPM tissue shape changes.

Alterations in Nodal signaling resulted in L LPM F-actin reorganization

To test if the observed F-actin asymmetries were under the control of Nodal signaling, we utilized our grafting system to flip L-R situs, a technique previously established by our lab (Ohi and Wright, 2007). To reverse the L-R axis, embryos were engrafted at stage 17 on the R side with an LPM graft from an equivalently staged embryo, which had been previously injected in the four L-sided cells with pCSKA-Xnr1 and βGal at the 8-cell stage. Engrafted embryos were then cultured until stage 38, fixed, cryosectioned, analyzed for F-actin and imaged at 40x and 100x magnification by confocal microscopy. Acquired images were then examined for actin intensity at 40x and actin bundle features at 100x.

An A/P survey of transverse cryosections from the experiment described above showed, preliminarily, that the observed F-actin asymmetry is responsive to Nodal signaling. A R/L ratio (described in Fig 4.5) for F-actin intensity was generated in MetaMorph® after analysis of 40x L and R LPMs.

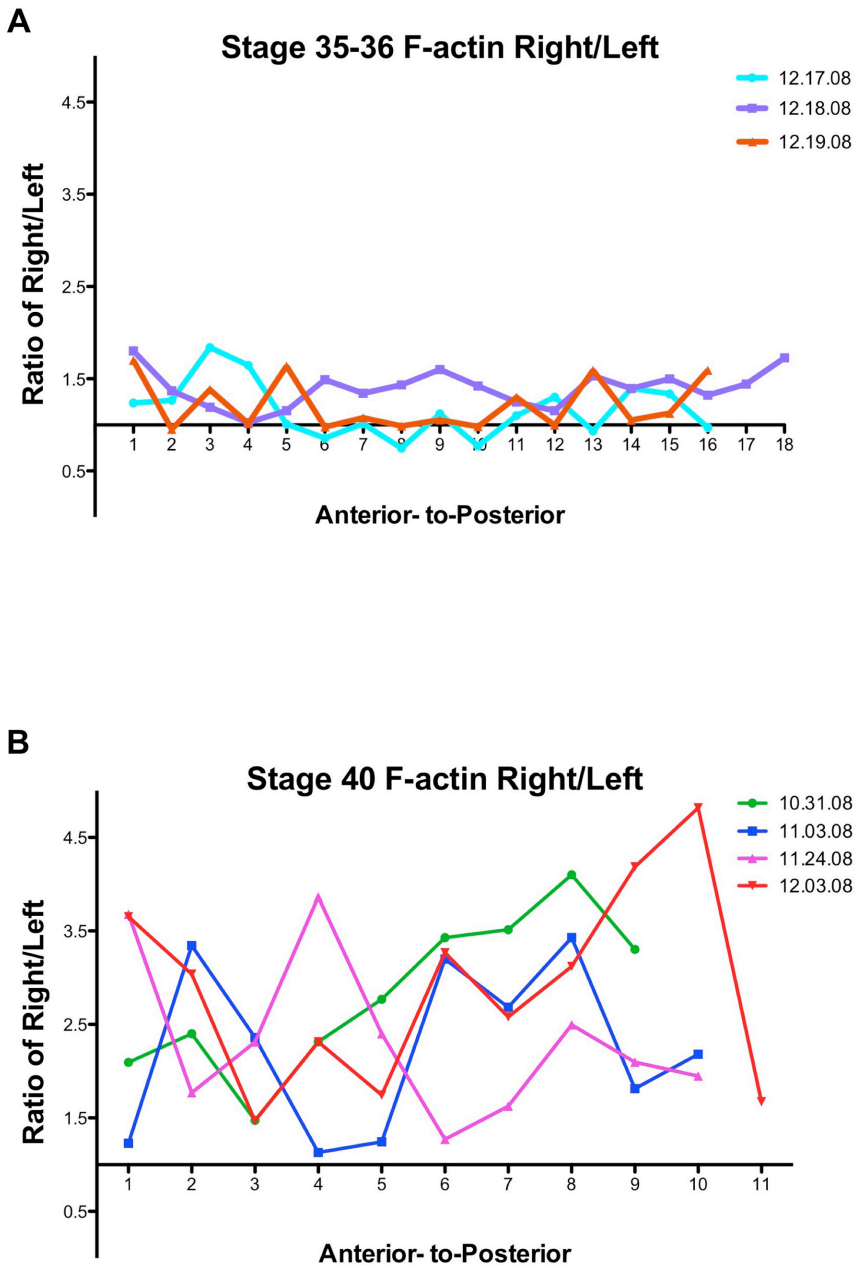

Figure 4.5 Quantification of R/L LPM focal F-actin intensity along the A/P length of stage 35/36 and stage 40 embryos. R/L F-actin intensity quotient was measured using morphometric analysis software. **Top Panel:** At stage 35/36, small peaks of R>L F-actin intensity were observed in the anteriormost and posteriormost parts of the embryo, rather than broadly across the entire A/P length. **Bottom Panel:** By stage 40, after gut coiling had initiated anteriorly, larger R-sided F-actin intensity peaks were observed throughout the length of the gut tube, including more posterior areas that had yet to begin coiling.

We observed a partial reversal of F-actin intensity, such that L LPM now showed increased actin intensity equivalent to what was seen in the R LPM of unmanipulated controls (Fig. 4.6). This L LPM intensity was greater than that of the R at many points along the A/P axis. We did not, however, see a concomitant relaxation and spreading of the R LPM F-actin in Xnr1-grafted embryos. It is possible, however, that our grafting technique incompletely reconfigured the R LPM to be the new 'L' side (Fig. 4.6). A better experiment, which will be expanded upon in the discussion section, would have been to posteriorly crop embryos at stage 17, which effectively removes endogenous *Nodal* expression, to observe what the 'default' state would be in the absence of Nodal signaling.

Examination of 100x z-stacked images from the same L and R LPM samples no longer showed dispersed F-actin in the L LPM, but rather thicker actin cables, with an increase in localization at the cell periphery, similar to control, unengrafted R LPMs. We did not observe an equivalent decrease in R LPM actin thickness (to WT L LPM levels).

Figure 4.6 R-sided Xnr1 graft alters L LPM F-actin bundling. (**A**) 40x transverse cryosections detecting F-actin (via phalloidin; grayscale) showed that L LPM F-actin from R-side Xnr1-engrafted embryos resembled the R LPM F-actin from unmanipulated embryos. (**B**) 100x images from the images in (A) showing that the L LPM F-actin appears more thickly bundled in engrafted embryos. (**C**) Morphometric analysis of R/L LPM F-actin intensity shows that the L intensity is now greater than the R in some locations (asterisk).

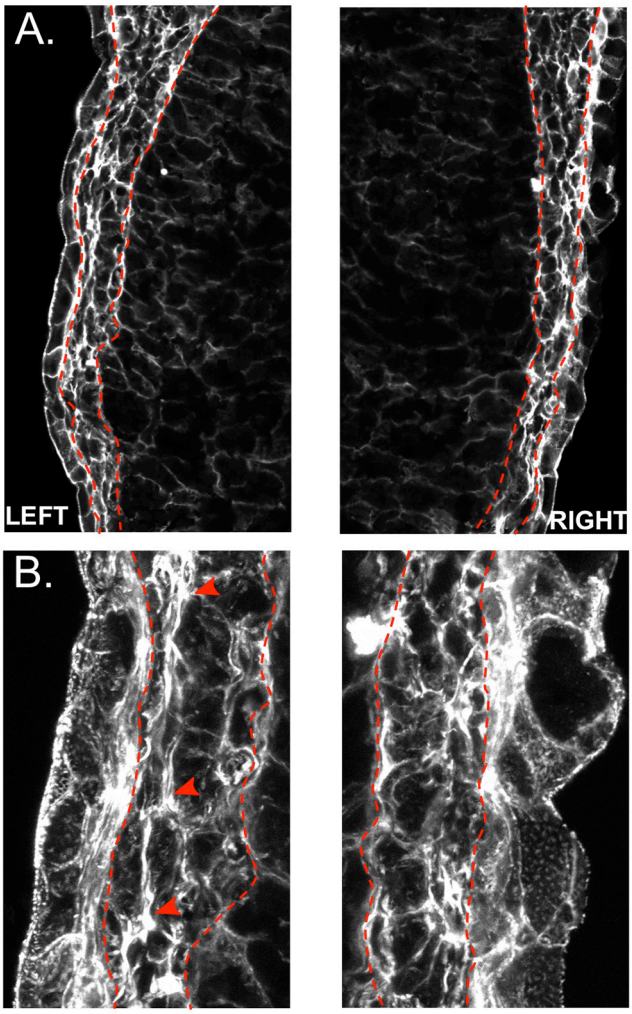
A.
LEFT
RIGHT
B.

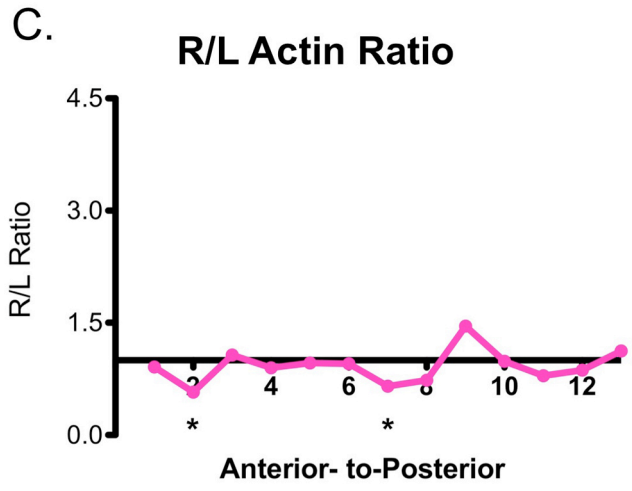
C.
R/L Actin Ratio
R/L Ratio
4.5
3.0
1.5
0.0
4
6
10
12
*
*
Anterior- to-Posterior

Discussion

Although significant time has been invested in understanding the reaction-diffusion nature of Nodal and Lefty ligands during the early stages of L-R axis specification, very little attention has focused on the downstream responses to Nodal signaling. As I mentioned in the introduction to this chapter, the stereotypical directional coiling events of the *Xenopus* gut tube have been described (Chalmers and Slack, 1998; Chalmers and Slack, 2000; Chalmers et al., 2000), but only in stages after the first signs of asymmetric morphogenesis are evident. The goal of the research presented within this chapter was to characterize the L and R LPM in the stages following asymmetric *Xnr1* expression to better evaluate LPM contribution to gut morphogenesis. My initial findings showed that there was a focal reorganization of R LPM F-actin along the A/P axis, which was detected prior to morphological gut asymmetry. There is a significant amount of work left to do, as the experiments for this project took a backseat when more pressing experiments (presented in Chapter III) arose. The results presented within this chapter lay the foundation for future explorations of LPM-specific responses to Nodal signaling.

Confocal characterization of morphogenetic changes within the L and R LPM before asymmetric gut displacement revealed a non-equivalence in R versus L LPM F-actin bundling and localization. Thickening of R LPM F-actin bundling was apparent several hours before asymmetric gut movements, beginning at stage 35-36 whereas L LPM F-actin remained dispersed. Preliminarily, morphometric analysis showed that these differences did not occur broadly across the A/P length of the R LPM but rather focally. Interestingly, prior to any observed gut asymmetries, the focal actin intensity peaks were more apparent in the anterior and posterior regions of the gut tube, which correspond to areas of future significant morphogenetic movements. For example, the

observed peaks in the anterior regions of the gut tube may signify areas where gut morphogenetic movements initiate and the focal peaks observed in the posterior may indicate where the 'anteriorward' retraction of the gut tube begins.

The R-sided F-actin redistribution we observed was somewhat contrary to what we predicted. Because *Pitx2c* is asymmetrically expressed in the L LPM and given the implications of Pitx family members in cell shape changes (Kurpios et al., 2008), we assumed we would see dynamic cell shape alterations occurring within the L LPM. Instead, we saw focal areas of F-actin rearrangement in the R LPM. In the last figure of this chapter, we presented preliminary evidence that the observed L-R differences in F-actin might be responsive to Nodal signaling. A R-sided Nodal graft, which flips the L and R sides, caused L-sided F-actin organization such that the bundles appeared thickened, as they do on the R LPM. This experiment suggests that the broad expression of *Pitx2c* on the L side might be informing L LPM cells to stay more 'spread' or to prevent thicker bundling, while the cells on the R focally rearrange their cytoskeleton to appear more contracted, with thicker actin cables. It may be that the focal actin redistribution primes the areas for future morphogenetic movements. From these studies, I am proposing that L-sided *Xnr1* expression induces L-sided *Pitx2c*, which subsequently turns on downstream effector proteins that instruct L LPM cells to maintain a more relaxed actin cytoskeleton. In Chapter V, I will discuss several future experiments that are necessary to better address this hypothesis.

CHAPTER V

SUMMARY AND FUTURE AIMS

TGFβ family members, whose functions are highly conserved across vertebrates, play indispensable roles in embryonic development. For example, formation of the primary germ layers, patterning of the embryonic axes and organ morphogenesis involve the exquisite coordination of many different TGFβ signaling pathways, including the Nodal, BMP, GDF and TGFβ members proper. In all vertebrates examined to date, as well as some invertebrates, the Nodal signaling pathway is required for mesendoderm induction in the gastrula stage and later during tailbud stages for patterning the L-R axis or generating chirality. During my thesis research, I investigated the routes and rates of transport of the Nodal ligand, and its antagonist Lefty, in the tailbud stage embryo during L-R patterning. Although Nodal and Lefty ligand dynamics have been somewhat described in the gastrula, it is likely that the drastically different architecture during tailbud stages affects the way both Nodal and Lefty signal in and between these more complex and mature tissues. Moreover, ligand behavior in the past has mostly been inferred through assessment of target gene activation, as tissue-immunodetection-competent antibodies to Nodal and Lefty do not exist. Since *Nodal* and *Lefty* are only asymmetrically expressed within the L LPM, it was important to determine if the mature ligands were also limited to transport within the L LPM. Genetic evidence from previous studies in our lab and others suggested that Lefty would travel to the contralateral R LPM, but such movement was so far not shown at the protein level. Additionally, I sought to characterize the tissue architectural features of L and R LPM during asymmetric Nodal signaling to determine if inherent features within the LPM might promote rapid transfer of the Nodal signal along the L LPM.

The *Xenopus* embryo is highly suited to the type of studies described herein, because the abundant, synchronously developing progeny are amenable to DNA/RNA microinjections and can rapidly recover from surgical manipulation. Because of the ease of engraftment, I was able to 'pulse' tailbud stage embryos with localized sources of Nodal and Lefty from animal cap (AC) grafts (described in Chapter III), to place our proteins of interest in the right place at the right time for characterization of function and movement directly during L-R patterning stages. From the studies presented in Chapter III, we generated robust biochemical data showing that functional, tagged Nodal and Lefty were properly secreted, cleaved and post-translationally modified in host embryos when supplied from an animal cap (AC) source. Analysis of L and R LPM cytoarchitecture revealed that the L and R LPM were both nonpolarized bilayers encased in ECM with no overt L-R differences before or during asymmetric *Xnr1* expression. It appeared, however, that the ECM adjacent to the LPM, specifically the somatic LPM:epidermal surface, might be a significant influence in Nodal signaling, because I detected Nodal and Lefty proteins predominantly at LPM and periaxial ECM surfaces. Additionally, CSPGs localized periaxially were present in a graded fashion, with protein levels enhanced anteriorly, which was an interesting observation given the directional posterior-to-anterior shift of the *Xnr1* expression wave. Assessment of ligand movement and clearance rates showed the relatively faster movement and increased stability of Lefty ligand compared to Nodal. We made a connection between the fast, long-range movement of Nodal to sGAGs within the ECM. Chemical-mediated inhibition of sGAG synthesis resulted in decreased Nodal ligand on ECM surfaces. We propose Nodal:sGAG interactions would serve two purposes: first, to facilitate rapid transfer of the Nodal ligand anteriorwards, potentially towards higher levels of CSPG and second, to keep the level of Nodal signaling in the vicinity of the responsive LPM high enough to maintain its feedforward loop.

In Chapter IV, I presented preliminary findings in which I sought to better characterize the downstream morphological consequences of Nodal signaling in L versus R LPM cells. A time course analysis of L and R LPM cells after *Xnr1* expression but prior to asymmetric organ morphogenesis demonstrated that R LPM cells displayed overt rearrangements in their actin cytoskeleton such that thicker actin cables were apparent. L LPM cells, however, did not undergo overt cytoskeletal changes and F-actin appeared more disperse.

This final chapter will address the future directions that have arisen and potential future experiments that have arisen from the experiments presented in Chapter III and IV.

Future Directions: Chapter III

Structural features within the LPM are integral in L-R patterning

When I began my graduate training, a previous graduate student, Yuki Ohi, was finishing her thesis project that evaluated the rapid, dynamic shifting of asymmetric *Xnr1* expression. Through a combination of tissue explantation, overexpression and grafting experiments, Yuki demonstrated that the rapid shifting of *Xnr1* expression required an intact LPM for planar tissue communication as well as Xnr1 autoinduction between neighboring cell fields (Ohi and Wright, 2007). If asymmetric *Xnr1* expression is limited to the L LPM, were there features unique to LPM tissue architecture that could facilitate this rapid transport of Nodal? We had previously speculated that the Nodal autoregulatory loop, working in a cell-to-cell-to-cell relay fashion, might be incapable of working fast enough to expand the *Xnr1* expression domain along the entire length of the LPM within the short period of expression (see Chapter III). Additionally, it was

apparent from an extensive search of the literature that the LPM architecture was not well described for *Xenopus*.

As presented in Chapter III, the L and R LPM displayed no overt architectural differences from one another, suggesting that there are not L LPM-specific features that would promote rapid ligand transport. We did, however, note differences in ECM composition on the somatic versus the splanchnic LPM surfaces, with increased levels of laminin and HSPG on at the somatic LPM:epidermal interface. From the perspective of understanding Nodal and Lefty transport, asymmetric deposition of ECM proteins on a particular face of the LPM immediately raised several questions. Do Nodal and/or Lefty utilize the ECM for transport, and if so, was there a preferred 'cocktail' of ECM proteins required for interaction? If Nodal/Lefty interact with the ECM, does is the ECM interaction facilitative or restrictive role during signaling? L LPM delivery of tagged Nodal and Lefty from an AC graft source showed that both ligands localized primarily at ECM surfaces surrounding the LPM and periaxial structures, and in fact, signal was detected quite distant (>500 μm) from the graft source. Lefty was also detected in the adjacent endoderm, lateral to the L LPM, indicating potentially differing affinities that Nodal and Lefty might have for the ECM surfaces adjacent to the LPM. One interesting observation was that it appeared that Xnr1 and Lefty preferentially localized to the epidermal-somatic LPM ECM surface, which we characterized as having a more mature basement membrane.

Predating the discovery of asymmetric *Nodal* expression, the Yost lab showed that pharmacological interference with the decoration of ECM proteins by sulfated glycosaminoglycans (sGAGs; e.g. HSPG, CSPG) using β-D-xylopyranoside (xyloside) resulted in midline, unlooped hearts (Yost, 1990). Subsequent experiments by the Hamada lab demonstrated that xyloside treatment of mouse embryos prevented the transport of asymmetric signals from the node to the L LPM, thus preventing the initiation

of asymmetric *Nodal* expression (Oki et al., 2007). After repeating the above experiments and confirming that there was a conserved requirement for sGAGs in perinodal transfer of asymmetric signals to the L LPM, we showed that Xnr1$^{6YMC-CS}$ *ligand* movement in sGAG-depleted embryos was significantly altered and Xnr1 association with LPM ECM disrupted, with a noticeable decrease in ECM-associated Xnr1 dorsally and laterally and a concurrent increase in endodermal Xnr1 signal. The more intense Xnr1$^{6YMC-CS}$ signal that was observed at the somatic LPM-epidermal interface in untreated embryos was altered, such that there was relatively more on the splanchnic LPM-endodermal ECM. These findings provide evidence that xyloside treatment has had also a biological consequence on HSPG levels in the LPM-adjacent ECM, an effect we were unable to detect immunofluorescently (see Chapter III). In sGAG-depleted embryos, the increased signal at the splanchnic:endodermal ECM, interstitial signal in the endoderm and reduced rate of transfer suggest that the sGAG-decorated somatic LPM-epidermal ECM is the most effective route of ligand transport as Xnr1$^{6YMC-CS}$. The following sections present future directions relevant to experiments presented in parts of Chapter III to address ligand:ECM interactions and the role of ECM in Nodal signaling.

Analysis of Nodal and Lefty ligand affinity for sGAGs

These experimental results have generated several unanswered questions. Does Nodal have a higher affinity for sGAGs than Lefty? Does sGAG disruption affect Lefty transport rate? Are there specific CSPG or HSPG proteins that interact with Nodal? Given that sGAGs are important for Nodal transport rate and ECM-association, it may be that Nodal has a higher affinity for sGAGs than Lefty, though we have not yet addressed if the transport route for Lefty and/or rate is affected after sGAG depletion. In the context of maintaining separate L and R compartments within the embryo, this

difference in affinity makes sense. The SELI model proposes that Lefty should be able to move to the R side, either directly from the L LPM or via a relay mechanism from dorsal structures, but Nodal should be restricted from such movement. Because the Nodal/Xnr1 signal is relatively unstable compared to Lefty, limiting the range of transfer will keep the local L LPM concentration of Nodal ligand above the threshold needed to maintain autoactivation. This idea that the sGAG interaction locally maintains a high concentration of Nodal must also take into account the on-off rates of Nodal ligand on the ECM, such that sufficient Nodal ligand is released to the LPM to activate the signaling pathway. Future experiments should address Nodal and Lefty affinities for sGAGs, specifically chondroitin sulfate (CS) or heparan sulfate (HS). AC secretion assays (see Chapter III, Fig. 3.14) to produce conditioned medium enriched in tagged Nodal or Lefty can be applied to an affinity column with CS or HS-conjugated beads and relative affinities of Nodal and Lefty for HSPGs and CSPGs can then be evaluated by competing the tagged proteins off of the column with buffers of differing ionic strength. Alternatively, microfluidic chambers with CS or HS-coated surfaces could also be used in combination with Nodal or Lefty-containing conditioned medium to establish differential diffusion rates over these different surfaces.

Identification of specific sGAGs that interact with Nodal and Lefty

It is currently unclear what the nature of the ligand:ECM interaction is, and more is required to dissect it. It could be that there is one major ligand:sGAG ECM protein interaction, or there could be multiple distributed interactions of several parts of the ligand with one or more than one sGAG ECM protein. Additionally, significant influences may also result from glycosylation of the mature ligand, which could cause an sGAG:N-linked glycosylation interaction. It is somewhat difficult to address protein-carbohydrate interactions, especially when the carbohydrate-modified proteins are in the ECM.

Immuno-mass spectrometry is a potential approach to identifying the proteins and carbohydrates that are interacting with Nodal and/or Lefty. This type of experiment can be performed at Vanderbilt in collaboration with the Monoclonal Antibody Core and Proteomics Core. Briefly, this experiment would be performed in posteriorly-truncated embryos, to remove endogenous Nodal and Lefty, that were subsequently AC-engrafted to provide an exogenous source of tagged Nodal or Lefty. Embryos would be cultured for 4.5 hours, a time period sufficient for Nodal or Lefty to be secreted from the AC graft into the host embryo, then the AC graft would be removed and the embryo would be subjected to a membrane-impermeable cross-linking reagent, such as DTSSP (Chen and Shen, 2004; Cheng et al., 2004). Because the cross-linking reagent is membrane-impermeable, we should be enriching our search for potential ECM interactors. After cross-linking, Immunoprecipitation (IP) for Myc from embryonic lysate would then pull down Xnr1$^{6MYC-CS}$ and physically associated molecules. Given the high affinity of the 6xMyc epitope tag for its antibody and the strength of the cross-linking reagent, the large ligand:ECM complexes that may result from IP can be subjected to harsh RIPA and SDS washes to effectively denature the complexes into smaller components. Reversal of cross-linking with a reducing agent then releases only the target proteins, which could then be analyzed by mass spectrometry and, with the help of a bioinformatics analysis, the candidate proteins could be identified.

Is the anterior enrichment of CSPG a directional cue for the Nodal ligand?

Another future experiment should test the whether anteriorly enhanced CSPG is a directional cue driving the forward movement of the Nodal ligand, helping to ensure the complete, rapid extension of the *Xnr1* expression domain into the anteriormost regions of the embryo. The Nodal signal must traverse the entire L LPM during a short time period, approx. 7 hours. If Nodal does not travel the full length of the LPM, anterior

structures such as the heart or foregut will not undergo proper L-R morphogenesis. The ideal experiment would be, for example, to reverse the CSPG gradient, by providing more CSPG on the ECM in regions that are posterior to an Xnr1 graft source. Because CSPG refers to a large family of CS-modified proteoglycans there is a technical problem in that this experiment would potentially require trying to posteriorly overexpress pathway components/enzymes of CSPG synthesis to enrich for CSPGs posteriorly. A large number of problems arise with any method related to this general concept. For example, a manipulated AC graft would have to secrete/target the ECM protein or enzyme to the proper location within the host. Then, presumably this would be followed by a second engraftment (to introduce the tagged ligand), with an increased likelihood of significant structural problems within the host embryo. Second, interference with ECM components or protein-modifying enzymes, with for example MO-knockdown, would disrupt critical processes such as gastrulation and neurulation, precluding analysis at later stages. One could potentially address directional attraction to CSPG in an AC sandwich experimental approach where an Xnr1$^{6MYC\text{-}CS}$-injected AC could be sandwiched between an uninjected AC (does not express CSPG) and an AC injected with a sulfotransferase to promote the overexpression of CSPGs on the cell surface. ACs could then be examined immunofluorescently or biochemically for directional movement of the tagged ligand toward a CSPG source.

Lefty and Nodal properties fit a reaction-diffusion paradigm

Before the central molecular players involved in embryonic pattern formation were known, or the appropriate analytical tools had arisen to study them, mathematical modeling utilized partial differential equations to reduce the complex process of pattern formation to the chemical reactions of individual proteins. In his seminal paper, “The

chemical basis of morphogenesis", Alan Turing theorized that two 'substances' with differential diffusion rates could generate patterns in a developing embryo (1990). Gierer and Meinhardt subsequently refined this model to better define Turing's two 'substances' (1972; 2009; 1974; 1990). In the model, one substance is a short-range activator, with 'locally restricted self-enhancing" capabilities while the other substance is an inhibitor, which is both rapidly diffusing and antagonistic to the activator. This mechanism of pattern formation is known as the reaction-diffusion model and has been used to describe how Lefty and Nodal behave in mesendodermal induction and during L-R patterning. With a temporal delay caused by the time to receive the signal, carry out its nuclear transduction and induce gene expression effects, Nodal positively autoregulates its own expression and, also induces its inhibitor Lefty. Lefty then antagonizes the spread of Nodal signaling within the tissue by traveling farther and faster than Nodal. The ultimate dynamics of an activator/inhibitor pair are governed by balancing effects, with the relative speeds of movement, ligand stability and the timing of activator versus inhibitor activation all serving as significant factors. The tenets of the reaction-diffusion relationship were explored by Hamada and colleagues by focally electroporating mouse $Nodal^{GFP}$ or $Lefty2^{GFP}$ expression construct into the lateral regions of chicken embryos during L-R patterning stages, and observing the distance each traveled over time (Sakuma et al., 2002). Lefty2 traveled farther and faster than Nodal (Sakuma et al., 2002), but as I have mentioned previously, the authors did not address the mechanisms of ligand transport used, relative ligand stability rates, or even the accuracy of electroporation into the LPM. More importantly, however, the authors never addressed whether the GFP-tagged protein migrating within the embryo was the cleaved, mature ligand rather than a non-functional proprotein precursor. While I confirmed the finding that tagged Lefty has a faster relative movement than Nodal, I also demonstrated that the tagged proteins were properly cleaved and that Lefty is more

stable than Nodal, which contributes to the distances Lefty is able to travel. In addition to careful analysis of Nodal and Lefty ligand transport rates, I was able to evaluate the relative clearance rates and different transport routes utilized by each ligand. By establishing that both Nodal and Lefty are cleared quite rapidly in the absence of continuous replenishment from an AC source, we have demonstrated that ligand interactions with ECM surfaces is not the result of ligand overstabilization from epitope tagging.

A major proposal of the SELI model (Chapter III) is that Lefty travels to the contralateral side to squelch the Nodal autoregulatory loop, but this movement has never been directly shown. Because ligand signal is seen on LPM and dorsal midline ECM, Lefty movement to the R side could be from either source or both. Therefore, we believe it is highly significant that we detected the ability for Lefty to move, within 3 hours, to the R LPM from the contralateral L LPM. A significant fraction of Lefty is transferred from the L to R LPM, even more by 6 hours (Chapter III), providing a significant period of anti-Nodal influence over the entire embryo. A high fractional transfer of Lefty likely primarily serves to suppress inappropriate activation of a R-sided Nodal autoregulatory loop. Additionally, a long-lived, pan-embryonic suppressive influence by Lefty might promote tissue maturation processes as well as the eventual epigenetic silencing of Nodal. The following sections will focus on future analyses of Nodal/Lefty movement to better address why Lefty travels farther than Nodal.

Live imaging of Nodal and Lefty at single molecule resolution

In the future, it might be possible to apply live imaging techniques to AC-engrafted embryos to observe single ligand molecule movement in real time. Brighter, more stable fluorophores such as quantum dot (Qdot®) nanocrystals now afford live imaging at single molecule resolution. Ideally, a reduction in the overall size of the

fluorophore would also be beneficial for this type of experiment, as the addition of larger, bulkier tags are known to disrupt ligand function.

Biochemical assessment of ligand clearance rates

Now that I have applied biochemical methods to address Nodal and Lefty protein behavior *in vivo*, it will be important to reassess our clearance rate assays, under the following reasoning. A biochemical approach affords more sensitivity than our previous immunofluorescence analysis. These experiments are already in progress, in collaboration with a new graduate student, Jessica Sweatt. Although our current analysis of Nodal and Lefty stability has provided a foundation for the relative clearance rates of each ligand, the immunofluorescence technique we used is notoriously non-quantitative and issues such as inherent yolk autofluorescence make distinguishing signal from noise difficult. These experiments also only addressed the relative rates at which Nodal and Lefty were removed from extracellular (i.e. ECM) surfaces and taken up by responding cells; tagged ligand is not detectable intracellularly by the current immunofluorescent methods we are using. Performing these experiments biochemically followed by immunoprecipitation affords increased sensitivity and allows us to better address how long it takes for tagged ligands, presumably taken up by cells into endosomal vesicles, to be degraded. Naturally occurring embryo-to-embryo variation from our immunofluorescence approach is diminished as each time point obtained biochemically results from homogenization of several embryos, allowing us to extend the clearance assays to later time points. Additionally, we can better address how soon Lefty arrives at on the contralateral R LPM by examining time points earlier than 3 hours post-engraftment (Chapter III, Fig. 3.10). We are also using these biochemical methods to better examine if there is biased transport of Nodal or Lefty anteriorwards from the AC graft. Our immunofluorescence analysis of ligand transport indicated that Nodal and

Lefty preferentially move towards anterior regions of the embryo. By dissecting embryos into anterior-dorsal, anterior-lateral, posterior-dorsal and posterior-lateral quadrants, we can establish more precisely, and with a higher sample number, the preferential movement of both ligands.

Cell memory of the Nodal signal: pSmad2 analysis

Cell memory of the Nodal signal is being assessed by examining the nuclear residence of the downstream signaling component, pSmad2. As I stated in the introduction, Nodal ligand binds its receptors and subsequently phospho-activates Smads2/3, which enter the nucleus to alter transcription. The current antibodies against pSmad2/3 are notoriously difficult to use in immunodetection on tissues. Angela Halstead in our lab has generated new antibodies against pSmad2/3 in an effort to better detect active Nodal signaling. Presumably, the nuclear residence time of pSmad2/3 should yield a good estimate of the length each cell 'remembers' receiving the Nodal ligand.

Live imaging analysis of ligand:receptor interactions and kinetics

Although we have observed that both Nodal and Lefty ligands are capable of traveling great distances within the embryo, we are currently unable to address what portion of the observed signal constitutes ligand that is actively engaged with its receptor, versus ligand that is in the process of being cleared or will shortly be cleared, or actively moving along ECM to more distant tissue locations. In the future, it might be possible to develop FRET-type assays in LPM explants, expressing ligand coupled to one fluorophore (e.g. CFP) in an embryo carrying (perhaps via a transgenic approach) Alk4, which is currently believed to be the primary Nodal receptor, coupled to another fluorophore (e.g. YFP). Close physical interaction, if the fluorophores are appropriately

placed, might then allow fluorescence energy transfer between CFP and YFP only when ligand and receptor are engaged. Another option might be a split-GFP assay in which the N-terminal half of GFP could be coupled to the extracellular portion of the Nodal receptor and the C-terminal half of GFP coupled to the ligand, resulting in GFP fluorescence only when the ligand engages its receptor. The discovery of smaller fluorophores, which would have less impact on the overall structure of the ligand, could only improve these types of assays.

Structure:function analysis of Nodal and Lefty

As I described previously in Chapter I, there is a substantial body of literature illustrating the importance of secreted ligand:ECM interactions, which can either be facilitative or restrictive on ligand travel. Previous research has implicated small motifs of consecutive basic or acidic residues in secreted ligands as being required for interaction with sGAGs (Jing et al., 2006; Ohkawara et al., 2002). To better understand the nature of Nodal and Lefty ligand interactions with ECM, a region of future exploration should include a search for such motifs within Nodal and Lefty. Are there any motifs in Xnr1 but not Lefty that might be required for its ECM tethering? If small motifs are identified, site-directed mutagenesis of these regions could be used to test for their requirement, using immunofluorescence to observe ligand localization and biochemical approaches to assess stability. It may be that there are several low-affinity motifs throughout each protein, indicating that identification of a single motif required for ECM interactions might be impossible.

Work from the Yost lab has indicated that HSPGs, specifically syndecans, play integral roles in L-R patterning (Arrington and Yost, 2009; Kramer et al., 2002; Kramer and Yost, 2002). Although we were unable to visually detect a significant reduction of

HSPGs after xyloside treatment, increased signal on splanchnic LPM:endodermal ECM surfaces indicates that HSPGs had been perturbed. Previously published morpholino-oligonucleotide knockdown of syndecans only assessed their role prior to gastrulation, rather than how they might additionally affect ligand transport. We can assess the role HSPGs such as syndecans play by utilizing our AC grafting system to supply an exogenous source of tagged Nodal to embryos previously injected with morpholinos against different syndecans to determine if their loss affects Nodal movement.

Identification of ECM-interacting domains within Nodal and Lefty

A primary future direction should include the dissection of potential domains present in Nodal or Lefty that allow Lefty to move more freely. This may tie in intricately with points that I raised in a previous section of this chapter regarding differing affinities of Nodal and Lefty for sGAGs, in which Lefty may not interact as strongly, or at all, with sGAGs within the ECM, allowing it to move more freely outside of the LPM. Careful structure-function dissection of specific regions of Lefty and Nodal might identify previously uncharacterized motifs present in one protein but absent in the other that would be involved in the ECM interaction. It may be difficult to address this question, however, by typical experimental methods such as domain swapping for reasons we have already mentioned previously. Nodal function is highly sensitive to manipulations of its sequence. Engineering of Lefty domains into Nodal may render the protein inactive, which would make it difficult to assess any specific effects on ligand localization or transfer rate. Although previous stretches of primary sequence in BMPs have been implicated in ECM interactions, it may be that two or more parts of the Nodal or Lefty polypeptide contribute to a tertiary structure capable of interacting with the ECM. Forcing a predicted structure for the Nodal primary sequence against the known crystal structure of BMP2 or TGFβ is likely inadequate to identify these types of ECM-binding

structures. In the future, it will be important to determine the crystal structures of Nodal and Lefty. Because Lefty protein is drastically different from Nodal, it may be that it has an alternative strategy for ECM interaction and information provided from the crystal structures of each protein will help elucidate these differences.

Evolutionary adaptations of different sized embryos to maintain dynamic and rapid Nodal transport in L LPM

One of the interesting questions that arose during our analysis of Nodal signaling in the tailbud stage *Xenopus* embryo is to understand what features we have described might be frog-specific. In different species, the Nodal interactions with ECM may have become adapted to each other in accordance with the embryo's morphology, size, and developmental mechanism. The *Xenopus* embryo is a relatively large embryo and might need more ECM-interacting features in order to maintain a threshold sufficient to propagate the *Nodal* expression wave in a given responsive period within the L LPM. For example, mature *Xenopus* Nodal (and zebrafish Southpaw) is glycosylated while mouse, chicken and human Nodal are not. We believe that glycosylation might be an evolutionary adaptation to allow Nodal to move within the L LPM to maintain the proper reaction-diffusion relationship with Lefty. In a publication from the Constam laboratory, it was proposed that glycosylation of the mature Nodal ligand might confer extra stability (Le Good et al., 2005).

Is glycosylation of mature Nodal or Lefty required during L-R Patterning?

A previous graduate student, JJ Westmoreland, sought to understand the role that post-translational N-linked glycosylation of Lefty ligand played during mesendoderm induction. JJ assessed Lefty secretion, cleavage, inhibitory function and travel range in an effort to better understand the purpose of glycosylation on a secreted ligand. JJ

generated a non-glycosylated Lefty (Lefty^{NGM}) but no changes in Lefty production, function or behavior were observed during mesendoderm induction (Westmoreland et al., 2007). Several of the *Xenopus* Nodal-related (Xnrs) proteins also contain glycosylation motifs. JJ used site-directed mutagenesis to mutate the glycosylation site in the mature Xnr2 ligand (Xnr2^{NGM}) but Xnr2^{NGM} still effectively induced mesodermal gene expression in animal cap assays, indicating that its signaling properties were not disrupted in cell-autonomous mesoderm induction experiments. We are now interested in understanding what role N-linked glycosylation of Lefty and Nodal might serve during L-R patterning stages. Given the dramatic architectural changes that occur between the gastrula and tailbud stages, N-linked glycosylation may only be required in the later stages when factors such as ECM interaction and long-range transport are relevant. In blastula-gastrula embryos, JJ demonstrated that Lefty ligand moved interstitially between cells (Westmoreland et al., 2007) and a recent publication from the DeSimone lab indicates that the first embryonic basement membrane in *Xenopus* is not assembled until the beginning of gastrulation, after Nodal signaling has begun (Dzamba et al., 2009), which indicates that ligand transport along ECM is likely not a factor during mesendoderm induction. Glycosylation of mature Nodal and Lefty ligands may serve as an additional mechanism during L-R patterning to aid in ligand interaction with the ECM for rapid, long-distance transport. In addition to Lefty^{NGM} (now referred to as Lefty$^{6MYC/NGM}$), generated by JJ, I have also generated a non-glycosylatable variant of Xnr1$^{6MYC-CS}$ (Xnr1$^{6MYC/NGM}$) to assess the requirement of N-linked glycosylation for each ligand during asymmetric Nodal signaling (Fig. 5.1). Previously published mesoderm induction assays and animal cap secretion assays demonstrated that Lefty^{NGM} is secreted, processed and functional as a Nodal inhibitor (Westmoreland et al., 2007). Given that the non-glycosylatable Xnr2 (Xnr2^{NGM}) maintained function and that it has high sequence similarity to Xnr1, we expected that function of the non-glycosylatable

Xnr1$^{6MYC/NGM}$ would not be affected by mutagenesis of the glycosylation motif. To confirm that Xnr1$^{6MYC/NGM}$ function was not affected, Xnr1$^{6MYC-CS}$ (positive control) or Xnr1$^{6MYC/NGM}$ RNA was injected into 1-cell stage embryos, animal caps explanted at stage 8-9 and cultured overnight. Xnr1$^{6MYC/NGM}$ equivalently caused significant elongation of animal caps, indicating that it was still capable of cell-autonomously inducing mesoderm (Fig. 5.1).

Figure 5.1 Generation and assessment of function of Xnr1$^{6MYC/NGM}$ and Lefty$^{6MYC/NGM}$. (**A**) Site-directed mutagenesis was used to mutate the 'NET' glycosylation site in the Nodal ligand domain to 'AET' to generate an Xnr1$^{6MYC-CS}$ glycosylation mutant (Xnr1$^{6MYC/NGM}$). (**B**) Xnr1$^{6MYC/NGM}$-containing AC grafts secreted only the non-glycosylated Xnr1 proprotein (Pro) and ligand (Mat) into host embryos, in comparison to Xnr1$^{6MYC-CS}$, which secreted both glycosylated (Pro^{G}, Mat^{G}) and non-glycosylated (Pro, Mat) proprotein and ligand. (**C**) Xnr1^{NGM} induces mesoderm equivalently to Xnr1$^{6MYC-CS}$ in an animal cap extension assays. (**D**) Site-directed mutagenesis was used to mutate the 'NRT' glycosylation motif to 'ART' to generate a Lefty$^{6MYC-CT}$ glycosylation mutant (Lefty$^{6MYC/NGM}$). (**E**) Animal cap secretion assays showed the non-glycosylated version of Lefty$^{6MYC/NGM}$ was properly produced, cleaved (Pro, Mat) and secreted. (**F**) Lefty$^{6MYC/NGM}$ equivalently inhibits mesoderm gene induction in animal caps as compared to Lefty$^{6MYC-CT}$ (Westmoreland et al., 2007).

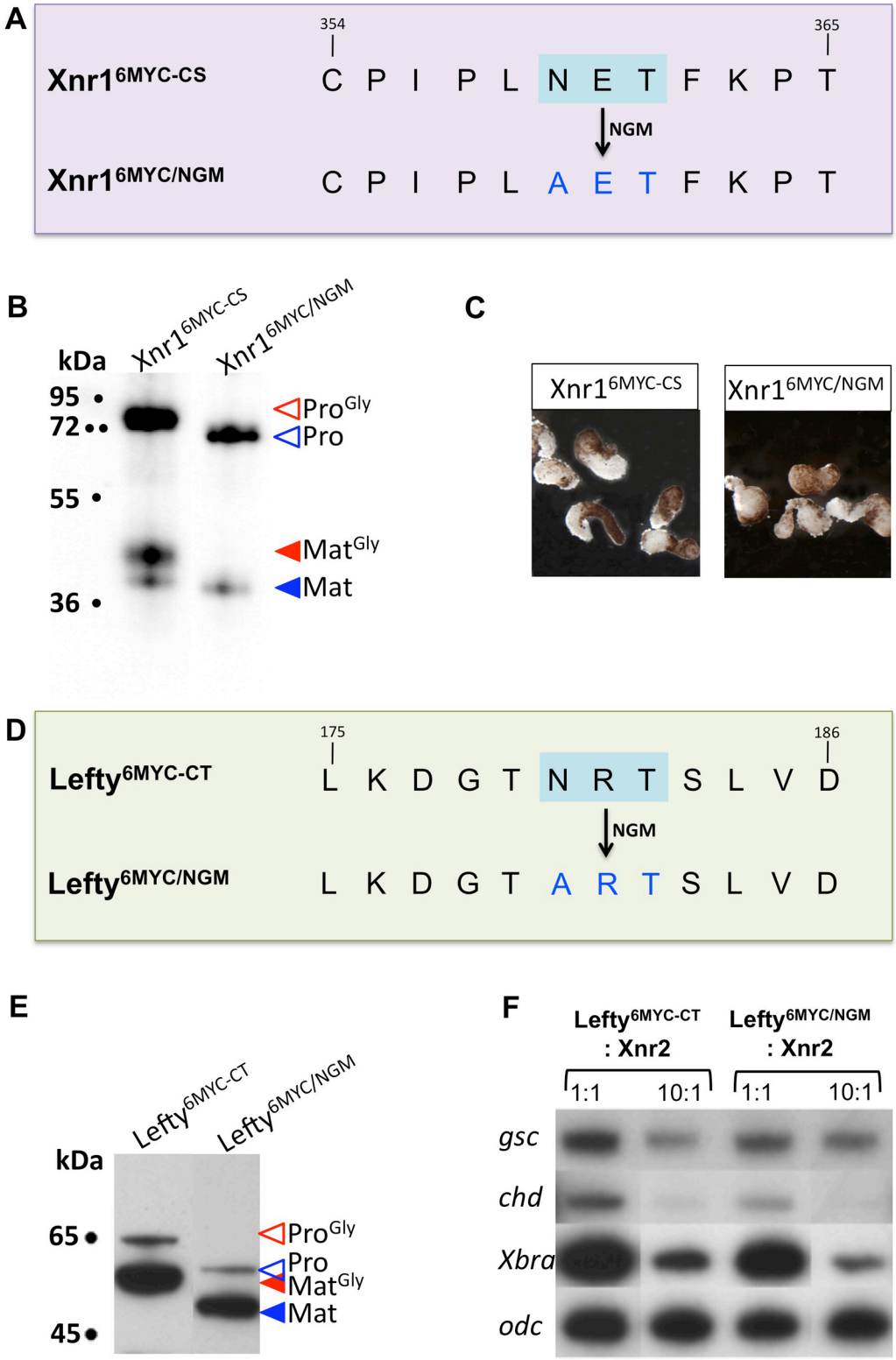

(E & F: from Westmoreland et al., 2007)

We are currently addressing how loss of glycosylation in Xnr1 and Lefty affects ligand localization, route and rate of transport as well as overall stability. One way in which we are beginning to address this issue is by examining R LPM explants from L LPM-AC-engrafted embryos to determine if Xnr1^{NGM} can now move into the endoderm and over into the R side, which may occur if glycosylated Nodal ligand is relatively well-tethered to the L LPM ECM as we have speculated in chapter III (Fig. 5.2). Preliminarily, we do not detect such a contralateral movement by Xnr1$^{6MYC/NGM}$. Several experiments proposed here are in collaboration with Jessica Sweatt, who will extend this project for her own thesis work. To address how removal of N-linked glycosylation affects Xnr1 movement, similar experiments to those presented in Chapter III will be performed using Xnr1$^{6MYC/GM}$. For example, to address the stability of Xnr1$^{6MYC/NGM}$ and Lefty$^{6MYC/NGM}$ during tailbud stages, AC-graft removal experiments will be performed (for experimental design, see Fig. 3.10) and compared to the glycosylated Xnr1 and Lefty. The Constam lab observed a stabilizing effect on mature human Nodal ligand in cell culture secretion assays when the *Xenopus* glycosylation motif was introduced (Le Good et al., 2005) indicating that non-glycosylatable *Xenopus* Nodal and Lefty might be destabilized.

Glycosylation may also be important for low-affinity interactions between Nodal for Lefty with the ECM. In our NGM proteins, we may observe a decrease in the distance traveled if glycosylation is integral to maintaining ligand:ECM interaction. We can also address whether or not both Nodal and Lefty still preferentially move anteriorly versus posteriorly in the absence of glycosylation. Although we did not observe R-sided Xnr1^{NGM} accumulation, it will be important to assess immunofluorescently whether or not Xnr1^{NGM} remains solely ECM-associated or if endodermal signal can now be detected, as was the case when sGAGs were removed.

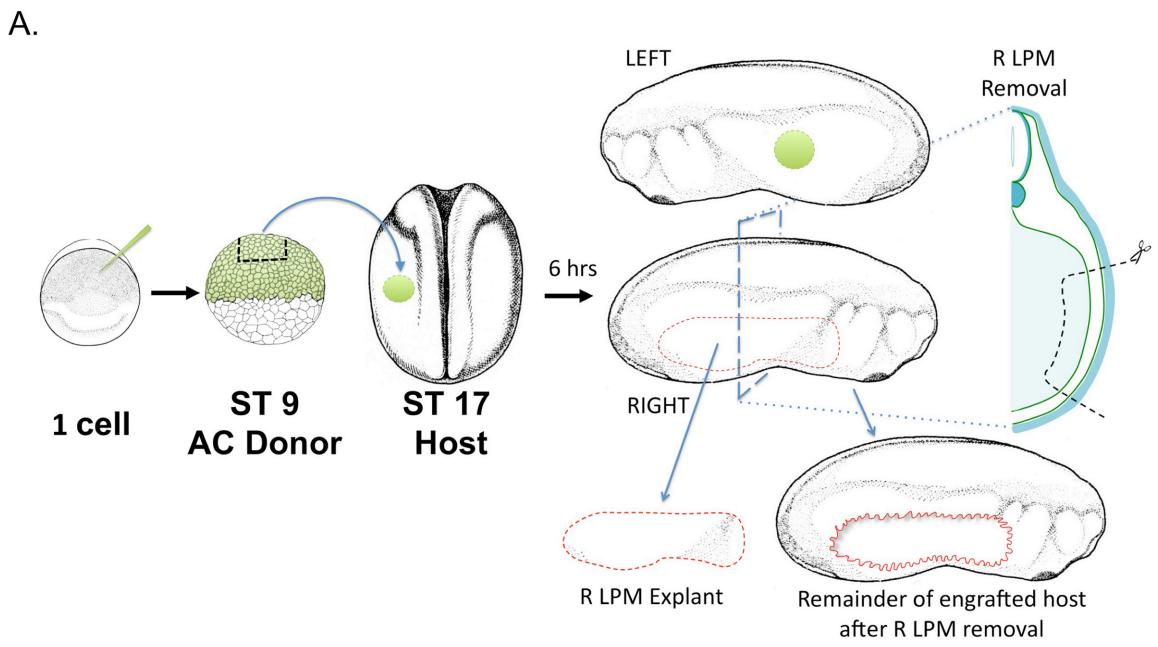

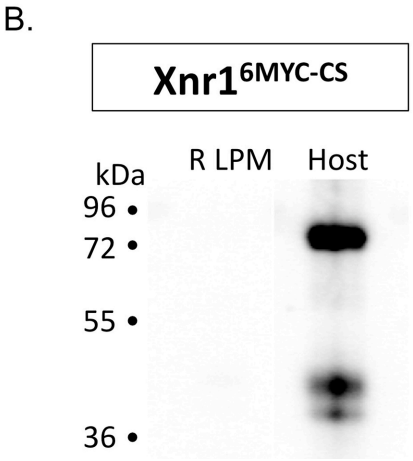

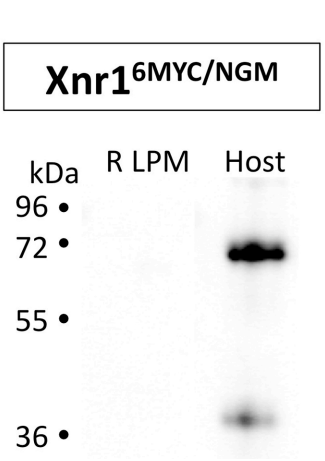

Figure 5.2 Xnr1$^{6MYC/NGM}$ is not detected in the R LPM after AC-engraftment on the L LPM. (**A**) Experimental design used to assess if Xnr1$^{6MYC/NGM}$ moved to the contralateral R LPM (see chapter III, Fig. 3.9). (**B,C**) Like Xnr1$^{6MYC-CS}$, Xnr1$^{6MYC/NGM}$ was not detected within the contralateral R LPM after 6 hours of engraftment.

We can also address whether or not Xnr1^{NGM} is still capable of mounting a forward-rolling wave of *Xnr1* expression in the absence of glycosylation. If we observe differences in the distance Xnr1 and Lefty are able to move in a given time period, this may indicate that Xnr1 can no longer properly positively autoregulate its own expression. Or, we may see a delay in the timing it takes the *Xnr1* expression wave to reach the anterior of the embryo.

Finally, we can also assess how Xnr1^{NGM} behaves in the absence of sGAGs by culturing Xnr1^{NGM}-containing AC-engrafted embryos in xyloside. Removal of sGAGs may further reduce Xnr1^{NGM} localization with ECM proteins as well as the distance traveled.

Future Directions: Chapter IV

Identification of the downstream effectors of Nodal signaling

In an attempt to identify other genes that might be differentially expressed between the L and R LPM, a former graduate student, Young Cha, and I performed a microarray experiment (see Chapter II) during my first few months in the Wright lab (Cha, 2006). These experiments were performed by isolating L and R LPMs at stage 23 (when *Nodal* and *Lefty* were both robustly expressed), extracting RNA, and hybridizing the RNA to a *Xenopus* Affymetrix™ microarray. From this experimental setup, we were unable to indentify any genes that were consistently differentially expressed between the L and R samples, aside from our positive controls, Nodal and Lefty.

Methods to identify targets of Nodal signaling

Given our findings in Chapter IV that intracellular alterations in F-actin do not appear until stages after *Xnr1* expression, it might be better to perform a microarray-

based approach in older embryos (after stage 25 but prior to stage 38), which could help us to identify targets, potentially downstream of Pitx2c, within the L LPM. It might also be, however, that a microarray-type experiment is not the correct approach, as there may not be any other L-R asymmetrically expressed genes in *Xenopus*. Rather, there may be post-translational modifications that occur asymmetrically, which would not be detected in our microarray experiment. There is a precedent for this idea. Research from the Yost lab has shown that while *Syndecan2* is symmetrically expressed within the *Xenopus* gastrula, Syndecan2 is phosphorylated by aPKCγ in R-sided cells only (Kramer et al., 2002; Kramer and Yost, 2002).

Cytoskeletal alterations as a readout of Nodal signaling in gut morphogenesis

One of the bigger questions about Nodal signaling, which we raised in the introduction of Chapter IV, is to understand how this signaling event is 'remembered' on the L side such that Nodal and Pitx2c instruct morphogenetic events. As a field, we still have very little understanding how broad L-sided expression of *Nodal* becomes translated into the stereotypical asymmetric placement of organs. There are two key sets of experiments that need to be performed to evaluate the significance and/or requirement of R LPM cytoskeletal rearrangements in gut morphogenesis. The first set of experiments entail a detailed dissection of the mechanism of R-sided F-actin rearrangement to address whether or not F-actin alterations are downstream of Nodal signaling. The second set of experiments will further describe the F-actin reorganization in better detail, by addressing the 3D shape of R versus L LPM cells.

The role of Nodal signaling in F-actin redistribution

At present, our results addressing the relationship of Nodal signaling to the cytoskeletal rearrangements seen on the R side of the embryo are preliminary and therefore inconclusive. One way to better assess the relationship of Nodal signaling with R LPM F-actin redistribution is to analyze the R and L LPM in embryos that do not express asymmetric *Xnr1*. Yuki Ohi, a former graduate student, previously showed that posterior truncation of embryos at stage 15/16 effectively removes the bilateral *Xnr1* expression domains in the region equivalent to the node (*Xenopus* gastrocoel roofplate), which prevents transfer of the asymmetric signal to the L LPM to initiate asymmetric *Xnr1* expression (Ohi, 2007; Ohi and Wright, 2007). This experimental manipulation generates a post-gastrulation, 'Nodal-null' embryo that will also lack L LPM *Lefty* and *Pitx2c* expression. If Nodal signaling is upstream of F-actin reorganization, we would propose that Pitx2c would no longer be present to instruct L LPM cells to remain spread. Instead, we would expect to see the L LPM look like the R LPM, with thicker actin cables at focal points along the A/P axis.

After establishing what L LPM F-actin organization looks like in the absence of *Nodal*, we could then perform 'rescue' type experiments, in which we reintroduce Nodal to the embryo. To do this, an *Xnr1*-containing animal cap (AC) source would be engrafted into the embryo (as described in chapter III) on either the L or R side after truncation. Based on previous results from Ohi and Wright (Ohi and Wright, 2007), we know that the Xnr1 graft location will determine which side becomes the dominant "L" side. We would predict that cells on the engrafted side should display a "L-like" phenotype with diffuse F-actin whereas cells on the side contralateral to the graft should have thick actin cables, with enhanced localization at the cell periphery. These experiments, in combination with the ones mentioned in the previous paragraph, would

better evaluate if Nodal signaling is driving the downstream changes in cytoskeletal architecture.

We will also need to assess if Pitx2c is serving as the instructive mediator for Nodal. Ideally, we could generate an inducible version of Pitx2c, which could be injected into early embryos, but would not be activated until later stages. To do this, we could make a glucocorticoid-activatable Pitx2c (Pitx2c-GR) construct, which would produce a Pitx2c-GR fusion protein that is held inactive in the cytoplasm. Addition of dexamethasone (Dex), however, promotes nuclear translocation of Pitx2c-GR and allows the protein to be transcriptionally active. This type of experiment was already performed in animal caps by the Wallingford lab (Chung et al., 2010) with Pitx1, thus lending strong support that this is a feasible experimental direction. By targeted injection of Pitx2-GR to either the R or L LPM in posteriorly truncated embryos (no *Pitx2*c expression), we can assess what happens to the cytoskeleton of cells where *Pitx2c* has been expressed. We would predict that Pitx2+ cells would display a more diffuse F-actin cytoskeleton, similar to L LPM cells in unmanipulated embryos. We could also address if Pitx2 is capable of having a community effect in a cell population by turning Pitx2-GR on in smaller groups/clumps of cells in posteriorly truncated embryos by using targeted injections in later staged embryos (e.g. 1 cell injected at the 32-64 cell stage).

An alternative approach to address the role of Pitx2c in cytoskeletal rearrangements would be to inject Pitx2c RNA into 1-cell stage embryos and look for changes in F-actin distribution in stage 9 ACs in comparison to uninjected control ACs. If Pitx2c affects F-actin organization, the cells of the animal cap might appear more spread, with dispersed F-actin. We could also address whether there was a concomitant increase in cell-cell contacts, by co-staining for β-catenin or N-cadherin, which were implicated by the Adelstein lab (Wei and Adelstein, 2002) as being downstream of *Pitx2* expression in HeLa cells. We have had difficulty in identifying cell adhesion proteins that

are strongly expressed within the L LPM during the stages leading up to gut morphogenesis. Because we have already identified cell adhesion proteins present in ACs, we can determine if *Pitx2c* misexpression changes cell adhesion protein levels or localization. Using small molecule inhibitors of Rho/Rac GTPases published previously, we can then address if Pitx2c works through the same downstream effectors as Pitx2a (Wei and Adelstein, 2002).

Descriptive analyses to characterize the morphological changes occurring in the L and R LPM

In addition to addressing how Nodal signaling triggers L-R differences in the LPM cytoskeleton, it will be necessary to determine if the F-actin changes are indicative of more global, ongoing cell shape changes in R versus L cells. To answer this question, thicker cryosections or vibratome sections should be imaged confocally to generate z-stacks. Then, the acquired images could be analyzed with 3D rendering software (e.g. Volocity, Imaris) to assess L-R differences in cell shape as well as the plane of F-actin orientation. In the Results section, we proposed that Nodal signaling may be triggering a D/v to A/P polarity change in the F-actin network and 3D analyses of the L versus R LPM would address this. Experiments to address L-R differences in cell shape could easily be performed by injecting RNA at the two-cell stage, such that R-sided cells were injected with membrane-bound GFP (mGFP; see Chapter II for description) and L-sided cells with membrane-bound RFP (mRFP). After sectioning embryos from stage 34-40, we could compare cell shape, volume, and orientation in the X/Y/Z planes over time. Additionally, the thick sections could also be stained with Phalloidin to address the orientation of the cytoskeletal network with respect to cell orientation within the LPM.

When we began these later-stage studies, we quickly realized that the current published images for Pitx2c are low-resolution. *Pitx2c* expression needs to be studied

over several stages, in whole-mount as well as in sectional analysis. Specifically, remains to be seen if *Pitx2c* expression becomes limited to the splanchnic mesoderm at some point, which could help us better determine if both the somatic and splanchnic LPM are involved in gut morphogenesis. To address if *Pitx2c* becomes restricted to one LPM layer, it will be best to use fluorescent in situ hybridization on cryosections that have been co-stained with an ECM protein such as Laminin to delineate the LPM boundaries.

Although we have confirmed via sectional analysis that a rightward tilt of the liver is the first internal morphological asymmetry, it will be informative to generate better whole-mount images to describe gut tube morphology, similar to the descriptive analyses previously published (Chalmers and Slack, 1998; Chalmers and Slack, 2000; Chalmers et al., 2000), in the hours leading up to asymmetric morphogenesis through stages where gut bending has begun. The gut tube should be imaged dorsally and ventrally over time, especially in the stages prior to stage 39, as they were not included in the descriptive studies by Chalmers and Slack (Chalmers and Slack, 1998). By describing the external morphology of the gut tube, it will allow us to make correlations between the areas of focal F-actin redistribution and ongoing external morphological changes. If whole-mount bright field imaging does not provide sufficient resolution to describe rather minute changes in the gut tube anatomy, endoderm-targeted mGFP injections might allow fluorescent whole-mount imaging. Then, using the software described above, 3D reconstructions of the endoderm could be created.

REFERENCES

Adams, D. S. and Levin, M. (2006). Inverse drug screens: a rapid and inexpensive method for implicating molecular targets. *Genesis* **44**, 530-540.

Adams, D. S., Robinson, K. R., Fukumoto, T., Yuan, S., Albertson, R. C., Yelick, P., Kuo, L., McSweeney, M. and Levin, M. (2006). Early, H+-V-ATPase-dependent proton flux is necessary for consistent left-right patterning of non-mammalian vertebrates. *Development* **133**, 1657-1671.

Agius, E., Oelgeschläger, M., Wessely, O., Kemp, C. and De Robertis, E. M. (2000). Endodermal Nodal-related signals and mesoderm induction in *Xenopus*. *Development* **127**, 1173-1183.

Arrington, C. B. and Yost, H. J. (2009). Extra-embryonic syndecan 2 regulates organ primordia migration and fibrillogenesis throughout the zebrafish embryo. *Development* **136**, 3143-3152.

Beck, S., Le Good, J. A., Guzman, M., Ben Haim, N., Roy, K., Beermann, F. and Constam, D. B. (2002). Extraembryonic proteases regulate Nodal signalling during gastrulation. *Nat Cell Biol* **4**, 981-985.

Belenkaya, T. Y., Han, C., Yan, D., Opoka, R. J., Khodoun, M., Liu, H. and Lin, X. (2004). Drosophila Dpp morphogen movement is independent of dynamin-mediated endocytosis but regulated by the glypican members of heparan sulfate proteoglycans. *Cell* **119**, 231-244.

Bernfield, M., Gotte, M., Park, P. W., Reizes, O., Fitzgerald, M. L., Lincecum, J. and Zako, M. (1999). Functions of cell surface heparan sulfate proteoglycans. *Annu. Rev. Biochem.* **68**, 729-777.

Blanchet, M.-H., Le Good, J. A., Mesnard, D., Oorschot, V., Baflast, S., Minchiotti, G., Klumperman, J. and Constam, D. B. (2008). Cripto recruits Furin and PACE4 and controls Nodal trafficking during proteolytic maturation. *EMBO J* **27**, 2580-2591.

Bouwmeester, T., Kim, S., Sasai, Y., Lu, B. and De Robertis, E. M. (1996). Cerberus is a head-inducing secreted factor expressed in the anterior endoderm of Spemann's organizer. *Nature* **382**, 595-601.

Bowes, J., Snyder, K., Segerdell, E., Jarabek, C., Azam, K., Zorn, A. and Vize, P. (2010). Xenbase: gene expression and improved integration. *Nucleic Acids Res.* **38**, D607-612.

Branford, W. W. and Yost, H. J. (2002). Lefty-dependent inhibition of Nodal- and Wnt-responsive organizer gene expression is essential for normal gastrulation. *Curr. Biol.* **12**, 2136-2141.

Brennan, J., Norris, D. P. and Robertson, E. J. (2002). Nodal activity in the node governs left-right asymmetry. *Genes Dev* **16**, 2339-2344.

Campione, M., Steinbeisser, H., Schweickert, A., Deissler, K., van Bebber, F., Lowe, L. A., Nowotschin, S., Viebahn, C., Haffter, P., Kuehn, M. R. and Blum, M. (1999). The homeobox gene Pitx2: mediator of asymmetric left-right signaling in vertebrate heart and gut looping. *Development* **126**, 1225-1234.

Cartwright, J. H. E., Piro, O. and Tuval, I. (2004). Fluid-dynamical basis of the embryonic development of left-right asymmetry in vertebrates. *Proc Natl Acad Sci USA* **101**, 7234-7239.

Casey, B. (1998). Two rights make a wrong: human left-right malformations. *Hum. Mol. Genet.* **7**, 1565-1571.

Casey, B. and Hackett, B. P. (2000). Left-right axis malformations in man and mouse. *Curr. Opin. Genet. Dev.* **10**, 257-261.

Cha, Y. (2006). Positive and negative regulation of pattern formation during *Xenopus* embryogenesis. *Cell & Developmental Biology Dissertation*, 1-179.

Cha, Y., Takahashi, S. and Wright, C. (2006). Cooperative non-cell and cell autonomous regulation of Nodal gene expression and signaling by Lefty/Antivin and Brachyury in Xenopus. *Dev Biol* **290**, 246-264.

Chalmers, A. D. and Slack, J. M. (1998). Development of the gut in Xenopus laevis. *Dev Dyn* **212**, 509-521.

Chalmers, A. D. and Slack, J. M. (2000). The Xenopus tadpole gut: fate maps and morphogenetic movements. *Development* **127**, 381-392.

Chalmers, A. D., Slack, J. M. and Beck, C. W. (2000). Regional gene expression in the epithelia of the Xenopus tadpole gut. *Mech Dev* **96**, 125-128.

Chen, C. and Shen, M. (2004). Two Modes by which Lefty Proteins Inhibit Nodal Signaling. *Curr Biol* **14**, 618-624.

Chen, Y. and Schier, A. (2002). Lefty proteins are long-range inhibitors of squint-mediated Nodal signaling. *Curr Biol* **12**, 2124-2128.

Chen, Y. and Schier, A. F. (2001). The zebrafish Nodal signal Squint functions as a morphogen. *Nature* **411**, 607-610.

Cheng, A. M., Thisse, B., Thisse, C. and Wright, C. V. (2000). The Lefty-related factor Xatv acts as a feedback inhibitor of Nodal signaling in mesoderm induction and L-R axis development in *Xenopus*. *Development* **127**, 1049-1061.

Cheng, S. K., Olale, F., Brivanlou, A. H. and Schier, A. F. (2004). Lefty blocks a subset of TGFβ signals by antagonizing EGF-CFC coreceptors. *PLoS Biol* **2**, 215-226.

Choi, W.-Y., Giraldez, A. J. and Schier, A. F. (2007). Target protectors reveal dampening and balancing of Nodal agonist and antagonist by miR-430. *Science* **318**, 271-274.

Chung, M.-I., Nascone-Yoder, N. M., Grover, S. A., Drysdale, T. A. and Wallingford, J. B. (2010). Direct activation of Shroom3 transcription by Pitx proteins drives epithelial morphogenesis in the developing gut. *Development* **137**, 1339-1349.

Collignon, J., Varlet, I. and Robertson, E. J. (1996). Relationship between asymmetric nodal expression and the direction of embryonic turning. *Nature* **381**, 155-158.

Conlon, F. L., Lyons, K. M., Takaesu, N., Barth, K. S., Kispert, A., Herrmann, B. and Robertson, E. J. (1994). A primary requirement for nodal in the formation and maintenance of the primitive streak in the mouse. *Development* **120**, 1919-1928.

Constam, D. B. and Robertson, E. J. (1999). Regulation of bone morphogenetic protein activity by pro domains and proprotein convertases. *J Cell Biol* **144**, 139-149.

Cui, Y., Hackenmiller, R., Berg, L., Jean, F., Nakayama, T., Thomas, G. and Christian, J. L. (2001). The activity and signaling range of mature BMP-4 is regulated by sequential cleavage at two sites within the prodomain of the precursor. *Genes Dev.* **15**, 2797-2802.

Daopin, S., Piez, K. A., Ogawa, Y. and Davies, D. R. (1992). Crystal structure of transforming growth factor-beta 2: an unusual fold for the superfamily. *Science* **257**, 369-373.

Davis, N., Kurpios, N., Sun, X., Gros, J., Martin, J. and Tabin, C. (2008). The chirality of gut rotation derives from left-right asymmetric changes in the architecture of the dorsal mesentery. *Dev Cell* **15**, 134-145.

Deimling, S. J. and Drysdale, T. A. (2009). Retinoic acid regulates anterior-posterior patterning within the lateral plate mesoderm of Xenopus. *Mech. Dev.* **126**, 913-923.

Droguett, R., Cabello-Verrugio, C., Riquelme, C. and Brandan, E. (2006). Extracellular proteoglycans modify TGF-beta bio-availability attenuating its signaling during skeletal muscle differentiation. *Matrix Biol* **25**, 332-341.

Dyson, S. and Gurdon, J. B. (1998). The interpretation of position in a morphogen gradient as revealed by occupancy of activin receptors. *Cell* **93**, 557-568.

Dzamba, B. J., Jakab, K. R., Marsden, M., Schwartz, M. A. and DeSimone, D. W. (2009). Cadherin adhesion, tissue tension, and noncanonical Wnt signaling regulate fibronectin matrix organization. *Dev Cell* **16**, 421-432.

Essner, J. J., Vogan, K. J., Wagner, M. K., Tabin, C. J., Yost, H. J. and Brueckner, M. (2002). Conserved function for embryonic nodal cilia. *Nature* **418**, 37-38.

Fischer, A., Viebahn, C. and Blum, M. (2002). FGF8 acts as a right determinant during establishment of the left-right axis in the rabbit. *Curr Biol* **12**, 1807-1816.

Gaio, U., Schweickert, A., Fischer, A., Garratt, A. N., Müller, T., Ozcelik, C., Lankes, W., Strehle, M., Britsch, S., Blum, M. and Birchmeier, C. (1999). A role of the cryptic gene in the correct establishment of the left-right axis. *Curr Biol* **9**, 1339-1342.

García-García, M. J. and Anderson, K. V. (2003). Essential role of glycosaminoglycans in Fgf signaling during mouse gastrulation. *Cell* **114**, 727-737.

Gierer, A. and Meinhardt, H. (1972). A theory of biological pattern formation. *Kybernetik* **12**, 30-39.

Grande, C. and Patel, N. H. (2009). Nodal signalling is involved in left-right asymmetry in snails. *Nature* **457**, 1007-1011.

Green, J. B., New, H. V. and Smith, J. C. (1992). Responses of embryonic Xenopus cells to activin and FGF are separated by multiple dose thresholds and correspond to distinct axes of the mesoderm. *Cell* **71**, 731-739.

Green, J. B. and Smith, J. C. (1990). Graded changes in dose of a *Xenopus* activin A homologue elicit stepwise transitions in embryonic cell fate. *Nature* **347**, 391-394.

Gritsman, K., Zhang, J., Cheng, S., Heckscher, E., Talbot, W. S. and Schier. (1999). The EGF-CFC protein one-eyed pinhead is essential for Nodal signaling. *Cell* **97**, 121-132.

Gros, J., Feistel, K., Viebahn, C., Blum, M. and Tabin, C. J. (2009). Cell movements at Hensen's node establish left/right asymmetric gene expression in the chick. *Science* **324**, 941-944.

Guo, Z. and Wang, Z. (2009). The glypican Dally is required in the niche for the maintenance of germline stem cells and short-range BMP signaling in the Drosophila ovary. *Development* **136**, 3627-3635.

Gurdon, J. B., Mitchell, A. and Mahony, D. (1995). Direct and continuous assessment by cells of their position in a morphogen gradient. *Nature* **376**, 520-521.

Hagos, E. G. and Dougan, S. T. (2007). Time-dependent patterning of the mesoderm and endoderm by Nodal signals in zebrafish. *BMC Dev Biol* **7**, 1-18.

Hamada, H. (2008). Breakthroughs and future challenges in left-right patterning. *Dev. Growth Diff.* **50**, S71-78.

Hecksher-Sørensen, J., Watson, R. P., Lettice, L. A., Serup, P., Eley, L., De Angelis, C., Ahlgren, U. and Hill, R. E. (2004). The splanchnic mesodermal plate directs spleen and pancreatic laterality, and is regulated by Bapx1/Nkx3.2. *Development* **131**, 4665-4675.

Hemmati-Brivanlou, A. and Thomsen, G. H. (1995). Ventral mesodermal patterning in Xenopus embryos: expression patterns and activities of BMP-2 and BMP-4. *Dev. Genet.* **17**, 78-89.

Horne-Badovinac, S., Rebagliati, M. and Stainier, D. Y. R. (2003). A cellular framework for gut-looping morphogenesis in zebrafish. *Science* **302**, 662-665.

Hummel, K. P. and Chapman, D. B. (1959). Visceral inversion and associated anomalies in the mouse. *J Hered* **50**, 10-13.

Ishimaru, Y., Yoshioka, H., Tao, H., Thisse, B., Thisse, C., C, V. E. W., Hamada, H., Ohuchi, H. and Noji, S. (2000). Asymmetric expression of antivin/lefty1 in the early chick embryo. *Mech Dev* **90**, 115-118.

Itoh, K. and Sokol, S. Y. (1994). Heparan sulfate proteoglycans are required for mesoderm formation in Xenopus embryos. *Development* **120**, 2703-2711.

Jing, X., Zhou, S., Wang, W. and Chen, Y. (2006). Mechanisms underlying long- and short-range nodal signaling in Zebrafish. *Mech. Dev.* **123**, 388-394.

Jones, C. M., Armes, N. and Smith, J. C. (1996). Signalling by TGF-beta family members: short-range effects of Xnr-2 and BMP-4 contrast with the long-range effects of activin. *Curr. Biol.* **6**, 1468-1475.

Jones, C. M., Kuehn, M. R., Hogan, B. L., Smith, J. C. and Wright, C. V. (1995). Nodal-related signals induce axial mesoderm and dorsalize mesoderm during gastrulation. *Development* **121**, 3651-3662.

Jullien, J. and Gurdon, J. (2005). Morphogen gradient interpretation by a regulated trafficking step during ligand-receptor transduction. *Genes Dev* **19**, 2682-2694.

Kingsley, D. M. (1994). The TGF-beta superfamily: new members, new receptors, and new genetic tests of function in different organisms. *Genes Dev* **8**, 133-146.

Kofron, M., Demel, T., Xanthos, J., Lohr, J., Sun, B., Sive, H., Osada, S., Wright, C., Wylie, C. and Heasman, J. (1999). Mesoderm induction in Xenopus is a zygotic event regulated by maternal VegT via TGFbeta growth factors. *Development* **126**, 5759-5770.

Kramer, K. L., Barnette, J. E. and Yost, H. J. (2002). PKCgamma regulates syndecan-2 inside-out signaling during Xenopus left-right development. *Cell* **111**, 981-990.

Kramer, K. L. and Yost, H. J. (2002). Ectodermal syndecan-2 mediates left-right axis formation in migrating mesoderm as a cell-nonautonomous Vg1 cofactor. *Dev. Cell.* **2**, 115-124.

Kucenas, S., Takada, N., Park, H.-C., Woodruff, E., Broadie, K. and Appel, B. (2008). CNS-derived glia ensheath peripheral nerves and mediate motor root development. *Nat. Neurosci.* **11**, 143-151.

Kurpios, N. A., Ibañes, M., Davis, N. M., Lui, W., Katz, T., Martin, J. F., Belmonte, J. C. I. and Tabin, C. J. (2008). The direction of gut looping is established by changes in the extracellular matrix and in cell:cell adhesion. *Proc Natl Acad Sci USA* **105**, 8499-8506.

Le Good, J. A., Joubin, K., Giraldez, A. J., Ben-Haim, N., Beck, S., Chen, Y., Schier, A. F. and Constam, D. B. (2005). Nodal stability determines signaling range. *Curr. Biol.* **15**, 31-36.

Lee, M. A., Heasman, J. and Whitman, M. (2001). Timing of endogenous activin-like signals and regional specification of the Xenopus embryo. *Development* **128**, 2939-2952.

Levin, M., Johnson, R. L., Stern, C. D., Kuehn, M. and Tabin, C. (1995). A molecular pathway determining left-right asymmetry in chick embryogenesis. *Cell* **82**, 803-814.

Levin, M. and Mercola, M. (1998). Gap junctions are involved in the early generation of left-right asymmetry. *Dev Biol* **203**, 90-105.

Levin, M. and Mercola, M. (1999). Gap junction-mediated transfer of left-right patterning signals in the early chick blastoderm is upstream of Shh asymmetry in the node. *Development* **126**, 4703-4714.

Levin, M., Thorlin, T., Robinson, K. R., Nogi, T. and Mercola, M. (2002). Asymmetries in H+/K+-ATPase and cell membrane potentials comprise a very early step in left-right patterning. *Cell* **111**, 77-89.

Logan, M., Pagán-Westphal, S. M., Smith, D. M., Paganessi, L. and Tabin, C. J. (1998). The transcription factor Pitx2 mediates situs-specific morphogenesis in response to left-right asymmetric signals. *Cell* **94**, 307-317.

Long, S., Ahmad, N. and Rebagliati, M. (2003). The zebrafish nodal-related gene southpaw is required for visceral and diencephalic left-right asymmetry. *Development* **130**, 2303-2316.

Lopes, S. S., Lourenco, R., Pacheco, L., Moreno, N., Kreiling, J. and Saude, L. (2010). Notch signalling regulates left-right asymmetry through ciliary length control. *Development* **137**, 3625-3632.

Lowe, L. A., Supp, D. M., Sampath, K., Yokoyama, T., Wright, C. V., Potter, S. S., Overbeek, P. and Kuehn, M. R. (1996). Conserved left-right asymmetry of nodal expression and alterations in murine situs inversus. *Nature* **381**, 158-161.

Lugemwa, F. N. and Esko, J. D. (1991). Estradiol beta-D-xyloside, an efficient primer for heparan sulfate biosynthesis. *J Biol. Chem.* **266**, 6674-6677.

Marques, S., Borges, A. C., Silva, A. C., Freitas, S., Cordenonsi, M. and Belo, J. A. (2004). The activity of the Nodal antagonist Cerl-2 in the mouse node is required for correct L/R body axis. *Genes Dev* **18**, 2342-2347.

Martello, G., Zacchigna, L., Inui, M., Montagner, M., Adorno, M., Mamidi, A., Morsut, L., Soligo, S., Tran, U., Dupont, S., Cordenonsi, M., Wessely, O. and Piccolo, S. (2007). MicroRNA control of Nodal signalling. *Nature* **449**, 183-188.

Massagué, J. (1998). TGF-beta signal transduction. *Annu. Rev. Biochem.* **67**, 753-791.

McCrea, P. D., Brieher, W. M. and Gumbiner, B. M. (1993). Induction of a secondary body axis in Xenopus by antibodies to beta-catenin. *J. Cell Biol.* **123**, 477-484.

McDowell, N., Zorn, A. M., Crease, D. J. and Gurdon, J. B. (1997). Activin has direct long-range signalling activity and can form a concentration gradient by diffusion. *Curr. Biol.* **7**, 671-681.

McGrath, J., Somlo, S., Makova, S., Tian, X. and Brueckner, M. (2003). Two populations of node monocilia initiate left-right asymmetry in the mouse. *Cell* **114**, 61-73.

Meier, S. (1979). Development of the chick embryo mesoblast. Formation of the embryonic axis and establishment of the metameric pattern. *Dev. Biol.* **73**, 24-45.

Meier, S. (1980). Development of the chick embryo mesoblast: pronephros, lateral plate, and early vasculature. *J. Embryol. Exp. Morphol.* **55**, 291-306.

Meinhardt, H. (2009). Models for the generation and interpretation of gradients. *Cold Spring Harb Perspect Biol* **1**, 1-14.

Meinhardt, H. and Gierer, A. (1974). Applications of a theory of biological pattern formation based on lateral inhibition. *J. Cell Sci.* **15**, 321-346.

Meno, C., Gritsman, K., Ohishi, S., Ohfuji, Y., Heckscher, E., Mochida, K., Shimono, A., Kondoh, H., Talbot, W. S., Robertson, E. J., Schier and Hamada, H. (1999). Mouse Lefty2 and zebrafish antivin are feedback inhibitors of Nodal signaling during vertebrate gastrulation. *Mol Cell* **4**, 287-298.

Meno, C., Saijoh, Y., Fujii, H., Ikeda, M., Yokoyama, T., Yokoyama, M., Toyoda, Y. and Hamada, H. (1996). Left-right asymmetric expression of the TGF beta-family member lefty in mouse embryos. *Nature* **381**, 151-155.

Molloy, S. S., Bresnahan, P. A., Leppla, S. H., Klimpel, K. R. and Thomas, G. (1992). Human furin is a calcium-dependent serine endoprotease that recognizes the sequence Arg-X-X-Arg and efficiently cleaves anthrax toxin protective antigen. *J Biol Chem* **267**, 16396-16402.

Muller, J. K., Prather, D. R. and Nascone-Yoder, N. M. (2003). Left-right asymmetric morphogenesis in the Xenopus digestive system. *Dev Dyn* **228**, 672-682.

Nakamura, T., Mine, N., Nakaguchi, E., Mochizuki, A., Yamamoto, M., Yashiro, K., Meno, C. and Hamada, H. (2006). Generation of robust left-right asymmetry in the mouse embryo requires a self-enhancement and lateral-inhibition system. *Dev. Cell.* **11**, 495-504.

Nieuwkoop, P. D. and Faber, J. (1967). Normal table of Xenopus laevis: A systematical and chronological survey of the development from the fertilized egg till the end of metamorphosis. Amsterdam: North-Holland Publishing Company.

Nonaka, S., Tanaka, Y., Okada, Y., Takeda, S., Harada, A., Kanai, Y., Kido, M. and Hirokawa, N. (1998). Randomization of left-right asymmetry due to loss of nodal cilia generating leftward flow of extraembryonic fluid in mice lacking KIF3B motor protein. *Cell* **95**, 829-837.

Ohi, Y. (2007). Long-range Nodal signaling in vertebrate left-right specification. *Cell & Developmental Biology Dissertation*, 1-157.

Ohi, Y. and Wright, C. (2007). Anteriorward shifting of asymmetric Xnr1 expression and contralateral communication in left–right specification in Xenopus. *Dev. Biol.* **301**, 447-463.

Ohkawara, B., Iemura, S.-i., ten Dijke, P. and Ueno, N. (2002). Action range of BMP is defined by its N-terminal basic amino acid core. *Curr. Biol.* **12**, 205-209.

Okada, Y., Nonaka, S., Tanaka, Y., Saijoh, Y., Hamada, H. and Hirokawa, N. (1999). Abnormal nodal flow precedes situs inversus in iv and inv mice. *Mol Cell* **4**, 459-468.

Oki, S., Hashimoto, R., Okui, Y., Shen, M. M., Mekada, E., Otani, H., Saijoh, Y. and Hamada, H. (2007). Sulfated glycosaminoglycans are necessary for Nodal signal transmission from the node to the left lateral plate in the mouse embryo. *Development* **134**, 3893-3904.

Oki, S., Kitajima, K., Marques, S., Belo, J. A., Yokoyama, T., Hamada, H. and Meno, C. (2009). Reversal of left-right asymmetry induced by aberrant Nodal signaling in the node of mouse embryos. *Development* **136**, 3917-3925.

Osada, S. I. and Wright, C. V. (1999). Xenopus nodal-related signaling is essential for mesendodermal patterning during early embryogenesis. *Development* **126**, 3229-3240.

Piccolo, S., Agius, E., Leyns, L., Bhattacharyya, S., Grunz, H., Bouwmeester, T. and De Robertis, E. M. (1999). The head inducer Cerberus is a multifunctional antagonist of Nodal, BMP and Wnt signals. *Nature* **397**, 707-710.

Piedra, M. E., Icardo, J. M., Albajar, M., Rodriguez-Rey, J. C. and Ros, M. A. (1998). Pitx2 participates in the late phase of the pathway controlling left-right asymmetry. *Cell* **94**, 319-324.

Pohl, B. S., Rössner, A. and Knöchel, W. (2005). The Fox gene family in Xenopus laevis: FoxI2, FoxM1 and FoxP1 in early development. *Int. J. Dev. Biol.* **49**, 53-58.

Ramos, J. W. and DeSimone, D. W. (1996). Xenopus embryonic cell adhesion to fibronectin: position-specific activation of RGD/synergy site-dependent migratory behavior at gastrulation. *J. Cell Biol.* **134**, 227-240.

Ramsdell, A. (2005). Left–right asymmetry and congenital cardiac defects: Getting to the heart of the matter in vertebrate left–right axis determination. *Dev. Biol.* **288**, 1-20.

Ramsdell, A. F. and Yost, H. J. (1998). Molecular mechanisms of vertebrate left-right development. *Trends Genet.* **14**, 459-465.

Raya, Á. and Belmonte, J. C. I. (2006). Left–right asymmetry in the vertebrate embryo: from early information to higher-level integration. *Nat. Rev. Genet.* **7**, 283-293.

Reissmann, E., Jornvall, H., Blokzijl, A., Andersson, O., Chang, C., Minchiotti, G., Persico, M. G., Ibanez, C. F. and Brivanlou, A. H. (2001). The orphan receptor ALK7 and the Activin receptor ALK4 mediate signaling by Nodal proteins during vertebrate development. *Genes Dev* **15**, 2010-2022.

Rodríguez Esteban, C., Capdevila, J., Economides, A. N., Pascual, J., Ortiz, A. and Izpisúa Belmonte, J. C. (1999). The novel Cer-like protein Caronte mediates the establishment of embryonic left-right asymmetry. *Nature* **401**, 243-251.

Ryan, A. K., Blumberg, B., Rodriguez-Esteban, C., Yonei-Tamura, S., Tamura, K., Tsukui, T., de la Peña, J., Sabbagh, W., Greenwald, J., Choe, S., Norris, D. P., Robertson, E. J., Evans, R. M., Rosenfeld, M. G. and Izpisúa Belmonte, J. C. (1998). Pitx2 determines left-right asymmetry of internal organs in vertebrates. *Nature* **394**, 545-551.

Saka, Y., Hagemann, A. I., Piepenburg, O. and Smith, J. C. (2007). Nuclear accumulation of Smad complexes occurs only after the midblastula transition in *Xenopus*. *Development* **134**, 4209-4218.

Saka, Y., Hagemann, A. I. and Smith, J. C. (2008). Visualizing protein interactions by bimolecular fluorescence complementation in *Xenopus*. *Methods* **45**, 192-195.

Sakuma, R., Ohnishi Yi, Y.-i., Meno, C., Fujii, H., Juan, H., Takeuchi, J., Ogura, T., Li, E., Miyazono, K. and Hamada, H. (2002). Inhibition of Nodal signalling by Lefty mediated through interaction with common receptors and efficient diffusion. *Genes Cells* **7**, 401-412.

Sampath, K., Cheng, A. M., Frisch, A. and Wright, C. V. (1997). Functional differences among Xenopus nodal-related genes in left-right axis determination. *Development* **124**, 3293-3302.

Schier, A. F. (2003). Nodal signaling in vertebrate development. *Annu. Rev. Cell Dev. Biol.* **19**, 589-621.

Scholpp, S. and Brand, M. (2004). Endocytosis controls spreading and effective signaling range of Fgf8 protein. *Curr. Biol.* **14**, 1834-1841.

Schweickert, A., Vick, P., Getwan, M., Weber, T., Schneider, I., Eberhardt, M., Beyer, T., Pachur, A. and Blum, M. (2010). The Nodal inhibitor Coco is a critical target of leftward flow in *Xenopus*. *Curr Biol* **20**, 738-743.

Schweickert, A., Weber, T., Beyer, T., Vick, P., Bogusch, S., Feistel, K. and Blum, M. (2007). Cilia-Driven leftward flow determines laterality in Xenopus. *Curr. Biol.* **17**, 60-66.

Shi, Y. and Massagué, J. (2003). Mechanisms of TGF-beta Signaling from Cell Membrane to the Nucleus. *Cell* **113**, 685-700.

Shimizu, K. and Gurdon, J. B. (1999). A quantitative analysis of signal transduction from activin receptor to nucleus and its relevance to morphogen gradient interpretation. *Proc Natl Acad Sci USA* **96**, 6791-6796.

Shiratori, H., Sakuma, R., Watanabe, M., Hashiguchi, H., Mochida, K., Sakai, Y., Nishino, J., Saijoh, Y., Whitman, M. and Hamada, H. (2001). Two-step regulation of left-right asymmetric expression of Pitx2: initiation by Nodal signaling and maintenance by Nkx2. *Mol Cell* **7**, 137-149.

Sive, H. L., Grainger, R. M. and Harland, R. M. (2000). Early Development of Xenopus laevis: A Laboratory Manual. Cold Spring Harbor, NY: Cold Spring Harbor Laboratory Press.

Slack, J. M. and Tannahill, D. (1992). Mechanism of anteroposterior axis specification in vertebrates. Lessons from the amphibians. *Development* **114**, 285-302.

Sokol, S., Christian, J. L., Moon, R. T. and Melton, D. A. (1991). Injected Wnt RNA induces a complete body axis in Xenopus embryos. *Cell* **67**, 741-752.

Sokol, S., Wong, G. G. and Melton, D. A. (1990). A mouse macrophage factor induces head structures and organizes a body axis in *Xenopus*. *Science* **249**, 561-564.

Song, H., Hu, J., Chen, W., Elliott, G., Andre, P., Gao, B. and Yang, Y. (2010). Planar cell polarity breaks bilateral symmetry by controlling ciliary positioning. *Nature* **466**, 378-82.

Stevens, R. L. and Austen, K. F. (1982). Effect of p-nitrophenyl-beta-D-xyloside on proteoglycan and glycosaminoglycan biosynthesis in rat serosal mast cell cultures. *J Biol. Chem.* **257**, 253-259.

Tabin, C. (2006). The key to left-right asymmetry. *Cell* **127**, 27-32.

Tanaka, C., Sakuma, R., Nakamura, T., Hamada, H. and Saijoh, Y. (2007). Long-range action of Nodal requires interaction with GDF1. *Genes Dev* **21**, 3272-3282.

Tanaka, Y., Okada, Y. and Hirokawa, N. (2005). FGF-induced vesicular release of Sonic hedgehog and retinoic acid in leftward nodal flow is critical for left–right determination. *Nature* **435**, 172-177.

Tanegashima, K., Haramoto, Y., Yokota, C., Takahashi, S. and Asashima, M. (2004). Xantivin suppresses the activity of EGF-CFC genes to regulate nodal signaling. *Int J Dev Biol* **48**, 275-283.

Thisse, C. and Thisse, B. (1999). Antivin, a novel and divergent member of the TGFbeta superfamily, negatively regulates mesoderm induction. *Development* **126**, 229-240.

Tseng, H.-T., Shah, R. and Jamrich, M. (2004). Function and regulation of FoxF1 during Xenopus gut development. *Development* **131**, 3637-3647.

Turing, A. M. (1990). The chemical basis of morphogenesis. 1953. *Bull. Math. Biol.* **52**, 119-153.

Vonica, A. and Brivanlou, A. H. (2007). The left-right axis is regulated by the interplay of Coco, Xnr1 and derrière in *Xenopus* embryos. *Dev Biol* **303**, 281-294.

Wallingford, J. B., Rowning, B. A., Vogeli, K. M., Rothbacher, U., Fraser, S. E. and Harland, R. M. (2000). Dishevelled controls cell polarity during Xenopus gastrulation. *Nature* **405**, 81-85.

Wang, X. and Yost, H. J. (2008). Initiation and propagation of posterior to anterior (PA) waves in zebrafish left-right development. *Dev. Dyn.* **237**, 3640-3647.

Weeks, D. L. and Melton, D. A. (1987). A maternal mRNA localized to the vegetal hemisphere in Xenopus eggs codes for a growth factor related to TGF-beta. *Cell* **51**, 861-867.

Wei, Q. and Adelstein, R. S. (2002). Pitx2a expression alters actin-myosin cytoskeleton and migration of HeLa cells through Rho GTPase signaling. *Mol Biol Cell* **13**, 683-697.

Westmoreland, J. J., Takahashi, S. and Wright, C. V. E. (2007). Xenopus Lefty requires proprotein cleavage but not N-linked glycosylation to inhibit Nodal signaling. *Dev. Dyn.* **236**, 2050-2061.

Williams, P. H., Hagemann, A., González-Gaitán, M. and Smith, J. C. (2004). Visualizing long-range movement of the morphogen Xnr2 in the Xenopus embryo. *Curr. Biol.* **14**, 1916-1923.

Wright, C. V. (2001). Mechanisms of left-right asymmetry: what's right and what's left? *Dev. Cell.* **1**, 179-186.

Xu, L., Chen, Y. G. and Massague, J. (2000). The nuclear import function of Smad2 is masked by SARA and unmasked by TGFbeta-dependent phosphorylation. *Nat Cell Biol* **2**, 559-562.

Yamamoto, M. (2003). Nodal signaling induces the midline barrier by activating Nodal expression in the lateral plate. In *Development*, vol. 130 (ed., pp. 1795-1804.

Yamamoto, M., Mine, N., Mochida, K., Sakai, Y., Saijoh, Y., Meno, C. and Hamada, H. (2003). Nodal signaling induces the midline barrier by activating Nodal expression in the lateral plate. *Development* **130**, 1795-1804.

Yokouchi, Y., Vogan, K. J., Pearse, R. V. and Tabin, C. J. (1999). Antagonistic signaling by Caronte, a novel Cerberus-related gene, establishes left-right asymmetric gene expression. *Cell* **98**, 573-583.

Yokoyama, T., Copeland, N. G., Jenkins, N. A., Montgomery, C. A., Elder, F. F. and Overbeek, P. A. (1993). Reversal of left-right asymmetry: a situs inversus mutation. *Science* **260**, 679-682.

Yoshioka, H., Meno, C., Koshiba, K., Sugihara, M., Itoh, H., Ishimaru, Y., Inoue, T., Ohuchi, H., Semina, E. V., Murray, J. C., Hamada, H. and Noji, S. (1998). Pitx2, a bicoid-type homeobox gene, is involved in a lefty-signaling pathway in determination of left-right asymmetry. *Cell* **94**, 299-305.

Yost, H. J. (1990). Inhibition of proteoglycan synthesis eliminates left-right asymmetry in Xenopus laevis cardiac looping. *Development* **110**, 865-874.

Yu, S. R., Burkhardt, M., Nowak, M., Ries, J., Petrášek, Z., Scholpp, S., Schwille, P. and Brand, M. (2009). Fgf8 morphogen gradient forms by a source-sink mechanism with freely diffusing molecules. *Nature*, 1-5.

Zhou, X., Sasaki, H., Lowe, L., Hogan, B. L. and Kuehn, M. R. (1993). Nodal is a novel TGF-beta-like gene expressed in the mouse node during gastrulation. *Nature* **361**, 543-547.

Zhu, L., Marvin, M. J., Gardiner, A., Lassar, A. B., Mercola, M., Stern, C. D. and Levin, M. (1999). Cerberus regulates left-right asymmetry of the embryonic head and heart. *Curr Biol* **9**, 931-8.